SANDIA REPORT
SAND2020-6295
Printed June 2020

Sandia National Laboratories

An Overview of the State-of-the-Art Reactor Consequence Uncertainty Assessment Accident Progression Insights

Kenneth C. Wagner
Christopher Faucett
Dusty Brooks
Aaron Krueger

Prepared by
Sandia National Laboratories
Albuquerque, New Mexico
87185 and Livermore,
California 94550

Issued by Sandia National Laboratories, operated for the United States Department of Energy by National Technology & Engineering Solutions of Sandia, LLC.

Available to DOE and DOE contractors from
U.S. Department of Energy
Office of Scientific and Technical Information
P.O. Box 62
Oak Ridge, TN 37831

Telephone: (865) 576-8401
Facsimile: (865) 576-5728
E-Mail: reports@osti.gov
Online ordering: http://www.osti.gov/scitech

Available to the public from
U.S. Department of Commerce
National Technical Information Service
5301 Shawnee Rd
Alexandria, VA 22312

Telephone: (800) 553-6847
Facsimile: (703) 605-6900
E-Mail: orders@ntis.gov
Online order: https://classic.ntis.gov/help/order-methods/

ABSTRACT

The U.S. Nuclear Regulatory Commission (NRC) with Sandia National Laboratories (Sandia) have completed three uncertainty analyses (UAs) as part of the State-of-the-Art Reactor Consequence Analyses (SOARCA) program. The SOARCA UAs included an integrated evaluation of uncertainty in accident progression, radiological release, and offsite health consequence projections. The UA for Peach Bottom, a boiling-water reactor (BWR) with a Mark I containment located in the State of Pennsylvania, analyzed the unmitigated long-term station blackout SOARCA scenario. The UA for Sequoyah, a 4-loop Westinghouse pressurized-water reactor (PWR) located in the State of Tennessee, analyzed the unmitigated short-term station blackout SOARCA scenario, with a focus on issues unique to the ice condenser containment and the potential for early containment failure due to hydrogen deflagration. The UA for Surry, a 3-loop Westinghouse PWR with a sub-atmospheric large dry containment located in the State of Virginia, analyzed the unmitigated short-term station blackout SOARCA scenario including the potential for thermally-induced steam-generator tube rupture. These three UAs are currently documented in three NUREG/CR reports.

This report provides input to planned NRC documentation on the insights and findings from the SOARCA UA program. The purpose of the summary report is to provide a useful reference for regulatory applications that require the evaluation of offsite consequence risk from beyond design basis event severe accidents. This report focuses on the accident progression and source term insights developed from the MELCOR analyses. MELCOR is the NRC's best-estimate, severe accident computer code used in the SOARCA UAs.

In anticipation of the SOARCA UA insights work, NRC and Sandia benchmarked the response of the Peach Bottom model to selected reference calculations from the Peach Bottom SOARCA UA. Peach Bottom was the first SOARCA UA performed and was completed in 2015 using the MELCOR 1.8.6 code. The PWR SOARCA UAs evolved the original methodology and utilized the updated MELCOR 2.2 computer code. The Peach Bottom model has been systematically updated for other NRC research efforts and has been updated to MELCOR 2.2. computer code. The findings from the new reference calculations using the updated model with the MELCOR 2.2 code are also integrated into the report.

A second objective is an assessment of the applicability of the results to the other nuclear reactors in the U.S. As the key findings are reviewed, judgments are presented on the applicability of the results to other U.S. nuclear power plants. An important objective of the SOARCA program relied on high-fidelity plant-specific modeling. However, the nature of the insights and conclusions allowed judgements to be made on the applicability of the various insights to the same general classification of plant (i.e., BWR or PWR) or the entire fleet of plants.

Finally, the results from the SOARCA UA accident progression calculations contain a wealth of information not previously documented in the NUREG/CRs. This report includes new but related information that can be used to benchmark past or support future regulatory decisions related to severe accidents. The new work includes a benchmark of the NUREG-1465 licensing source term definitions, the variability of key accident progression events and timing to radionuclide release, and an improved understanding of the timing and source terms from consequential steam generator tube ruptures.

ACKNOWLEDGEMENTS

The Sandia authors gratefully acknowledge the significant technical and programmatic contributions from the NRC SOARCA team which are reflected throughout the report. Dr. Tina Ghosh has been involved throughout the SOARCA UAs, providing the primary managerial and technical oversight. The long lists of NRC and Sandia contributors from the SOARCA UAs are cited in the three NUREG/CRs and are also gratefully acknowledged by the small team of authors compiling the results of their efforts. Significant technical contributions, advice, and reviews were provided by Dr. Hossein Esmaili, Dr. Alfred Hathaway, and Dr. Edward Fuller (retired) of the NRC. Dr. Randal Gauntt (retired), Mr. Patrick Mattie, Mr. Joseph Jones (retired), and Dr. Doug Osborn from Sandia are recognized as the SOARCA UA managers guiding the past efforts. There is a comparable list of project managers at the NRC including Ms. Patricia Santiago, Dr. Salman Haq, and Mr. Jon Barr. Sadly, we have lost Mr. Charlie Tinkler and Mr. Robert Prato, who were important contributors to the original SOARCA project. Finally, Mr. Kyle Ross and Mr. Mark Leonard have also retired but were significant technical contributors. Mr. Kyle Ross was the technical lead on all three SOARCA UAs and the original pressurized water reactor SOARCA study. Mr. Leonard was the technical lead on the original boiling water reactor SOARCA study and a key contributor to the first Peach Bottom SOARCA UA.

CONTENTS

LIST OF FIGURES

LIST OF TABLES

ACRONYMS AND DEFINITIONS

Abbreviation	Definition
AC	alternating current
ACRS	Advisory Committee on Reactor Safeguards
AFW	auxiliary feedwater
AVB	anti-vibration bars
B&W	Babcock and Wilcox
BOC	beginning of cycle
BWR	boiling water reactor
CCI	core-concrete interactions
CE	Combustion Engineering
CEA	Atomic Energy and Alternative Energies Commission
CFD	computational fluid dynamics
C-SGTR	consequential steam generator tube rupture
DC	direct current
EFPY	effective full-power year
EOC	end of cycle
EPRI	Energy Power Research Institute
FOM	figure of merit
FTC	fail to close
FTO	fail to open
GE	General Electric
ISI	in-service inspections
LER	licensing event reports
LHF	lower head failure
LOCA	loss-of-coolant accident
LTSBO	long-term station blackout
MCCI	molten core concrete interaction
MOC	middle of cycle
MSIV	main steam isolation valves
MSL	main steam line
MSS	main steam system
NRC	United States Nuclear Regulatory Commission
NSSS	nuclear steam supply system
POD	probability of detection

Abbreviation	Definition
PRA	probabilistic risk assessment
PRT	pressurizer relief tank
PWR	pressurized water reactor
RCIC	reactor core isolation cooling
RCP	reactor coolant pump
RCS	reactor coolant system
RPV	reactor pressure vessel
Sandia	Sandia National Laboratories
SBO	station blackout
scfh	standard cubic feet per hour
scfm	standard cubic feet per minute
SAMG	Severe accident management guidelines
SG	steam generator
SLOCA	small-break loss-of-coolant accident
SOARCA	State-of-the-Art Reactor Consequence Assessment
SRV	safety relief valve
STSBO	short-term station blackout
SV	safety valve
UA	uncertainty analysis
U.S.	United States

1. INTRODUCTION

The U.S. Nuclear Regulatory Commission (NRC) with Sandia National Laboratories (Sandia) have completed three uncertainty analyses (UAs) as part of the State-of-the-Art Reactor Consequence Analyses (SOARCA) program. The SOARCA UAs included an integrated evaluation of uncertainty in accident progression, radiological release, and offsite health consequence projections. The UA for Peach Bottom, a boiling-water reactor (BWR) with a Mark I containment located in the State of Pennsylvania, analyzed the unmitigated long-term station blackout (LTSBO) SOARCA scenario [1]. The UA for Sequoyah, a 4-loop Westinghouse pressurized-water reactor (PWR) located in the State of Tennessee, analyzed the unmitigated short-term station blackout (STSBO) SOARCA scenario, with a focus on issues unique to the ice condenser containment and the potential for early containment failure due to hydrogen deflagration [2]. The UA for Surry, a 3-loop Westinghouse PWR with subatmospheric large dry containment located in the State of Virginia, analyzed the unmitigated STSBO SOARCA scenario including the potential for thermally-induced steam-generator tube rupture [3]. These three UAs are currently documented in three NUREG/CR reports totaling over 1800 pages of information.

The objectives of this report are described in Section 2. The report will organize and highlight the most important insights on the accident progression and radiological release from the three UAs. The SOARCA UA is a significant improvement in the state of understanding of accident progression responses and uncertainty. Previous assessment of severe accident risk often relied on expert judgment, separate effects codes, and/or experiments that lacked an integrated architecture for an integral assessment of effects important to key figures of merit (i.e., particularly the source term). The report objectives include providing guidance for other applications (e.g., recommendations for new work, extensions for accident management, and insights for regulatory applications). A strength of the SOARCA UA analyses was the focused specifications (e.g., plant-specific, a specific sequence, and limited operator interventions). It provided an in-depth uncertainty characterization of the specific accident at a specific plant that had not been done previously. Consequently, it is also appropriate to discuss the assumptions and limitations of the focused approach.

Section 3 contains the key insights from the three studies. The three SOARCA UAs are a rich source of information but have not been previously summarized with an integrated perspective. The overviews of the integration of insights started with a series of conference papers with varied scopes and objectives shown in Reference [4] through [8]. This report incorporates and organizes the findings cited in the conference papers but specifically within the scope of the accident progression insights rather than consequence or methodology insights.

In anticipation of the SOARCA insights summary report, the Peach Bottom model was updated and benchmarked to selected reference calculations from the Peach Bottom SOARCA UA using MELCOR 2.2. The Peach Bottom LTSBO was the first SOARCA UA performed and was completed in 2015 using the MELCOR 1.8.6 code. The two PWR SOARCA UAs (Sequoyah and Surry) evolved the UA methodology and utilized the updated MELCOR 2.2 computer code. The new insights using an updated Peach Bottom model with the MELCOR 2.2 are integrated into this report.

The Peach Bottom UA calculations and report were nearly done at the time of the Fukushima Dai-chi reactor accidents occurred. The Peach Bottom UA report includes a discussion of the original Peach Bottom SOARCA calculations with respect to the events at the various Fukushima Dai-chi reactor accident [1]. The Fukushima Dai-chi accidents were complicated with operator actions and

mitigative efforts with uncertain effectiveness. The Peach Bottom UA notes many commonalities in the accident progression as well as differences. Several references are made to the Fukushima Dai-chi accidents in this report as well as NRC post-Fukushima orders to improve safety. Most importantly, the various UAs address attempt to answer the question, "how bad could it be?" using the risk dominant sequences identified in the respective SOARCA UA plant PRAs but with limited credit for any operator actions and no credit for mitigative actions. The Sequoyah UA report includes a sensitivity calculation to highlight the importance of post-Fukushima NRC orders to have an emergency power source for the hydrogen igniters, which prevented an early containment failure.

A second objective is an assessment of the applicability of the results to the other nuclear reactors in the U.S. As the key findings are reviewed, judgments are presented on the applicability of the results to other U.S. nuclear power plants. An important objective of the SOARCA program relied on high-fidelity, plant-specific modeling. In particular, the SOARCA program attempted to incorporate accurate plant-specific design information, system models, and operator actions. The SOARCA program included numerous onsite plant visits, industry and expert NRC Advisory Committee on Reactor Safeguards (ACRS) reviews, fact-checks and feedback solicitations with the plant staff, and public and NRC staff input from other NRC offices. Consequently, the results were intended to be only representative of the three specific plants for three specific accident sequences. However, the nature of the insights and conclusions allowed judgements to be made on the applicability of the various insights to the same general classification of plant (i.e., BWR or PWR) or the entire fleet of plants. When possible, recommendations and methods are suggested to generalize the specific findings to other plants.

Some recent work not previously discussed in the SOARCA UA NUREG/CRs is presented in Section 4. The new work highlights applications using the SOARCA calculations as a large database for investigations of the variability and uncertainty in severe accident progression. The results from the SOARCA UA accident progression calculations contain a wealth of information not previously documented in the NUREG/CRs. The new but related information can be used to benchmark past or inform new regulatory decisions related to severe accidents. The new work includes a benchmark of the NUREG-1465 licensing source term definitions, the variability of key accident progression events and timing to radionuclide release, and an improved understanding of the timing and source terms from consequential steam generator tube ruptures.

Recommendations for other applications and a summary is provided in Section 5. The recommendations highlight benefits from the SOARCA UA work including the data harvesting as identified in Section 4, guidance for future UA work, new insights with uncertainty characterization for emergency preparedness and accident management, and uncertainty-informed regulatory insights (e.g., licensing source term guidance).

2. OBJECTIVES OF THE INSIGHTS REPORT

The objectives of this report include providing an integrated summary of the key findings from the SOARCA UAs and their applicability to other plants and other accident sequences (see discussion in Section 2.1). The SOARCA program has already benefitted many activities at the NRC. Section 2.2 summarizes the objectives to applying the results and methodology to other applications. Finally, Section 2.3 describes the specifications and scope of the studies to frame the inherent limitations for other applications.

2.1. Key Objectives

The key objectives of the SOARCA UA insights report is to identify the most important insights on potential accident progression and radiological release from the SOARCA program.

- The new insights gained from the SOARCA UAs.
- How insights from each of the three UAs apply to accident scenarios that were not studied.
- How insights from each of the three UAs apply to the fleet of operating plants in the U.S., and to other sites.
- Important considerations in determining the applicability of insights to other plants and sites.

2.2. Recommendations for Other Applications

The SOARCA UAs have already provided considerable impact. They have assisted the regulatory evaluation of a variety of issues including the disposition of post-Fukushima Dai-chi accident regulatory initiatives and the consideration of emergency planning zone size. The SOARCA studies have also informed other NRC research projects, such as the NRC's Spent Fuel Pool Study published in 2013, and the NRC's on-going Site Level 3 Probabilistic Risk Assessment project.

The consolidated insights from the eventual NUREG report with both accident progression and offsite consequence insights are expected to provide guidance for emergency planning and emergency response. The existing results remain a wealth of additional insights. Examples are provided in Section 4 for the assessment of uncertainty in event timing and severity for decision makers in emergency management. For example, the timing uncertainty characterizations can be a resource for human reliability assessments for severe accident management guidelines. If the timing uncertainty is large relative to the time to perform the action, then an assessment can be made on the appropriateness on early actions versus implementing later actions. It may be more effective to bypass early actions in lieu of the latter actions (e.g., focusing on powering igniters in the containment versus water addition to the reactor when resources are limited).

Another example provides benchmarks for the phenomenological uncertainty displayed in the SOARCA results to the regulatory source term specifications provided in NUREG-1465 [9]. The techniques used for NUREG-1465 are dated relative to current simulation techniques and the uncertainty characterization used in the SOARCA UA. The information from the SOARCA UA results database compliments subsequent source term efforts such as References [10], [11], and [12] that revisit the regulatory guidance for light water reactor source terms. The example in Section 4 allows immediate quantitative data from the SOARCA UA work. The previously reported SOARCA UA results contain a wealth of new insights into figures of merit (FOM) available through advanced data-mining techniques.

2.3. Discussion of SOARCA UA Limitations

A strength of the SOARCA UA program was the plant-specific analysis of a specific accident sequence with limitations on operator actions for accident mitigation. The SOARCA UAs provide a focused evaluation of the accident progression and uncertainties within the scope of the current state-of-the-art of the computer models and our understanding of the important uncertain accident progression. The current state-of-the-art and associated computer codes have evolved since the inception of the licensing for commercial power reactors. While probabilistic risk assessments (PRA) have allowed significant progress in characterizing the plant-specific contributors to the core damage frequency (i.e., the Level I portion of the PRA), the understanding of the consequences to those vulnerable states has lagged due to the complexity of the phenomena, a limited experimental database, and the challenges of performing an integrated simulation. The SOARCA UAs provide an alternate and complimentary method to advance the understanding of the accident progression, the radionuclide source term, and the associated health consequences evaluations that are found in current PRA treatments. The insights from SOARCA UA helps improve the associated accident progression characterization in PRAs while PRAs identify those sequences and events most important for focused SOARCA UA studies.

The SOARCA UA results are particularly relevant for regulators and emergency preparedness planners. Due to the lack of mitigation and limited credit for operator actions, the SOARCA UAs investigate uncertainty in the magnitude and timing of the source term and the associated health consequences. In effect, they attempt to answer the question, "how bad could it be?" using the risk dominant sequences identified in the respective SOARCA UA plant PRAs. The fast-progressing STSBO without onsite AC or DC power in the PWR UAs have wide applicability to worst case events (e.g., the Fukushima Dai-chi accidents without the operator actions). The BWR UAs illustrate a more likely but slower progressing LTSBO with limited DC power for injection. The UA simulations characterize the uncertainties in the accident progression and the magnitude of the source term without complications of operator interventions. Consequently, the impact of the accident uncertainties can be evaluated without the potentially overwhelming course corrections from successful operator actions. Nevertheless, the SOARCA UA offer valuable information on timing windows and their uncertainties for mitigating actions (e.g., time to recover hydrogen igniters in the Sequoyah UA, see Section 3.2.4.2).

The strengths of current PRAs highlight the limitations of the SOARCA UAs but also their complimentary role. PRAs examine the full range of accidents with less detail but realistically consider operator actions. For example, PRAs typically address phenomenological uncertainties in a parametric manner without characterizing the range of outputs (e.g., a binary evaluation of a safety valve failure) and with limited consideration of simultaneously incorporating other uncertainties (e.g., timing in the accident and failure area).

A strength of the PRA is that it is not limited by code capabilities. Advanced separate effects code results, experiments, real accidents (e.g., insights from the Fukushima Dai-chi accidents), and expert judgment can be incorporated into the PRA without having those capabilities in an integral accident progression and source term code like MELCOR. Furthermore, advanced PRA techniques allow uncertainty quantification using methods like Fussell-Vesely, Risk Achievement Worth, or and Birnbaum. These techniques provide quantitative perspective on dominant contributors to risk and sensitivity of risk to changes in input values. Once the PRA is completed, these importance evaluations can be rapidly performed to assess a more complete understanding of the plant risk. Although additional data mining can be done on the SOARCA UA, the basic modeling assumptions

cannot be changed in the same manner. In contrast, re-running the SOARCA UA calculations and processing the results is a large effort.

The scope of the current SOARCA UAs have a very limited incorporation of operator actions or severe accident management actions. Since the SOARCA UAs focused on accidents that experienced core damage, it falls within the scope of the Level 2 and Level 3 portions of the PRA. An integrated PRA not only includes operator actions that prevent core damage in the Level I portion of the PRA, but accident management actions in the Level 2 and Level 3 portions of the PRA as well. However, future applications of SOARCA UA techniques could be expanded to include operator actions and the integrated impact on the accident progression and health consequences.

Finally, both a PRA and the SOARCA UA are highly plant specific. Great efforts are made to accurately describe the accident progression at a single nuclear reactor. The SOARCA UA is further limited by a single scenario. However, there is generic applicability from both a PRA and a SOARCA UA to other similar plants, the full class of plants (BWR or PWR), and all reactors. The translation of these insights is almost always qualitative. Since both techniques quantify and address uncertainty, the judgment of the impact to the variations in other designs is often within the characterized uncertainty of the plant-specific results. At the end of each of the insights subsections is an assessment of the applicability to other plants.

This page left blank

3. ACCIDENT PROGRESSION INSIGHTS

Section 3 presents the key insights from the SOARCA UAs. The accident progression insights reflect the uncertain parameter selections and their associated distributions. As described in Section 3.1, each UA had a specific focus and selected a small number of uncertain parameters judged to most impact the primary FOMs (i.e., the magnitude of the iodine and cesium release to the environment). The magnitude of the source term to the environment is impacted accident progression and its associated uncertainty. Section 3.2 discusses the key findings from the issues found to most impact the accident progression, which includes a summary of the insights with a focus on the source term insights, i.e., specifically the timing and the magnitude. The accident progression and source term issues are inherently related, so there are synergisms between their insights.

3.1. Uncertainty Parameter Selection and UA Focus

Although all three SOARCA UAs provided insights into accident progression and the source term, the scope of each project had different focuses that helped guide the uncertainty parameter selection and corresponding emphasis in the regression evaluations. Severe accidents include complex phenomena with many important aleatory and epistemic uncertainties that challenge their characterization and management. The approach in the UA was to limit, combine, and focus the number of uncertain parameters into a small set that focused on a few FOMs. The primary FOMs are the iodine and cesium release to the environment. Within the context of the primary FOM, each SOARCA UA had a specific focus that also helped with the selection of the uncertain parameters.

Table 3-1 summarizes the uncertainty parameters used in the three SOARCA UAs. The broad categories of uncertain parameters included the sequence definition (e.g., time in the fuel cycle, stochastic valve failure probability, pump and main steam isolation valve leakages), the in-vessel accident progression (e.g., fuel degradation parameters, oxidation kinetics), ex-vessel accident progression and containment response (e.g., the containment failure pressure, design leakage, hydrogen ignition criteria), and radionuclide behavior (e.g., chemical form of cesium and iodine, aerosol aerodynamic shape factor). A discussion of the emphasis in the three UAs is provided in the following paragraphs.

Most of the PWRs in the U.S. use a concrete reinforced containment and a U-tube steam generator (SG), which is the configuration for the Surry nuclear plant. The Surry SOARCA UA included a full set of uncertainty parameters appropriate for a PWR with the cited characteristics. However, due to the nature of a reinforced concrete containment, some specific focuses were parameters that could contribute to an early bypass of the containment via a consequential steam generator tube rupture and exploration of uncertain parameters promoting hydrogen burns that create an over-pressurization challenge. The Surry UA was the last study finished and reflects the most recent approach for some of the generic uncertain parameter selections and distributions. As shown in Table 3-1, it also has the largest list of uncertain parameters and the most complicated implementation of the radionuclide speciation and time in the fuel cycle. The study benefitted from two revisions with feedback from the ACRS between the two UA evaluations.

Most of the BWRs in the U.S. use a Mark I steel containment, which is the configuration of the Peach Bottom nuclear plant. The Peach Bottom plant also had a broad set of uncertain parameters but uniquely defined for a BWR. Similar to the Surry UA, the Peach Bottom UA included a focus on the parameters that promote an earlier failure of the containment via melting of the containment drywell steel liner by ex-vessel debris and leakage through the containment head seal. The Peach

Bottom UA was performed first and reflects the initial approach for some of the generic uncertain parameter selections and distributions. The Surry UA simulated a STSBO without any injection whereas the Peach Bottom UA used a LTSBO with 2 to 8 hours of injection. The LTSBO offered some new perspectives on a slower accident progression at a lower decay heat power (i.e., the reactor fission reaction shutdown occurs at the start of the station blackout).

Finally, the Sequoyah nuclear plant has an ice condenser containment design that is typical of 10 nuclear reactors at five sites in the U.S., which makes it the second most common PWR containment design in the U.S. Since Sequoyah is a PWR like Surry, the emphasis on the UA was shifted to primarily focus on the containment response. It included an emphasis on uncertain parameters that contribute an earlier failure of the containment. The Sequoyah UA was developed between the first and second revisions of the Surry UA and reflects a similar approach for some of the generic uncertain parameter selections and distributions. The Sequoyah UA also simulated a STSBO without any injection like the Surry UA. However, the Sequoyah UA scope did not include provisions for an evaluation of a consequential steam generator tube rupture and did not include many of the uncertain parameters related to the radionuclide source term used in the Surry UA. Instead, the Surry UA is used as for insights on consequential steam generator tube ruptures and PWR source term issues (i.e., particularly the in-vessel release) and the Sequoyah UA primarily addresses the ice condenser containment performance in a severe accident.

Each UA included some discovery and iteration to establish the list of uncertain parameters and their distributions. Some parameters were anticipated to be important but not realized as important in the initial Peach Bottom UA (i.e., the radial debris relocation time constants). Consequently, they were dropped from consideration in subsequent UA evaluations. Initial scoping studies allowed other uncertain parameters to be dropped (e.g., the PWR pressurizer safety valves [SVs] did not experience high temperatures for thermal failure mode evaluations). The consideration of the time in the fuel cycle was introduced after the Peach Bottom UA. The Surry UA source term had the highest level of sophistication and complication in the time of fuel cycle sampling and the cesium and iodine speciation sampling, which allowed new insights applicable for all reactor designs.

Table 3-1. Uncertain MELCOR parameters chosen for the SOARCA UAs

Peach Bottom – BWR with Mark I Containment	Sequoyah – PWR with Ice Condenser Containment	Surry – PWR with Large, Dry Sub-atmospheric Containment
Sequence Related Parameters		
• Safety relief valve stochastic failure to reclose • Battery duration	• Primary safety valve stochastic number of cycles until a failure to close • Primary safety valve open area fraction after failure • Secondary safety valve stochastic number of cycles until failure-to-close • Secondary safety valve open area fraction after failure	• Primary safety valve stochastic number of cycles until failure-to-close • Primary safety valve open area fraction after failure • Secondary safety valve stochastic number of cycles until failure-to-close • Secondary safety valve open area fraction after failure • Reactor coolant pump seal leakage • Normalized temperature of hottest steam generator tube • Steam generator non-dimensional flaw depth • Main steam isolation valve leakage
Time within the Fuel Cycle		
Not varied	Time in the cycle sampled at three points in the refueling cycle – near Beginning- (BOC), Middle- (MOC), and End-of-Cycle (EOC)	Time in the cycle was discretely sampled at 14 times from 0.5 days to 550 days
In-Vessel Accident Progression		
• Zircaloy melt breakout temperature • Molten clad drainage rate • SRV thermal seizure criterion • SRV open area fraction upon thermal seizure • Main steam line creep rupture area fraction • Fuel failure criterion • Radial debris relocation time constants	• Melting temperature of the eutectic formed from fuel and zirconium oxides • Oxidation kinetics model	• Zircaloy melt breakout temperature • Molten clad drainage rate • Melting temperature of the eutectic formed from fuel and zirconium oxides • Oxidation kinetics model

Table 3-1. Uncertain MELCOR parameters chosen for the SOARCA UAs

Peach Bottom – BWR with Mark I Containment	Sequoyah – PWR with Ice Condenser Containment	Surry – PWR with Large, Dry Sub-atmospheric Containment
Ex-Vessel Accident Progression and Containment Behavior		
• Debris lateral relocation – cavity spillover and spreading rate • Hydrogen ignition criteria • Railroad door open fraction • Drywell head flange leakage • Drywell liner failure flow area	• Lower flammability limit hydrogen ignition criterion for an ignition source in lower containment • Containment rupture pressure • Barrier seal open area • Barrier seal failure pressure • Ice chest door open fraction • Particle dynamic shape factor	• Hydrogen ignition criteria • Containment design leakage rate • Containment fragility curve • Containment convection heat transfer coefficient
Radionuclide Behavior		
• Chemical form of iodine • Chemical form of cesium • Particle density	• Particle dynamic shape factor	• Chemical form of iodine • Chemical form of cesium • Particle dynamic shape factor • Secondary side decontamination factor

3.2. Accident Progression Insights

The common elements from the accident progression insights from the three UA studies are organized in this section. The key insights are related to (a) the time in the fuel cycle (Section 3.2.1), (b) valve failures (Section 3.2.1), (c) consequential steam generator tube ruptures (C-SGTRs in Section 3.2.3), (d) hydrogen behavior (Section 3.2.4), (e) containment failure insights (Section 3.2.5), (f) primary seal leakage (Section 3.2.5), and (f) other source term insights not already covered in the proceeding sections (Section 3.2.6). Some sections have more information or applicability from one UA versus the other. However, each section also includes as discussion of the applicability of the UA findings to other plants.

3.2.1. Time in the Fuel Cycle

The time in fuel cycle parameter was included to understand the extent to which the fuel burnup influenced simulation results. This was accomplished by varying the point during the fuel burnup cycle at which the accident occurs. The time in the fuel cycle parameter directly affects the MELCOR accident progression through the magnitude of the decay heat power. It also affects the MELCOR and MACCS source term analysis through the mass and make-up of the fission product inventory. Although the inventories of shorter-lived isotopes increase with burnup only until secular equilibrium is established, the inventories of longer-lived isotopes grow throughout the cycle. For example, Cs-137 grows monotonically and can nearly double from the beginning to end of the fuel burnup cycle (see Figure 3-1). Because the longer-lived isotopes have an effect on latent cancer fatality risk, especially in the long-term phase, the time in the fuel cycle has high importance for consequence calculations (i.e., not discussed in this report).

The time in the fuel cycle was not addressed in the Peach Bottom UA. However, the Surry and Sequoyah UAs included the time in the cycle as an uncertain parameter that impacted the overall

decay heat power and the radionuclide inventory. The Sequoyah UA and the *draft* Surry UA used three representative times in the fuel cycle [2][3]. However, there is a significantly lower decay heat at beginning of the cycle (i.e., the BOC sample was specified close to the start of the fuel cycle) due to short recent irradiation time, which results in a lower inventory of the shorter-lived nuclides that dominate decay heat for a few hours after shutdown. Similarly, the radionuclide inventory at end of the cycle sample was near the maximum activity of the long-lived isotopes during the cycle, which will dominate the decay power for longer decay times. The inability to characterize the continuous variation from the start to the end of cycle with only three points was identified a weakness in the *draft* Surry and Sequoyah UAs. Consequently, the *final* Surry UA included fourteen evenly spaced samples [3].

The decay heat power samples from ORIGEN time of the cycle calculations supporting the Surry UA were integrated through four hours (see Figure 3-2). The integrated power during the first four hours (i.e., the core degradation phase of the STSBO accident) rapidly changes at the start of the cycle but subsequently stabilizes. The delineation between the startup phase of the cycle is approximately 100 days before the integrated decay heat is relatively constant. Consequently, the Surry UA provides more information on the transition from the start of the cycle to the more stable long-term decay heat power.

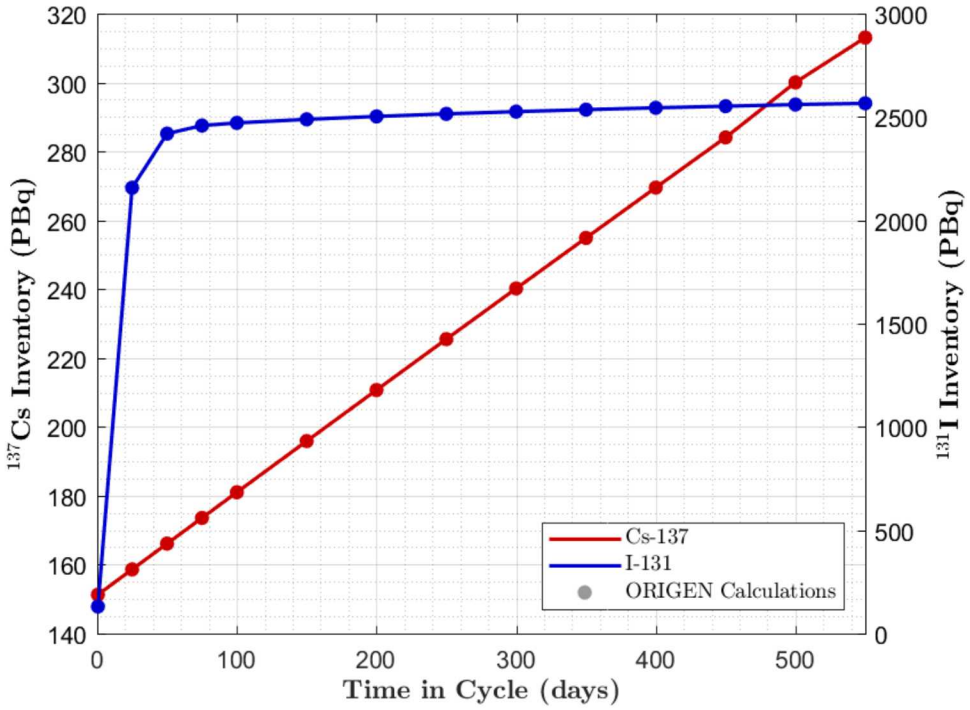

Figure 3-1. Activity levels for I-131 and Cs-137 with respect to time in the cycle

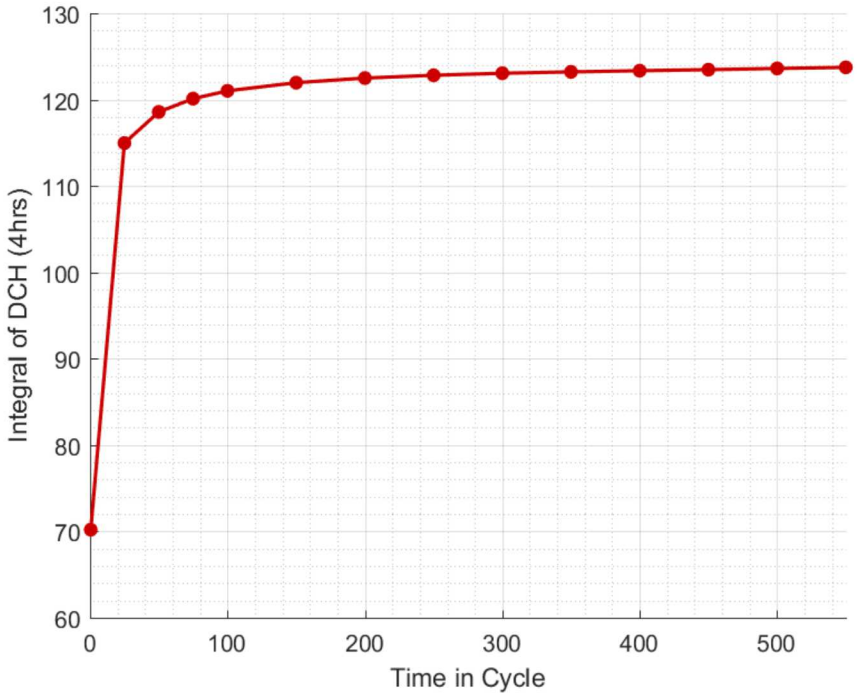

Figure 3-2. The 4-hr integrated decay heat for ORIGEN calculations used in the Surry UA

3.2.1.1. PWR UAs

The Surry and Sequoyah UAs showed that the time in the cycle influenced the timing of the events in the accident sequence. The following subsections highlight the key insights.

Insights from the Surry UA time in the cycle regressions

Regressions were performed in the Surry UA on the timing to a hot leg creep rupture failure and the reactor vessel lower head failure (LHF), which occurred in all completed realizations.[1] The time in the fuel cycle (i.e., the ORIGENDay uncertainty parameter) was identified as the most important parameter in both regressions. Figure 3-3 and Figure 3-4 show the hot leg and LHF timings as a function of the fourteen sampled times in the cycle. Both figures show a very large impact on the event timings for the first time in the cycle sample versus the other times in the cycle (i.e., the events occur much later due to the very low decay heat power). Similar to the trend for the integrated decay heat power Figure 3-2, the subsequent times in the cycle show a smaller impact on the timings, which occurred more quickly as the cycle continued. In both the hot leg failure and LHF regressions, the time in the cycle was the most important parameter affecting the timing (e.g., contributing over 30% to the variation in the timing to these two events and 17% of the conjoint influence[2]).

[1] There was one outlying realization that did not have a hot leg failure, which is discussed in the Surry UA report [3].

[2] The conjoint influence concerns two or more input parameters acting together. The conjoint influence may have synergistic effects that would not be uncovered by studying the influence of each parameter individually.

The realizations with the earliest time in the cycle (0.5 days) exhibited significantly different behavior than the other realizations. The containment did not significantly pressurize and there was no containment over-pressure failure prior to 72 hr (see Figure 3-6), which was different than all other realizations. Consequently, the accident progression at the start of the fuel cycle is not characteristic of the bulk of the fuel cycle.

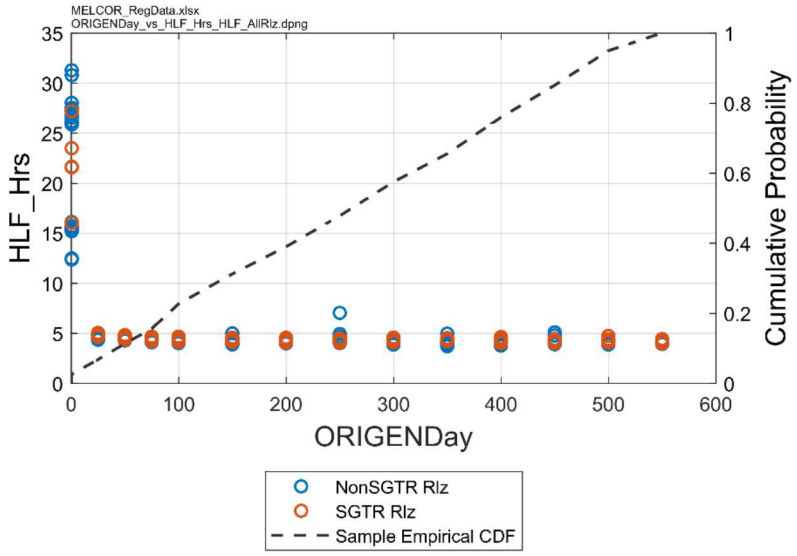

Figure 3-3. The reactor hot leg failure timing as a function of the time in the cycle

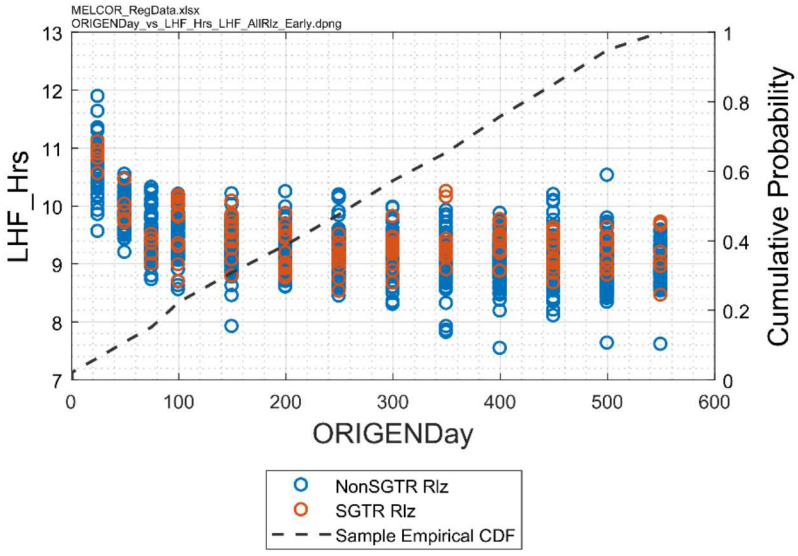

Figure 3-4. The reactor vessel lower head timing as a function of the time in the cycle (only realizations without a steam generator tube rupture)

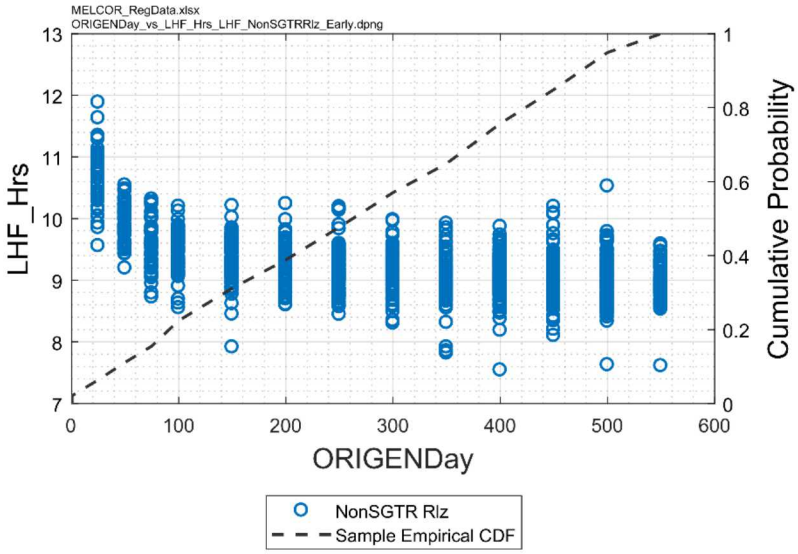

Figure 3-5. The containment failure timing as a function of the time in the cycle

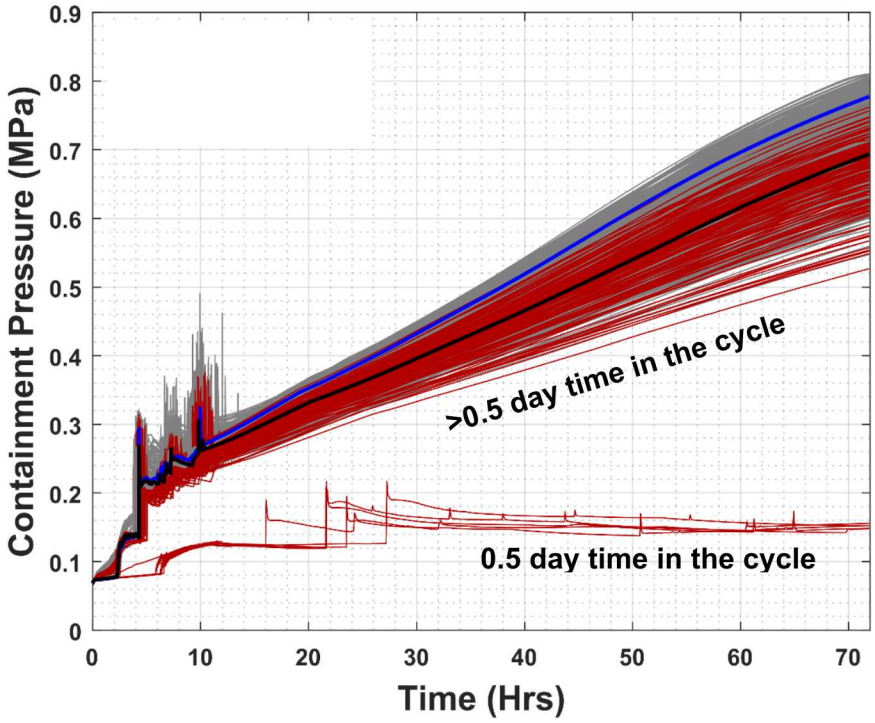

Figure 3-6. Containment pressure responses showing 0.5 day time in the cycle realizations versus the >0.5 day time in the cycle realizations

Insights from the Sequoyah UA time in the cycle results

The Sequoyah UA only sampled three times in the cycle, (i.e., beginning of cycle – BOC, middle of cycle – MOC, and end of cycle – EOC). Figure 3-7 shows the selected time in the cycle parameter. Three points in the cycle are taken as 'representative' times to constrain the problem. Using only three times in the cycle was criticized as too coarse in the Sequoyah UA, which led to the finer discretization in the Surry UA. Figure 3-8 shows the Sequoyah decay heat curves as a function of decay time for variable operating time (in days) into the last day in cycle. The BOC sample (6.25 days) has significantly less decay versus the MOC sample at 200 days. Similar to the Surry UA, the decay heat power does not change significantly from the MOC to the EOC value at 529 days.

The Sequoyah BOC sample time (i.e., 6.25 days) laid between the first two samples in the Surry UA (i.e., 0.5 and 25 days). The Surry UA showed no significant pressurization at 0.5 days but a containment pressurization to high containment pressure by 72 hr for a time in the cycle of 25 days and greater (i.e., Figure 3-7 only shows the 0.5 day decay heat cases not pressurizing the containment). The Sequoyah BOC samples showed an observable containment pressurization but significantly less than the MOC and EOC results (see Figure 3-8). Consequently, the Surry 0.5 day and the Sequoyah BOC results suggest the containment pressure responses are transitioning from almost no pressurization at 0.5 days to an observable pressurization at 6.25 days. By 25 days into the cycle, the Surry UA is showing a pressurization to containment failure prior to 72 hr. There are many plant specific factors affecting the two containment responses, but these results provide qualitative insights into the duration of the early burn-up phase.

The lower containment pressurization rate for BOC prevented long-term containment rupture before 72 hr.[3] The BOC realizations would have eventually ruptured the containment if the simulations were extended well beyond 72 hr. Some MOC and EOC realizations also did not reach containment failure within 72 hr, which was primarily due to high sampled rupture pressures. In the 600 Sequoyah UA calculations, 567 realizations completed to 72 hr. The end-states of the containment included:

- 4 containment failures following the sudden pressurization of the first hydrogen burn,
- 492 realizations that failed the containment between 36 hr and 72 hr after a gradual monotonic progression in pressure to rupture,
- 71 realizations did not fail containment by 72 hr, and
- None of the BOC realizations failed the containment prior to 72 hr.[4]

[3] Sequoyah has a free-standing steel containment consisting of a cylinder topped by a hemispherical dome. The containment failure studies indicate that the containment would rupture due to an over-pressurization near the large access penetration. Unlike the concrete-reinforced Surry containment, the tear would quickly depressurize the containment. A concrete-reinforced containment yields with increased leakage through the cracks in the concrete and tears in the internal steel liner.

[4] An early containment failure at BOC is judged possible but not encountered in the UA of 69 BOC realizations.

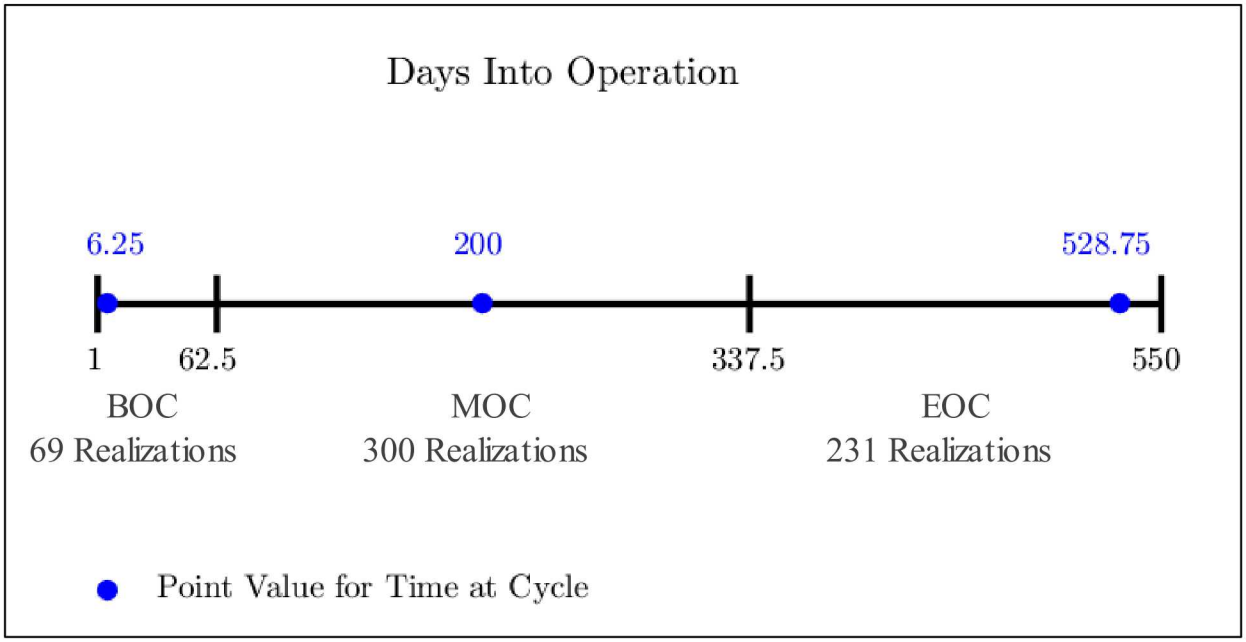

Figure 3-7. The Sequoyah UA specifics for the time in the cycle uncertainty sampling

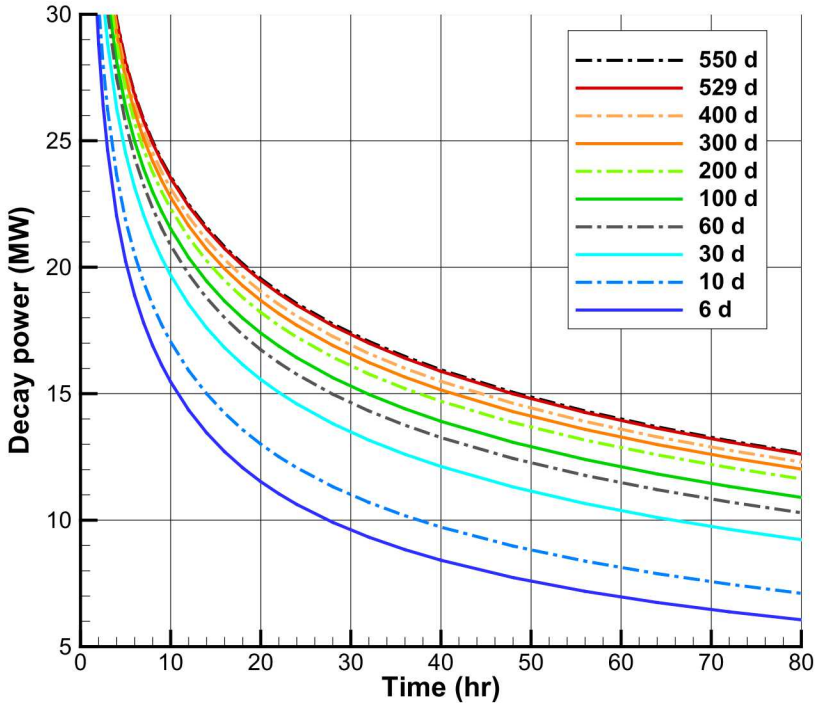

Figure 3-8. Variations in the Sequoyah decay heat power as a function of the time in the cycle

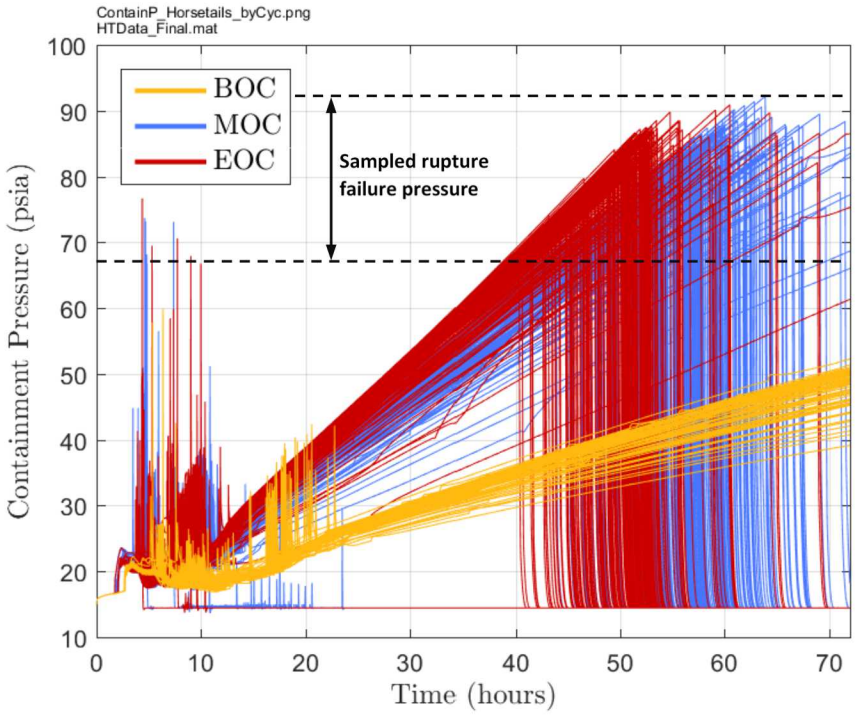

Figure 3-9. Sequoyah UA containment pressure response colored by the time in the cycle

In-vessel hydrogen generation regressions from the Surry UA

The time in the cycle was identified as the most important parameter for in-vessel hydrogen production in the Surry UA. Figure 3-10 shows the in-vessel hydrogen generations as a function of the time in the cycle. There is a trend for decreased hydrogen production as a function of the time in the cycle. The hydrogen production at 0.5 day time is significantly higher as emphasized in Figure 3-11. The low decay heat power led to a slower progression of the accident and a protracted hydrogen generation phase before significant core degradation. In contrast, the higher decay heat at later times in the cycle promoted a faster heatup through the fuel collapse with less complete oxidation. The impact is observable for a time in the cycle >25 days but smaller than the significant variation from 0.5 days to 25 days. The highest in-vessel hydrogen production was 777 kg, which occurred at 0.5 days into the fuel cycle and was over twice as large as the 310 kg median and 318 kg mean values.

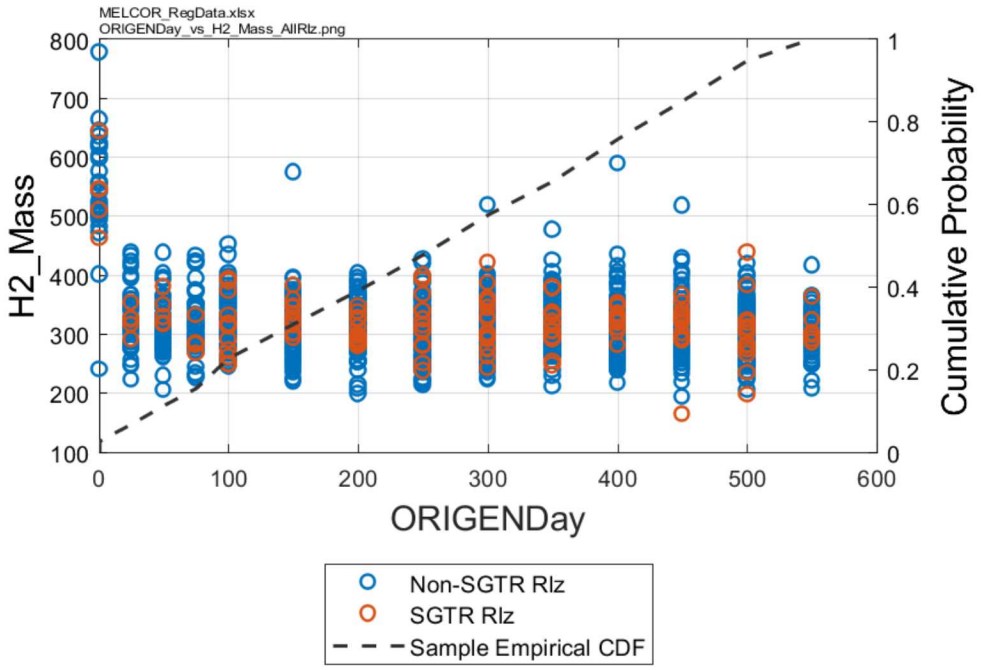

Figure 3-10. Scatterplot of in-vessel hydrogen production versus time in the cycle

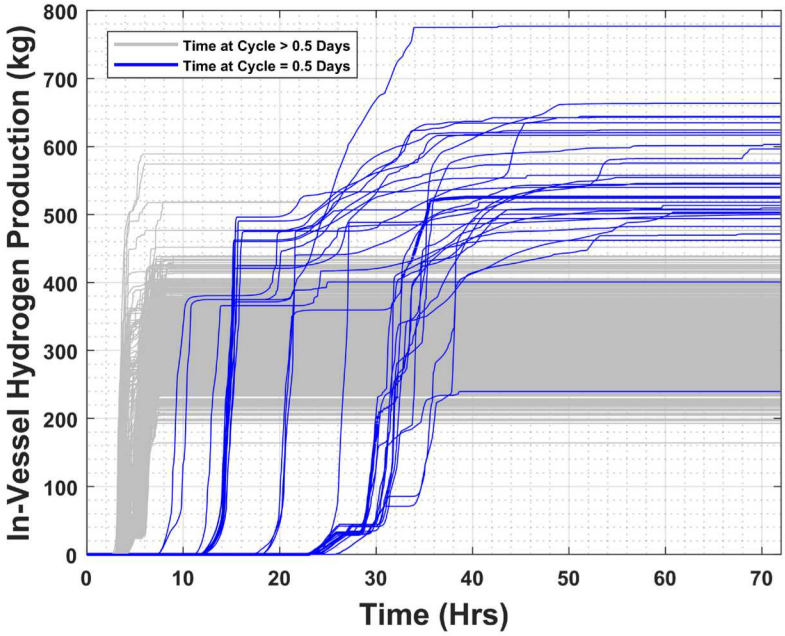

Figure 3-11. In-vessel hydrogen production with emphasis on the 0.5 day time in the cycle results

Source term insights versus the cycle results

The Surry and Sequoyah UAs also identified the time in the cycle as important parameters for source term to the environment. In the Surry UA, the time in the cycle was the second most important parameter in the realizations without a C-SGTR behind the fraction of iodine gas in the gap for the total iodine release to the environment. Although the iodine reached secular equilibrium after

~50 days at cycle, the higher decay heat impacted the iodine release by accelerating the containment failure and increasing revaporization. Figure 3-12 shows an increasing iodine mass release as a function of the time in the cycle.

The time in the cycle was also the second most important regression parameter for the cesium release to the environment behind the magnitude of the design leakage. Somewhat surprising, the time in the cycle importance for cesium was lower than for iodine. As shown in Figure 3-13, the trend is also less clear. The inventory of cesium nearly doubled from the start of the cycle to the end of the cycle, which is not evident in the trend of released *mass* versus time in the cycle. The difference in the iodine and cesium response is largely attributed to transport physics. The cesium release is less susceptible to revaporization due to the low vapor pressure of its dominant chemical form (i.e., cesium molybdate).[5] The cesium aerosols settle after their release to the containment, which largely occurs prior to the containment failure. Consequently, the cesium release to the environment is highly sensitive to the preexisting design leakage rate (i.e., the most important sampled variable). In contrast, the important iodine uncertain parameters include the amount of iodine gas and revaporized iodine gas that is less sensitive to the amount of the design leakage (i.e., the iodine gases will continue to be released well after the cesium aerosols have settled).

The time in the cycle is the most important parameter for the iodine release and the second most important parameter for the cesium release to the environment in the Sequoyah UA. The discretization of the Sequoyah UA results is more limited and biased due to only three time in the cycle samples and no containment failure with BOC sample, respectively. However, the Sequoyah UA MOC and EOC realizations showed the same trends observed in the Surry UA, see Figure 3-14 and Figure 3-15.[6]

[5] The less dominant form of cesium (i.e., cesium hydroxide) can chemisorb onto stainless steel and be retained in-vessel. The only significant example of the chemisorption behavior occurred in the Peach Bottom UA calculations with a delayed MSL failure [1]. Unlike a PWR, the hot gases with radionuclides exiting the core in a BWR flow directly into the stainless steel steam separators and dryers. The high surface areas of these stainless steel internals and the high temperature and pressure conditions in the Peach Bottom MSL failure accident progression contributed to higher levels of cesium chemisorption.

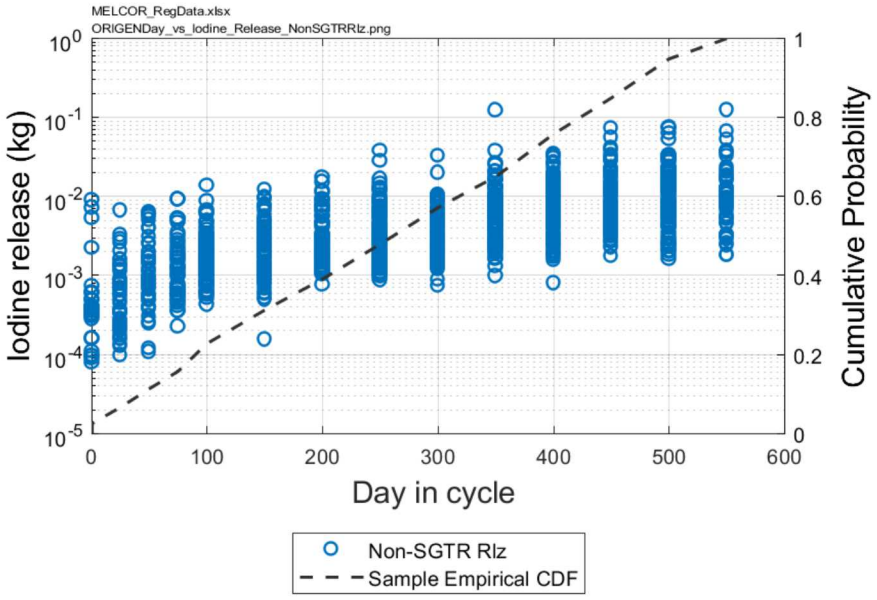

Figure 3-12. Scatterplot of iodine release mass versus the time in the cycle in the Surry UA

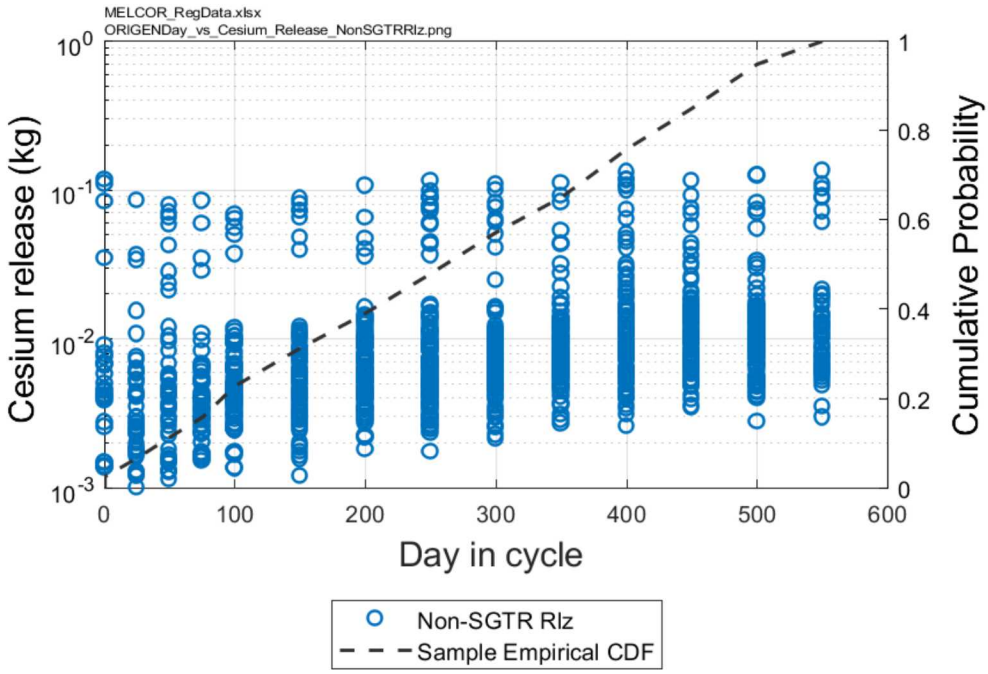

Figure 3-13. Scatterplot of cesium release mass versus the time in the cycle in the Surry UA

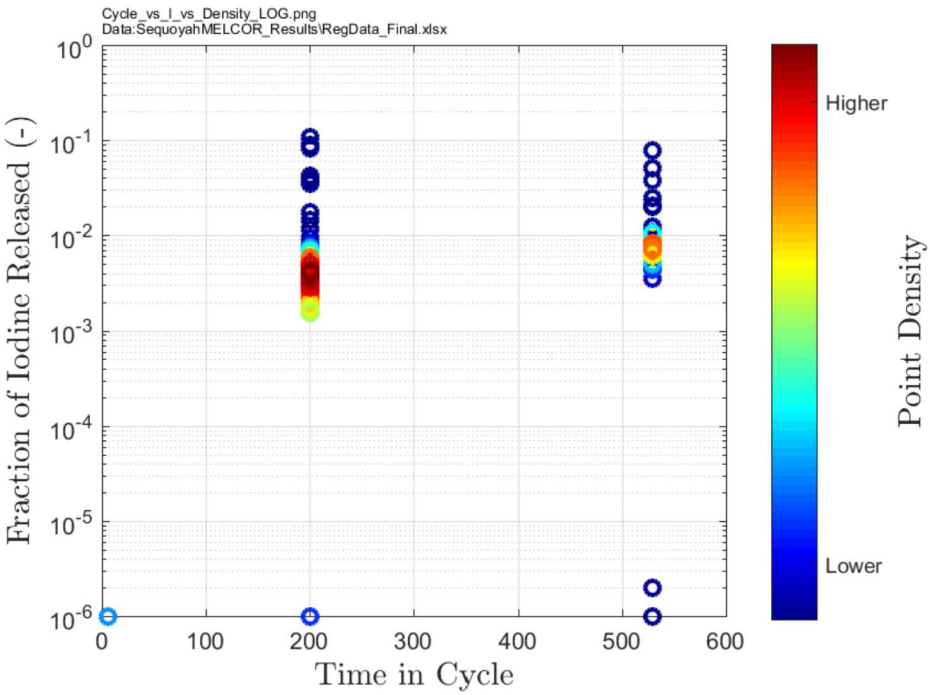

Figure 3-14. Scatterplot of iodine fraction released versus the time in the cycle in the Sequoyah UA[6]

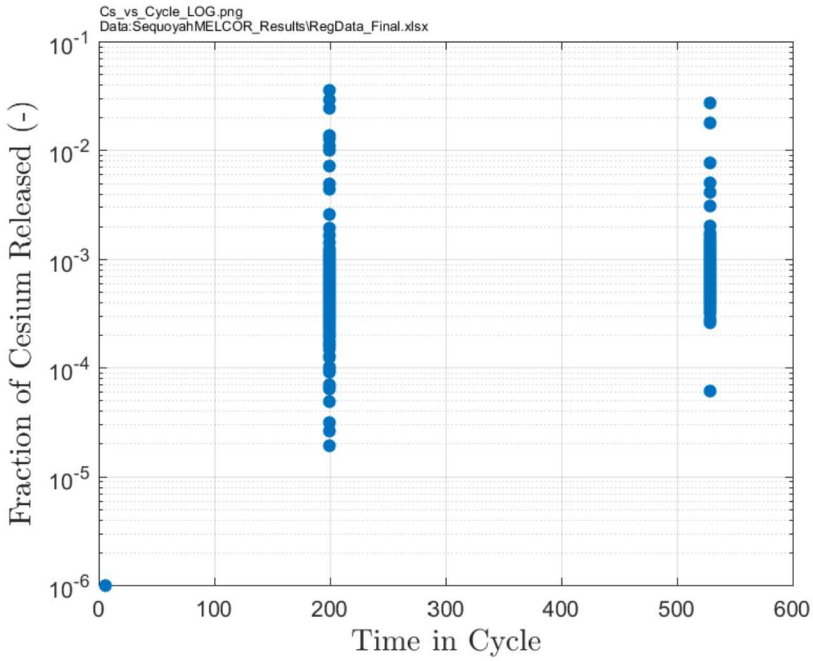

Figure 3-15. Scatterplot of cesium release fraction versus the time in the cycle in the Sequoyah UA[6]

[6] The Sequoyah reported the iodine and cesium released to the environment as a fraction of the initial inventory and therefore does not include the variation of the mass over the cycle.

3.2.1.2. Implications for Other Plants

The Surry and Sequoyah UA included variability of the accident time during the fuel cycle, which was not explored in the Peach Bottom UA. The uncertainty revealed large variations in the radionuclide inventories and decay heats from BOC to EOC. Relative to the timing of the accident progression, the earliest sampled times-in-cycle had significantly different behavior until the inventories of shorter-lived isotopes increase reached a secular equilibrium. An interpretation using the Surry and Sequoyah results suggest this occurs after 25 days. The accident progression near the full power start-up after refueling (i.e., the Surry UA sampled at 0.5 days) showed particularly slow developing behavior that did not progress to a containment over-pressure failure. This behavior is expected to be generally consistent throughout other PWR and BWRs.

The integrated decay heat power rises rapidly through 100 days at cycle but slowly thereafter. The regressions of the key accident event timings show a correlation of the time in the cycle to accelerating the accident progression including hot leg failure, reactor vessel lower head failure, and containment failure. The correlation of these items to a BWR would be the timing to a thermal failure of the SRV, reactor LHF, and containment failure.[7] The insights on the accident progression timing as a function of the time in the cycle are qualitatively applicable to all plants.

The time in the cycle was identified as the most important parameter for in-vessel hydrogen production in the Surry UA. The in-vessel hydrogen production is very important for early challenges to the containment integrity. The higher quantity of hydrogen at earlier times in the cycle with lower decay heat is expected to be applicable to all plants. As the cycle progresses, the increasing decay heat power with more time in the cycle accelerates the accident progression through the fuel collapse, which limits the in-vessel hydrogen production. The same trend will be applicable to other plants. For example, the time-in-cycle was the second most important parameter for the amount of hydrogen vented to the containment before hot leg failure as shown in the Sequoyah UA focused SRV study (i.e., see Section 3.2.5.3). The amount of hydrogen vented to the containment is directly related to the higher amount of in-vessel hydrogen production. Although the Peach Bottom UA did not vary the time in cycle, the trends observed in the PWR UAs are expected to show a high importance in BWRs too (i.e., the quantities of the in-vessel hydrogen production and fuel collapse timing versus decay heat levels have similarities).

The time in the cycle also had an important impact on the source term. The variations of the iodine and cesium radionuclides shown in Figure 3-1 illustrate important differences of the inventories where short-lived isotopes (e.g., ^{131}I) reach a secular equilibrium while longer-lived isotopes grow throughout the cycle. However, somewhat surprisingly, the time in the cycle was more important to the iodine release to the environment in both the Surry and Sequoyah UA than for the cesium release to the environment. The differences were attributed to an increased mobility (i.e., revaporization) and release of the iodine as a function of the decay heat. The qualitative implications for other plants are expected to be the same but quantitatively impacted by plant-specific containment leakage and failure attributes.

[7] The mode of containment failure in the Peach Bottom UA was a liner melt-through, which followed the reactor lower head failure. Consequently, the containment failure timing is related to the decay heat power that leads to the vessel lower head failure whereas the ex-vessel debris spreading and liner failure includes other physics in addition to the decay heat power (e.g., quenching, heat transfer, and chemical reactions).

3.2.2. Valve Failures

Following the loss of power in a station blackout (SBO) scenario without DC power, passive spring-operated safety valves (SVs) open to prevent over-pressurization.[8] This includes PWR pressurizer SVs, the PWR secondary system SVs, and BWR safety relief valves (SRVs). Valve failures have occurred during operations that are recorded in the utility's LERs to the NRC and in NUREG/CR-7037 [14]. The failure modeling of the safety valves was observed to be very important in the accident progression of all three UAs. In the Peach Bottom UA, the effect was notable on determining whether a main steam line (MSL) creep rupture occurs, which bypasses the benefits of wetwell scrubbing. In the Sequoyah UA, the effect was notable on in-vessel hydrogen release to the containment and its potential for causing an early containment failure. In the Surry UA, the effect was notable on whether a C-SGTR containment bypass event occurs.

Section 3.2.2.1 describes the methodology used for the PWR fail to close (FTC) modeling. The PWR UAs were performed after the Peach Bottom BWR UA and included new updates to the modeling. The plant-specific UA insights from the UAs are in discussed in Sections 3.2.2.2 through 3.2.2.3. An assessment of the applicability of the modeling and conclusions to other plants in Section 3.2.2.4.

3.2.2.1. SV FTC Modeling Insights

The following discussion describes the insights and approach to model PWR SV failures. While safety valve behavior was important in all three SOARCA UAs, there is sparse data and a lack of established expert consensus on how best to model the valve failure rates under severe accident conditions. There is some operational data on safety valve failure-to-close during non-severe accident conditions (i.e., main steam safety valves following scram events). However, the data is not under the exact conditions that the safety valves would experience in the SBO scenarios. Safety valve performance is clearly important in an SBO, yet the basis for a more confident modeling of the uncertainties in safety valve behavior is currently lacking. The SOARCA UA analyses attempt to address the lack of applicable data (with respect to both failure rates and failure mechanisms) on SV failure-to-close in a reasonable way that has been positively reviewed by experts outside the team [13].

Insights on PWR SV failure

The stochastic valve failure area was updated following an ACRS review after the *draft* Sequoyah UA was completed. The *draft* version of the Sequoyah UA used different assumptions for primary SV failure attributes [29]. The ACRS questioned an equal likelihood of failure from 1% to 100% open and recommended discussions with valve experts. Sandia contacted nuclear valve testing personnel and examined LERs with reported SV failures. The following conclusions and changes were made to the PWR SV modeling (i.e., applied to the final Surry and Sequoyah UAs).

- An SV FTC is most likely on the initial demand.
- If an SV functioned per design on the initial demand, then it would most likely function on all subsequent demands.
- SVs that fail to close are most likely to fail in either a weeping (i.e., mostly closed) or a mostly open position.

[8] The power-operated operation of the relief valves was not credited in the UAs.

- The probability per demand of a valve to fail to open (FTO) is sufficiently small compared to the FTC such that FTO may be neglected.
- A valve is more likely to fail if cold water flows through the valve than if saturated water flows through the valve.
- Applying MSL SV operational data to pressurizer SVs is acceptable due to the lack of pressurizer SV operational data.[9]

Based on these insights, the SV FTC failure was modified to emphasize mostly closed and mostly open failure area distributions. There was also no more consideration of FTO and failure due to flowing water.[10]

Technical rational for the PWR SV FTC distribution

The uncertainty characterization of stochastic SV failure was informed by NUREG/CR-7037 [14]. NUREG/CR-7037 (Table 20) reports on SV operation subsequent to actual scram events. Information is included for both the main steam system (MSS) SVs on the secondary side of the steam generators and the reactor coolant system (RCS) SVs on the pressurizer. The UAs assumed that the MSS data was most representative of valve failure during severe accident scenarios. NUREG/CR-7037 notes that the MSS and the pressurizer SVs are similar. Inquiries to SV testers revealed that these valves are similar but not identical in that there are some physical and maintenance differences. While there are differences between the MSS and pressurizer SVs, they are similar enough that in weighing the difference between the valves against the lack of operational data on the pressurizer SVs, it was judged a more defensible basis to rely on the MSS operational data for the pressurizer SVs too.

Only valve responses to actual scram events were considered. The data from valve testing reported in NUREG/CR-7037 was not considered. NUREG/CR-7037 (Table 22) reports on failure rates in SV testing but the rates differ markedly from the rates evidenced by actual plant events, suggesting that aspects of the testing were inconsistent with actual conditions experienced by an installed valve. To better understand the differences, Sandia made inquiries on valve testing and testing requirements. The testing is only required to demonstrate whether the valves will unseat at design pressures to relieve pressure during an overpressure event. The testing does not fully stroke an SV at pressure like an actual demand would. In fact, no testing facility in the U.S. has the flow capacity to fully stroke an SV. As such, the testing data was not considered applicable for the purpose of this UA.

The data from actual scram events typically includes a single SV cycle, so there may be some limitation in extrapolating to repeated valve cycles during a severe accident. Although the amount occurrences were limited, the actual plant events were judged as the best data source. There is sufficient resolution in the data to separate it into two groups. The first group consists of all of the initial demands and the number of valve failures on initial demand. There were no valves that failed after the initial demand, so the second group consists of the number of cases in which a subsequent demand occurred. This separation of the data suggests two separate failure probability distributions:

---

[9] NUREG/CR-7037 noted that although main steam system and reactor coolant system SVs are similar, the SV testers noted that the pressurizer and main steam SVs had characteristic physical and maintenance differences.

[10] The SV failure following water flow was essentially eliminated after the Energy Power Research Institute (EPRI) analyzed the events and issued recommendations to prevent standing, cold water upstream of the SVs [15].

one for the probability of failure on the initial demand, and another for the probability of failure on subsequent demands.

Description of the PWR SV FTC distribution

A beta-binomial distribution was used to model cycles until an FTC event. The sampling from this model was extended to include uncertainty in cycles-to-failure. For the FTC on the initial demand, the model consists of a beta distribution on the probability of an FTC event on initial demand and a binomial distribution on the cycles-to-failure. Similarly, for FTC on subsequent demand, the model consists of a beta distribution on the probability of an FTC event on subsequent demand and a negative binomial distribution on the subsequent cycles-to-failure. Hence, both for failure on the initial demand and failure on the subsequent demand, the beta-binomial model facilitates two stage sampling that incorporates both uncertainty in the probability of valve failure-to-close-on-demand, and in the cycles-to-failure experienced by a valve given that probability of failure. The beta distributions used the data from NUREG/CR-7047 to refine a Jeffreys uninformed beta distribution, which is commonly used as a prior distribution in Bayesian analysis with limited data [15].

Description of the BWR SRV FTC distribution

The BWR SRV construction is different from PWR SVs and monitored separately from the PWR SVs in NUREG/CR-7037 [13]. The operating mode of interest during an SBO is the "pressure mode," where the SRVs are actuated via a pilot sensing port that is internal to the valve (not the air actuator). However, the failure rate reflected in NUREG/CR-7037 is conceptually different from the situation modeled in a LTSBO. The historical failure events occurred after only a few valve cycles, although the precise number is difficult to determine from the available information in the LER (i.e., not reported). The failure rate after numerous cycles is non-existent because events involving numerous valve cycles are not observed. It was concluded that other unknown failure mechanisms would likely overwhelm those that lay behind the nominal failure rate. The FTC beta distribution for the Peach Bottom UA was ultimately developed from consideration from these uncertainties. The beta distribution from the utility covers the range of values that are needed to define the parametric relationship between the probability that the SRV will fail to close in a severe accident [16].

Summary of FTC Findings

In summary, the historical PWR SV FTC data suggested a lower likelihood of a valve failure after the first cycle, which was incorporated into the PWR UAs. The PWR FTC area is biased to weeping (i.e., mainly closed) and mainly open failure areas, which is also judged applicable to BWR SRVs. However, the Peach Bottom UA data did not include the complication of first and subsequent FTC distributions or the biases on failure areas. However, the Peach Bottom UA incorporated uncertainty from other unknown mechanisms involving numerous, continuous valve cycling.

Consequently, the SV or SRV FTC frequency conceptually consists of separate failure rates for the first valve demand, a short-term number of cycles, and long-term cycling. However, the historical data is very sparse to accurately quantify these parameters. Furthermore, the test data was judged inappropriate due to the lack of a prototypical full valve cycle and discrepancy with the historical rate of occurrences. Consequently, the valve FTC remains as having significant uncertainty and high importance (i.e., see Sections 3.2.2.2 and 3.2.2.3), which warrants its inclusion in characterizing the range of possible severe accident progressions.

The BWR SRVs also experience high thermal stresses during core degradation. The thermal failure of a BWR SRV was included in the Peach Bottom UA and further discussed in Section 3.2.2.3.

3.2.2.2. PWR UAs

The Surry and Sequoyah UAs included stochastic SV FTC on the MSS and pressurizer SVs. The two studies used the same FTC distributions and associated failure areas. Each valve had randomly selected failure cycles and failure areas. The two UAs illustrated different insights and have different ramifications based on the containment design. Unlike the BWRs, neither PWR UA showed any significant potential for a thermal failure of SVs. Consequently, the valve failures were limited to stochastic failures.

The Surry UA showed some key impacts from SV failures: (a) increased mechanic stress for a C-SGTR, (b) reduced stress for a hot leg failure, and (c) an increased radionuclide inventory discharged to the pressurizer relief tank (PRT), which may subsequently revaporize. However, the most likely outcome was normally operating MSS and pressurizer SVs. The MSS and pressurizer FTC parameters have the greatest impact on the potential for C-SGTRs if an MSS SV FTC occurs prior to core damage, and the associated heatup of the steam generator tube and a pressurizer SV FTC does not occur (i.e., maximum differential pressure across the tubes).

MSS valve failure influence on C-SGTRs

The MSS SVs only cycled until the water inventory in the SGs was vented away. The SGs subsequently depressurized due to MSL leakage, which stopped further cycling. The maximum number of MSS SV cycles was <130 cycles. Consequently, only sampled FTC failures within this range could possibly fail. The Surry UA MSS SV FTC results are shown in Table 3-2. For the 1,147 realizations included in the UA statistics, an MSS SV FTC occurred about 10% of the time on each SG. The regressions showed decreased strain of the SG tubes as a function of the number of MSS SV cycles. However, due to MSL leakage that also depressurized the SG, the MSS FTC cycle parameter only accounted for less than 1% of the strain evaluation (i.e., the creep rupture index). For example, the sampled parameter for the MSL sampled leakage accounted for more than 12% of the unflawed SG tube strain evaluation.[11]

[11] The best regressions for the MSS and RCS FTC parameters assessed the strain on an unflawed tube. The regressions for tubes with flaws were overwhelmed by the flaw depth. The unflawed regression was only performed for the hottest region of the thermal plume entering the steam generator, which was overwhelmed by an uncertainty parameter on the plume temperature. The MSL leakage, the MSS and RCS FTC parameters, and the pump seal leakage are the next most important influencing parameters.

Table 3-2. MSS SV FTC statistics

	MSL A	MSL B	MSL C
FTC occurrences	116	127	130
Mean cycles to FTC	26	26	23
Median cycles to FTC	24.5	19	15
Min cycles to FTC	1	1	1
Max cycles to FTC	102	93	92
Mean FTC open fraction	0.325	0.380	0.398
Median FTC open fraction	0.087	0.181	0.176
Mean time of FTC (hr)	0.617	0.644	0.490
Median time of FTC (hr)	0.563	0.537	0.309
Earliest FTC time (hr)	0.042	0.043	0.040
Latest FTC time (hr)	1.827	4.350	1.507

Impact of the leakage from the MSIV

While not a valve failure, the leakage past the PWR main steam isolation valves (MSIVs) or other isolating systems on the MSS can increase the mechanical stress across the SG tubes and contribute to a C-SGTR. PWRs do not have regulatory requirements to maintain MSIV leakage below a technical specification. However, the BWRs do have technical specifications and are often challenged to meet their technical specification limits. MSIV leakage and an MSS FTC are two mechanisms that can depressurize the SG. The resulting larger pressure difference between the primary and the secondary system increases the stress across the steam generator tubes and increases the likelihood of their failure. Furthermore, a C-SGTR along with the MSIV leakage, provides a release path for radionuclides to bypass containment and reach the environment.

To inform the uncertainty range for MSIV leakage, it was desirable to have the technical specification for a PWR. An in-depth search was conducted, both in-house and at NRC. This including checking the FSAR and plant data book for Surry, a search of licensee testing reports, and a discussion with a former PWR operator who is now with NRC. Although the PWR MSIV performance is controlled by technical specifications for closure timing, there is no requirement for leak-tightness. No direct information was obtained for measured leakage of PWR MSIVs.

The guidance for the PWR leakage was obtained from several sources, including technical specifications for BWR MSIV leakage, BWR Licensing Event Reports (LERs) concerning MSIVs, and PWR LERs concerning MSIVs [3]. Parametric MELCOR calculations were also performed to examine the secondary depressurization rate for a range of leak sizes. The hot leg failure of the reactor coolant system occurs at ~4 hr in the Surry STSBO without any SV FTC. Consequently, the secondary pressure at 4 hr has the most significance in the competition between a hot leg failure and a steam generator tube failure. After the hot leg failure, the primary system depressurizes and there is no more threat of a tube rupture. Figure 3-16 shows that leakages less than 0.025 in^2 do not show any significant depressurization within 4 hr whereas a leak of 0.2 in^2 or greater depressurizes the secondary below 1 MPa by 4 hr. To put the BWR technical specification into perspective, 0.1 in^2 and 0.5 in^2 leakages correspond to approximately 4600 and 23,000 scfh, respectively, which is very large compared to the BWR technical specification of 11.5 scfh. However, the value required by BWR technical specifications is offset by the lack of required testing for PWRs and the large number of

PWR LERs with MSIV issues.[12] The Surry UA sampled variable MSIV leakage from 0.01 in^2 to 1 in^2 using a uniform distribution.

In summary, a key insight is that MSIV leakage can be as effective as MSS SV FTC. In the regressions on the creep magnitude for an ideal tube in the peak temperature region, the MSIV leakage was the second most important parameter behind the peak temperature of the plume entering the SG. Although not evaluated, the most important parameter effecting the magnitude of the creep accumulation in hot upflow and cold regions of the SG is expected to be the magnitude of the MSIV leakage (i.e., the peak hot plume temperature parameter is not used in these bulk regions).

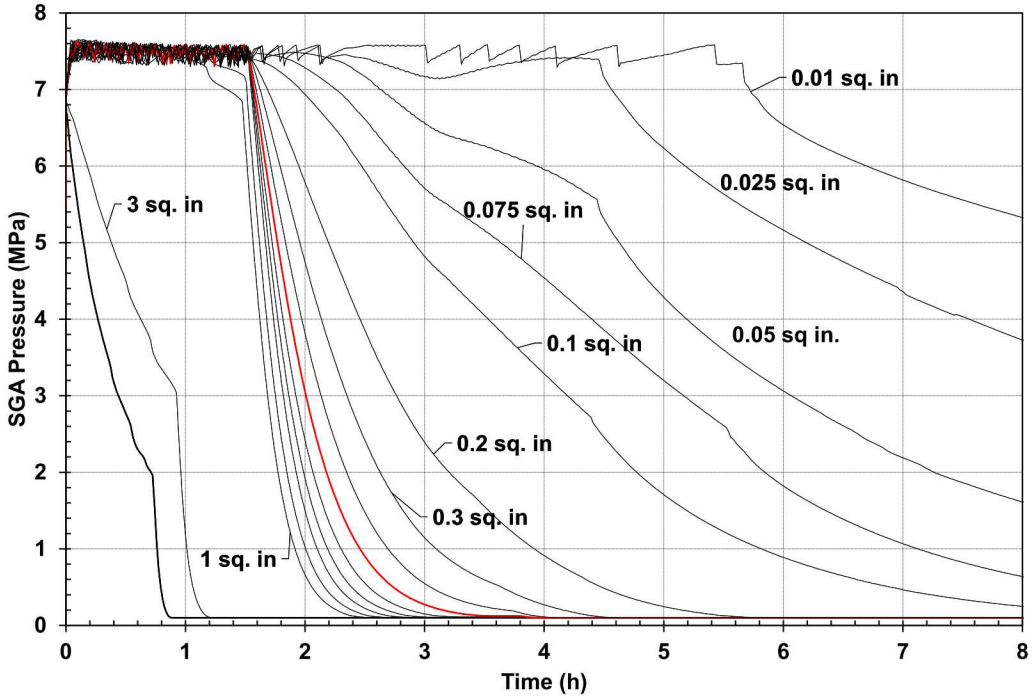

Figure 3-16. Steam generator pressure as a function of MSIV leakage size

Pressurizer valve failure influence on C-SGTRs

Similarly, the pressurizer SVs only cycled until a hot leg failure, which occurred after the primary system was vented away. The maximum number of pressurizer SV cycles was generally bounded due to the consequences of the inventory loss out of the vessel (i.e., typically <70 cycles[13]). Consequently, only sampled FTC failures within this range could fail. The Surry UA pressurizer SV FTC results are shown in Table 3-3. For the 1,147 realizations included in the UA statistics, a

[12] The size, design, and function of the PWR MSIV is judged similar to the BWR MSIV.

[13] The maximum number of SV cycles was dependent on the time in cycle and the magnitude of the pump seal leakage. It was typically <70 cycles. The SVs open to release steam, and then later hydrogen, out of the primary system. At approximately 70 cycles, the core has transitioned to a high-temperature, degrading state. The high temperature gases exiting the core caused to a hot leg failure under these conditions, which depressurized the primary system and prevented any further SV cycling. The cycle count was slightly higher for the earliest BOC realizations due to the very low decay heat power and slower core degradation (e.g., the Sequoyah BOC realizations).

pressurizer SV FTC occurred 120 times or about 10%. In 10 realizations, there were 2 SVs that failed to close. The regressions showed increased strain of the SG tubes as a function of the number of pressurizer SV cycles. However, the pressurizer SV FTC cycle did not appear as a significant contributor to the strain evaluation for the creep rupture index.[11] Figure 3-17 shows that most of the tube ruptures occurred when there were 50 or more pressurizer SV cycles. Furthermore, the failed SV leakage area was always less than ~10% of the SV flow area. These two factors contributed to keep the primary system pressure high to increase stress across the SG tubes.

Large pressurizer valve failure areas delaying or preventing an RCS hot leg failure

There was only one realization without a creep rupture failure of the hot leg during core degradation. The realization had an FTC that occurred at an optimum time with a large failure area. The optimum time occurred near the start of the core degradation that led to accumulator water injection while the system depressurized. The core degradation transitioned into a collapse onto the lower head and its subsequent failure. An earlier SV FTC did not promote a protracted accumulator injection during the critical core damage phase. All other combinations of SV FTC and valve failure area resulted in sufficient thermal-mechanical stress to fail the hot leg.

Small pressurizer valve failure areas accelerating hot leg failure

The earliest rupture of a hot leg nozzle in the UA occurred with a pressurizer FTC of the lowest set point pressurizer SV on the 1st cycle but with the valve leaving a small 0.096 fraction open. While these aspects served to reduce RCS pressure and hence the stress on the hot leg nozzles, they more importantly leaked RCS coolant relatively rapidly. The rapid loss of coolant resulted in a relatively early overheating of the fuel rods and the open SV kept a continuous flow of hot gas moving through the loop C hot leg nozzle. The creep damage accumulation in the nozzle started early and proceeded steadily to where the nozzle ruptured earlier than in any other calculation in the UA.

Valve failures leading to a cesium vapor source from the PRT

The pressure relief tank (PRT) was a location of substantial deposition and retention of fission products in the UA calculations. The degree of fission product retention in the tank was strongly influenced by whether the tank boiled dry. In all but two of the 56 realizations in the UA that experienced an FTC of a pressurizer SV in a substantially open position (>0.36 open area fraction), the PRT boiled dry (see Figure 3-18). The zero values in this figure indicate no valve failure (i.e., the pressurizer SVs operated per design). The decay heat in the retained fission products boiled the PRT dry. In the case of a stuck open SV, more fission products were vented to the PRT.

There is dramatic heating inside of the tank following the water boil-off. Figure 3-19 shows the corresponding history of the three chemical forms of Cs resident in the tank. Note the large steep decreases of the quantities of CsOH and CsI that occur when the tank heats and vaporizes the previously settled retained cesium compounds. The venting reduces the fission product decay power in the tank, which subsequently drops in temperature and ends the vaporization. All the Cs_2MoO_4 is retained in the tank due to its lower volatility. Although CsOH is the most volatile cesium compound in the PRT, the remaining amount chemisorbed from CsOH into the steel of the tank. A key modeling enhancement for the Surry UA included multiple heat structures on the PRT that separated regions for radionuclide settling after the pool evaporates versus the sides and the top of the tank.

The behavior of revaporized cesium from the PRT can be important to the environmental source term. It is a source of hot radionuclide vapors that will condense to form small, airborne aerosols in the containment atmosphere. The small aerosols are susceptible for release to the environment due

to design leakage and through the containment failure. However, the timing of the large cesium source following the PRT dryout occurs in the well before containment liner failure (see Table 3-4), which allows significant time for aerosol settling. Consequently, the PRT vapor source is most important if the pre-failure (design) leakage is high.

Table 3-3. Pressurizer SV FTC statistics

	SV-1	SV-2	SV-3
FTC occurrences	120	10	0
Mean cycles to FTC	17.667	5.800	-
Median cycles to FTC	11	5.5	-
Min cycles to FTC	1	1	-
Max cycles to FTC	63	15	-
Mean FTC open fraction	0.384	0.661	-
Median FTC open fraction	0.092	0.773	-
Mean time of FTC (hr)	2.468	2.512	-
Median time of FTC (hr)	2.204	2.295	-
Earliest FTC time (hr)	1.876	2.042	-
Latest FTC time (hr)	4.122	3.728	-

Table 3-4. Comparison of PRT dryout and containment liner failure statistics

Statistical Measure	PRT Dryout time (hr)	Containment Liner failure time (hr)
Mean	12.712	50.785
Median	10.116	50.058
Min	7.373	34.489
Max	66.212	71.915

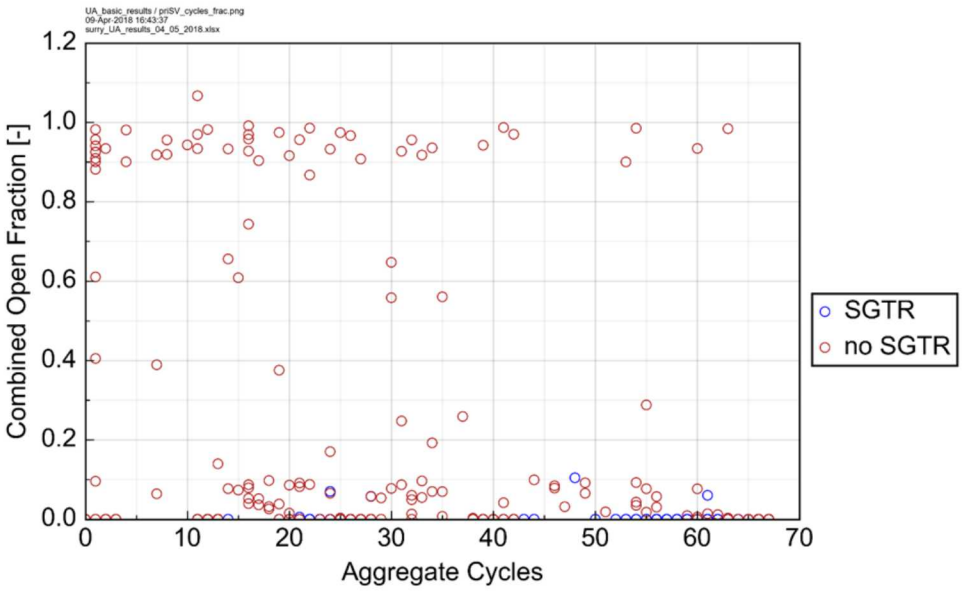

Figure 3-17. Aggregate pressurizer SV cycles and end-state open fraction

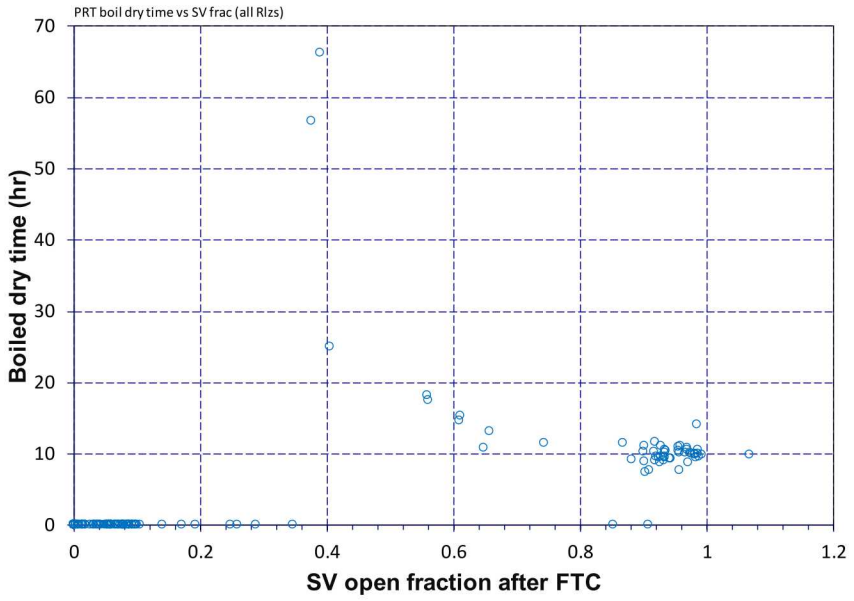

Figure 3-18. Time of PRT boiling dry versus pressurizer SV FTC open fraction

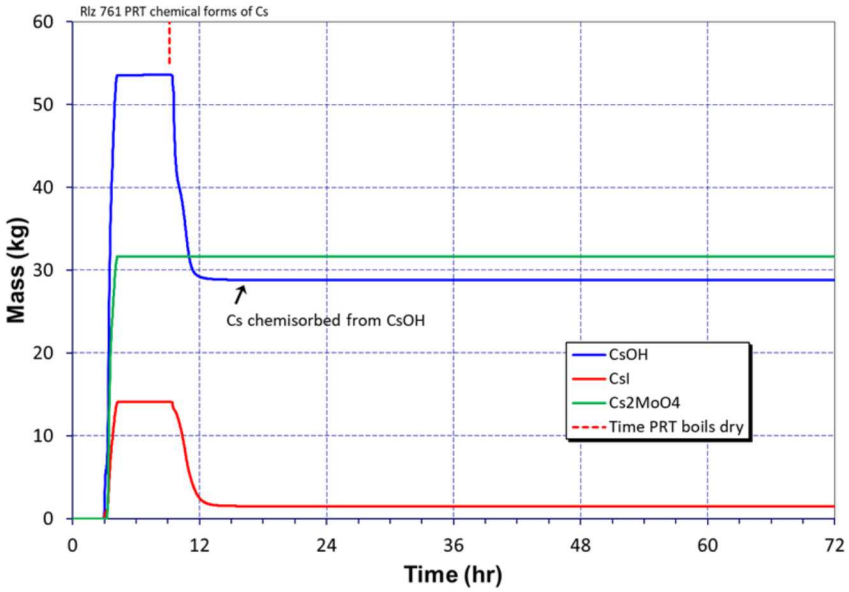

Figure 3-19 Example of cesium revaporization following PRT dryout.

All pressurizer valves fail to open

In the draft UA[38], pressurizer SV FTO was considered. If one SV failed to open, then the next one would be demanded. Although statistically possible, the likelihood of all valves failing to open was evaluated to be incredible and not considered for the final Surry UA [3]. Prior to that conclusion, a sensitivity study was performed to investigate the system response with all pressurizer SVs failing to open. The only mechanism of pressure relief was the reactor coolant pump (RCP) seal leakage or a C-SGTR, if present. Sensitivity calculations were performed that failed all three primary

SVs after only two cycles apiece. In the first sensitivity, the RCP seal leakage was left at 21 gpm/pump. Following this, two more sensitivities were run with enhanced leakage at 182 gpm/pump and 480 gpm/pump. With the nominal pump leakage of 21 gpm, the primary system would pressurize until there is another primary system structural failure (see Figure 3-20). Similarly, a leakage of 182 gpm/pump also does not prevent over-pressurization of the primary system. However, the largest leakage of 480 gpm/pump prevented a primary system over-pressure condition. Interestingly, the 480 gpm/pump calculation still progressed to a hot leg creep rupture failure despite depressurizing to less than 4 MPa during the initial core degradation phase. Consequently, a hot leg failure is still possible despite the lower primary system pressure from the three seal RCP failures (i.e., net 1440 gpm).

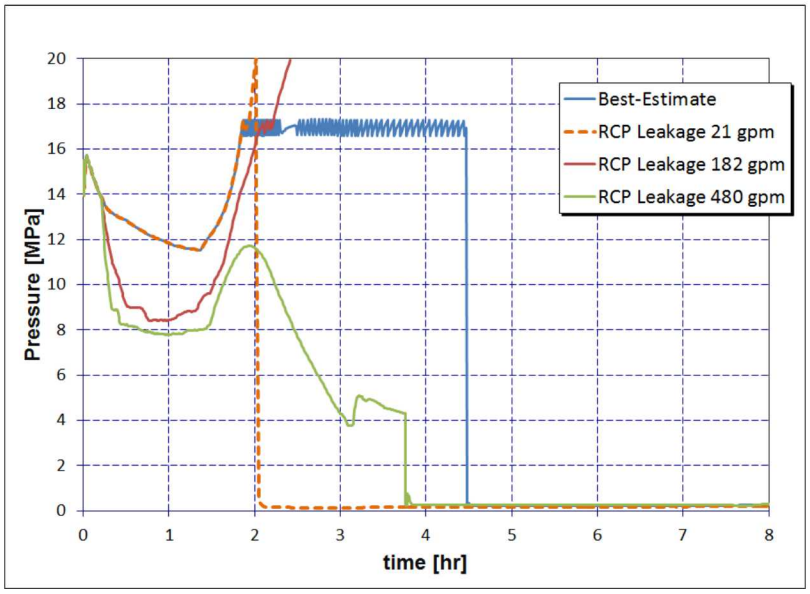

Figure 3-20. Comparison of primary pressures for select values of pump seal leakage

3.2.2.3. Peach Bottom UA

In the Peach Bottom UA, the valve response strongly affected the magnitude and timing of fission product releases to the environment. Whether an SRV sticks open before or after the start of core damage had a significant impact on the magnitude of the source term (i.e., the magnitude of cesium and/or iodine releases to the environment) and whether an MSL creep rupture occurs. The insights from the Peach Bottom UA are discussed in the following subsections.

BWR valve responses

Every Peach Bottom UA calculation experienced a failed SRV, which could be divided into three outcomes representing a distinct mode of venting the reactor pressure vessel (RPV) during much of the core degradation. The three groups are: (1) an SRV stochastic failure for ~50% of the realizations, (2) an SRV thermal failure without MSL creep rupture representing ~33% of the realizations, and (3) an SRV thermal failure with MSL creep rupture for ~17% of the realizations. The importance of these parameters is significant as their values strongly influence the releases of the iodine and cesium to the environment.

One of the most important parameters, both for amount of radionuclide release and hydrogen production is the uncertainty in the frequency of the SRV stochastic FTC. It has a strong negative

monotonic influence (indicating that fewer cycles before failing leads to higher releases). A longer period of SRV valve cycling will cause a thermal seizure of the SRV and potential MSL creep rupture, which ultimately leads to a larger source term release to the environment. Other regressions techniques indicate that it also has non-monotonic and conjoint influence. The conjoint influence is partly shared with the SRV open area fraction after thermal seizure. If the SRV thermal failure area is small, then the failed valve relieves steam more slowly with higher protracted pressures. The higher pressures result in elevated stresses in the MSL piping, which combine with elevated temperatures to accumulate creep damage over time that can lead to an MSL rupture. Combined, these parameters control the type of failure (SRV stochastic, SRV thermal seizure, or SRV thermal seizure with MLS creep rupture). The importance of failure mode is visible on Figure 3-21.

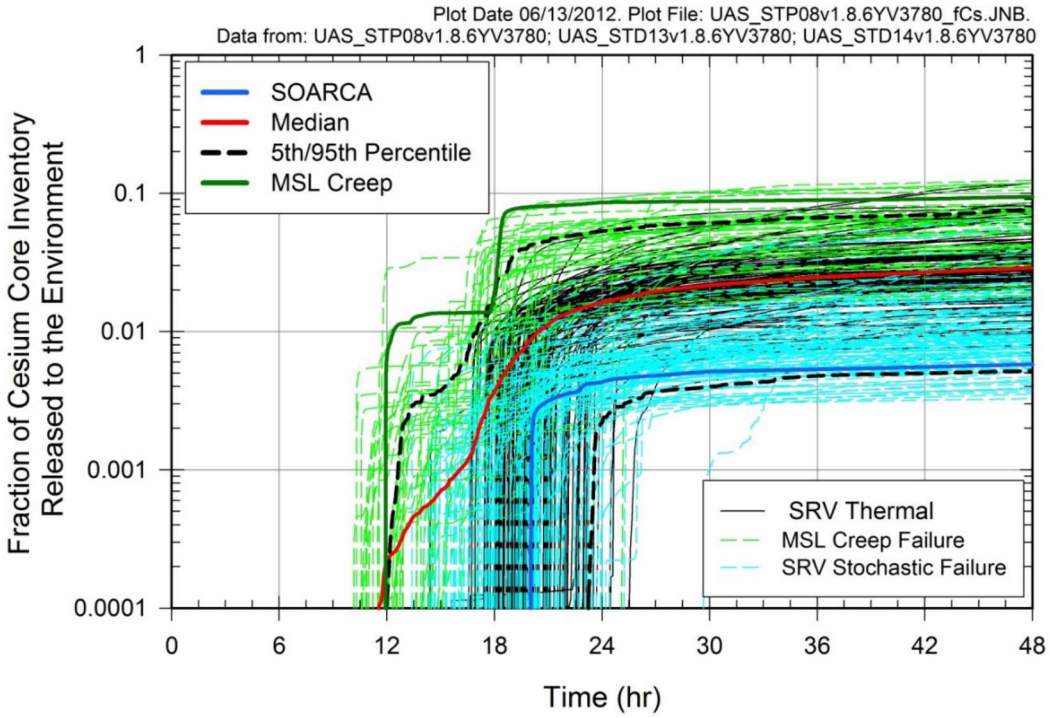

Figure 3-21. Cesium environmental release fraction as a function of valve failure mode for the Peach Bottom UA

Impact of additional manual BWR valve actions

A sensitivity study was carried out to determine the effect of manual operation of the SRV. The study varied the manual opening time of a single SRV. In order to depressurize the reactor vessel in a controlled manner, operators can manually open an SRV. The emergency depressurization action is described in the station emergency procedures to prevent excessive cycling of the SRVs [16]. The UA calculations include this operation action at 1.0 hr after the initiating event following discussions with plant staff. Four sensitivity variations on SRV operation considered opening at 0.5 hr, 2.0 hr, 3.0 hr, and not opening.

There was very little impact in the timings of key events between the 1.0 hr, 2.0 hr, 3.0 hr, and no operator actions. This showed the timing of the operator action or the lack of an operator action did not significantly impact the timing of the severe accident progression. The 0.5 hr differed from the other cases because the operator did not maintain adequate steam pressure for the reactor core

isolation cooling (RCIC) system.[14] The impact on any other SRV manual opening strategy would be similar if it inadvertently disabled RCIC.

Although the timings were not impacted, the probability of an SRV FTC increases with increasing delays to implement manual control of the SRV to stop valve cycling. Each of the sensitivity calculations used the same failure cycle specifications (i.e., 270 cycles to FTC), and therefore experienced earlier stochastic failures of the SRV due to a fast accumulation of SRV cycles as the manual operator action is delayed. The calculation with no operator actions predicted 4.6 hr to a stochastic failure of SRV whereas the 1, 2, and 3 hr cases were 8.2, 7.9, and 7.5 hr, respectively.

Similarly, the various manual SRV actions or lack of an action had a relatively small impact on the environment source term. All cases showed similar cesium release to the environment. However, the case without any operator actions had a higher iodine release attributed to higher in-vessel revaporization. The timing of the reactor depressurization due to an SRV FTC relative to the loss injection impacted the magnitude of the in-vessel iodine deposition available as a late-phase revaporization source. The small iodine source term differences were judged not significant within the variability of the other in-vessel accident progression uncertainties that could be considered for this comparison.

3.2.2.4. Implications for Other Plants

The MSS and pressurizer SV failures had significant impacts on all three UAs. The UA analyses identified SV FTC as the key or one of the key uncertain parameters increasing the source term. An SV FTC changes the course of the accident. As noted in Section 3.2.2.1, there is sparse data and a lack of established expert consensus on how best to model the failure rates under severe accident conditions. Nevertheless, the stochastic occurrence of a valve FTC is noted in plant LERs. Furthermore, the high-temperature conditions at BWR SRVs during a severe accident also strongly indicate thermal failure modes for BWRs. Although there is significant uncertainty in the FTC distributions and their associated failure flow areas, the possibility of these scenario-altering failures is a significant finding from the UAs.

General C-SGTR and accident progression insights

All PWRs include pressurizer and MSS SVs. In scenarios with a loss-of-power sequences like the SBOs in the Surry and Sequoyah UAs, the MSS and pressurizer SVs will cycle to release steam and prevent an over-pressurization of the secondary system. With respect to the uncertainty of their failure characteristics, the SV FTC characteristics used in the PWR UAs are judged representative of other PWRs in the U.S. The quantitative insights are dependent on many plant-specific factors that limit their direct applicability. However, the following qualitative insights are applicable,

- An MSS SV FTC weakly increases C-SGTR occurrences.
- A pressurizer SV FTC with a large failure area can prevent a C-SGTR whereas no FTC or an FTC with a small failure area promotes a C-SGTR.
- A pressurizer SV FTC with a large failure area can delay or prevent hot leg failure.

[14] The failed operator action to maintain adequate RPV pressure to prevent isolation of the RCIC was erroneously not included in the model control logic. The operator would carefully monitor the system pressure to maintain RCIC flow (i.e., extremely unlikely that an SRV would be opened and the system response was not monitored). Nevertheless, it does show the adverse impact of failing to perform this action. However, the alternate response is not relevant for the purpose of the sensitivity study on operator action timings.

- A pressurizer SV FTC can concentrate radionuclides in the PRT that may promote their late revaporization.

Reactors with a Babcock and Wilcox (B&W) design nuclear steam supply systems (NSSS) use once-through SGs that are less susceptible to hot natural circulation flows from the core flowing through the SG. Although the insights above increase mechanical stress (i.e., higher differential pressure) across the SG tubes, the B&W NSSS do not experience the same thermal stresses as Westinghouse and Combustion Engineering (CE) NSSS designs. Consequently, the B&W plants are less susceptible to a C-SGTR. However, the higher radionuclide loading to the PRT following a pressurizer FTC is common across all PWR designs.

Ice condenser over-pressure insights

The Sequoyah UA results show a dependence on a pressurizer SV FTC promoting a large deflagration that could fail the containment. However, a key insight from the Sequoyah UA is an early containment failure was very unlikely within the constraints of the study (e.g., uncertain parameters and ranges, ignition assumptions, and containment design). The 10 ice condenser plants are similar but not identical. All 10 ice condensers NSSSs are large 4-loop Westinghouse designs of similar power ratings and containment sizes. Eight of the 10 reactors have free-standing steel containments like Sequoyah. However, the two ice condenser units at the Donald C. Cook Nuclear Plant in Michigan have steel-reinforced concrete containments (i.e., similar to Surry). The qualitative insights that large hydrogen deflagrations challenge the containment over-pressure limits following a pressurizer FTC will be applicable to other ice condenser plant designs, with the possible exception of the Cook plant. The quantitative evaluation of that challenge includes the uncertainty in the hydrogen pressurization as well the specific geometry and pressure ratings of the containment. However, the impact of the design variations of the eight ice condensers with free-standing steel containment is expected to be smaller than the severe accident uncertainties, which should make the low likelihood of an over-pressure challenge applicable.

BWR accident progression insights

All BWRs in the U.S. are designed by General Electric (GE), although their size, safety system configuration, and containment design can vary significantly. In particular, there are several types of BWR SVs. NUREG/CR-7047 identifies that BWRs use code safety valves, direct-acting SRVs, and pilot-actuated SRVs. The SRVs include a pressure mode where they function as a code safety valve. Furthermore, there are three configurations of the pilot-actuated SRVs. The Peach Bottom uses three-stage Target Rock SRVs. However, the assessment for their stochastic FTC relied on generic data for all BWR SRVs. Consequently, the FTC distributions are judged to be applicable within the previously mentioned caveats on sparse data in accident conditions.

The thermal SRV FTC criteria and the corresponding failure area also have uncertainties, which were explored within our current understanding of their failure characteristics in the Peach Bottom UA. The location of the SRVs in all BWRs is similar and would flow very hot gases during a severe accident core degradation as simulated in the UA. However, the response of the valve components to flowing high temperature gas depends on the valve design and operation. For example, different thermal failure criteria were developed for the Grand Gulf and Peach Bottom MELCOR models because the plants have different types of SRVs [16].

The three-stage Target Rock SRVs are pilot operated and fully open when the pressure exceeds the setpoint and fully close when the pressure decreases below the closing set pressure. The movement of the valve disc is controlled by a pilot valve, which re-aligns the internal gas pressure in the valve

allowing the RPV pressure to the valve be closed up to the opening pressure and open until the closing pressure. The Dikkers SRVs in the Grand Gulf plant is a spring-loaded valve that pops open at the relief pressure and gradually closes as the pressure decreases. Consequently, the modeling and insights on the thermal SRV failures are expected to have variations. The thermal SRV failure challenge is expected for all BWRs but the resulting leakage area and failure criteria will have differences.

Overall, the Peach Bottom SRV failure insights are expected to have qualitative applicability to all BWRs. The stochastic and thermal failure characteristics are expected to be similar. The associated thermal challenges to the MSL are also expected to be applicable.

The impact of the source term from the various SRV and MSL failures is not expected to be generally applicable. All the Peach Bottom UA calculations include a liner melt-through shortly after the vessel failure. The timing and mode of containment failure for Peach Bottom Mark I containment is different than expected for the BWR Mark III containment and the various designs of the BWR Mark II containments.[15] Consequently, the hold-up and eventually release of radionuclides will be substantially different and not follow the characteristic cesium release insights observed in Figure 3-21. However, the responses of the other Mark I containments are expected to be similar with some variations in the timing of the liner melt-through due to the sump size and drywell wall and floor characteristics.

BWR Mark III over-pressure insights

Similar to the PWR ice condenser containment, the BWR Mark III containment is relatively small and not inerted. It is qualitatively expected to also be challenged by hydrogen burns following a collection of hydrogen in the containment from an SRV FTC. The steam reducing effects of the wetwell pool will increase combustibility and the flame speed in a manner similar to the ice condenser chests. However, the containment ignition sources for a BWR Mark III containment will be different than a PWR (e.g., no hot gases exiting a PRT and no hot leg failure). Similar to the ice condenser design, the ex-vessel debris is expected to be an important Ignition source in an unmitigated BWR Mark III loss-of-power sequence.

3.2.3. Consequential Steam Generator Tube Failure

Only the Surry UA performed an evaluation of consequential steam generator tube failures (i.e., consequential steam generator tube ruptures or C-SGTRs). The consequential response is due to hot thermal plumes generated during the core degradation circulating to the SG and failing the tubes. While C-SGTRs would also be expected in the Sequoyah plant, the Sequoyah UA did not include the uncertainty parameter additions and additional modeling needed to predict C-SGTRs. BWRs do not have SGs, so the issue is only applicable to PWRs. Section 3.2.3.1 discusses the key insights from the Surry UA and Section 3.2.3.2 discusses their applicability to other plants.

3.2.3.1. Surry UA

The Surry UA includes additional modeling to predict when an SGTR may be induced by evolving conditions in the unmitigated STSBO scenario. Similar to the Sequoyah PWR model, the Surry model includes in-vessel, hot leg, and SG natural circulation modeling. Natural circulation flows can occur in all three regions that transfer heat from the hottest regions of the core to a hot leg and the

[15] The Mark II containments had four different Architectural Engineering firms and have significant differences in the reactor pedestal and drywell floor design [35].

SGs (see Figure 3-22). As a special modeling addition for the Surry UA, a separate effects SG inlet model was imbedded in the model to predict the response from the peak temperature of the gas entering the SG. The separate effects model uses boundary conditions from the full plant model to specify the peak plume temperature entering the SG. The magnitude of the natural circulation flows and peak hot plume temperature modeling is guided by detailed computational fluid dynamics (CFD) work [17]. Furthermore, the peak plume temperature is an uncertain parameter derived from the variability observed in the CFD analyses. Finally, the Surry model includes a sampled flaw distribution in the cold, hot, and peak plume temperature regions of the three SGs. Creep rupture evaluations were performed to evaluate the potential for failure of flawed and unflawed tubes in the three regions.

Evaluation of SG tube flaws

The flaw size and frequency is guided by NRC research on consequential tube ruptures (i.e., NUREG-2195, [18]) and historical Surry in-service inspection (ISI) reports (e.g., References [19] and [20]). Surry adopted industry guidelines to maintain SG tube integrity for the operating interval between tube inspections. The technical specifications define what constitutes tube integrity through the establishment of performance criteria. However, the maintenance requirements are supplemented with some prescriptive requirements that includes 100% inspection of the tubes every two refueling outages.

The ISI reports include a table summarizing the wear observed at the Anti Vibration Bars (AVBs) at the top of the tube bundle, a location known for tube wear that is carefully monitored. The wear at these locations generally increases at a predictable rate and can be managed effectively in the ISI program. The second most common reason for plugging thermally treated Inconel 600 tubes is due to damage by loose parts. The Surry ISI reports include detailed information on every tube plugging not due to AVB wear, which includes loose parts damage and inadvertent maintenance damage from sludge cleanup tools. The Surry ISI reports show 76 incidences of tube plugging due to flaws during the SG's lifetimes.[16] Sixty-one percent of the identified flaws that led to tube plugging were located between the tube sheet and the second grid support, or close to the hot side of the SG inlet. The higher occurrence of flaws near the inlet of the hot side of the SG is significant because this location is susceptible to the highest temperatures during a severe accident [17]. These insights were incorporated into the hot and upflow region flaw sizes.

The NUREG-2195 statistical analysis and the Surry ISI reports are based on flaws that are detected. The number of flawed tubes from the two approaches does not account for the hidden flaws that are not detected during the SG ISIs. The larger and deeper the flaw, the higher the probability of detection (POD). NUREG-2195 cites NUREG/CR-6791 [21] as providing techniques for evaluating the POD and judges the impact is relatively small for deep flaws. The flaw estimation and judgment on the POD is important since the Surry UA results did not predict any failures in unflawed tubes.

Surry UA C-SGTR results

The occurrence of a C-SGTR required a substantial tube flaw depth and other contributing accident progression parameters characteristics. A C-SGTR occurred in 144 of the Surry realizations, or 12.5% of the completed calculations. In every realization with a C-SGTR, a hot leg nozzle rupture also occurred (i.e., the attributes that lead to a C-SGTR also promote a hot leg rupture). The hot leg

[16] The Surry SGs were replaced in 1980 and 1981.

failure terminated the high leakage flow rate through the C-SGTR. The high-level insights regarding C-SGTR occurrence include:

- The threat of a C-SGTR was not limited to the peak plume region in the SG tube bundle.
- The likelihood of a C-SGTR for the cold and hot upflow regions significantly increased if the non-dimensional flaw depths were respectively greater than 0.8 and 0.68, respectively.
- The likelihood of a C-SGTR in the peak temperature region significantly increased if either the non-dimensional flaw depth was greater than 0.42 or if the flaw depth was greater than 0.31 with a peak non-dimensional hot plume temperature greater than 0.48.

The consequences of the C-SGTR are significant because these realizations predict the largest and earliest cesium and iodine releases. Figure 3-23 and Figure 3-24 show time-dependent release of iodine and cesium mass to the environment, respectively. There is a clear bifurcation in the results, with the higher release masses representing C-SGTR realizations and the remainder of the realizations having much lower releases. The realizations with a C-SGTR have an early pathway to the environment through the failed tube and then either a failed open MSS SV (see Section 3.2.2.2) or via MSL leakage. On the semi-log scales of Figure 3-23 and Figure 3-24, the non-C-SGTR results show significant increases after 36 hr with the start of containment failures. However, most of the post-containment releases are relatively small in absolute magnitude as compared to the earlier C-SGTR releases. There was only design leakage[17] prior to the containment failure, which accounts for the early but small releases to the environment. The late releases result from lingering airborne radioactive aerosols and gases in the containment and late revaporization releases (e.g., see the PRT discussion in Section 3.2.2.2).

[17] The design leakage is a sampled uncertain variable. The uncertainty sampling ranges from 10% to 1000% of the technical specifications for containment leakage, i.e., 0.1% air volume per day at the containment design pressure.

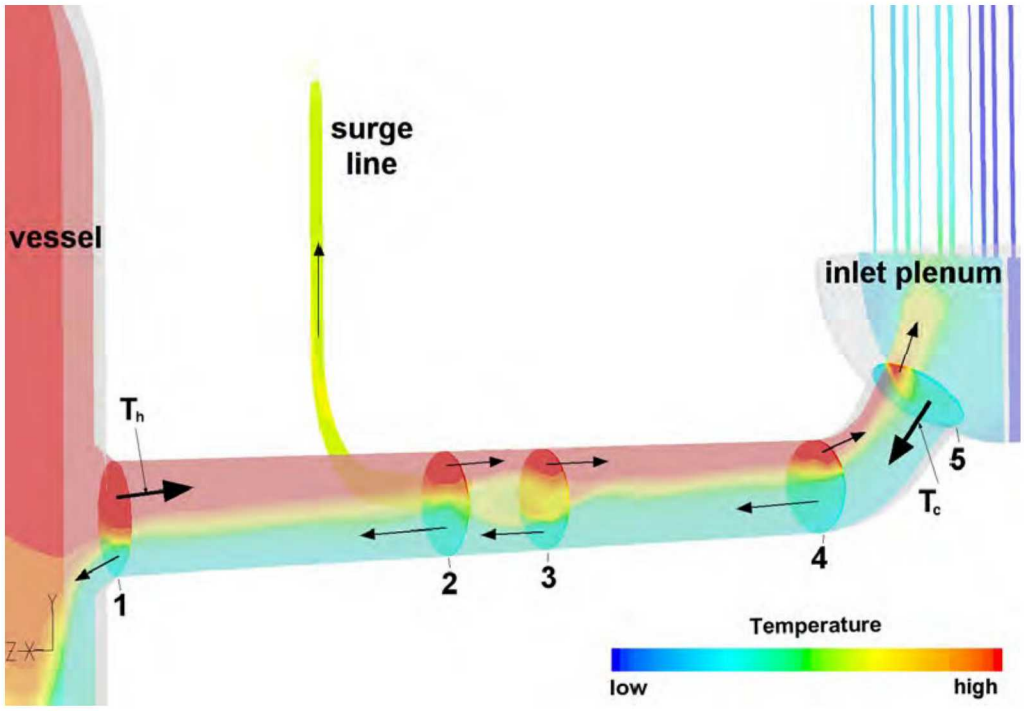

Figure 3-22. CFD simulation of hot natural circulation flows from the vessel to the steam generator [17]

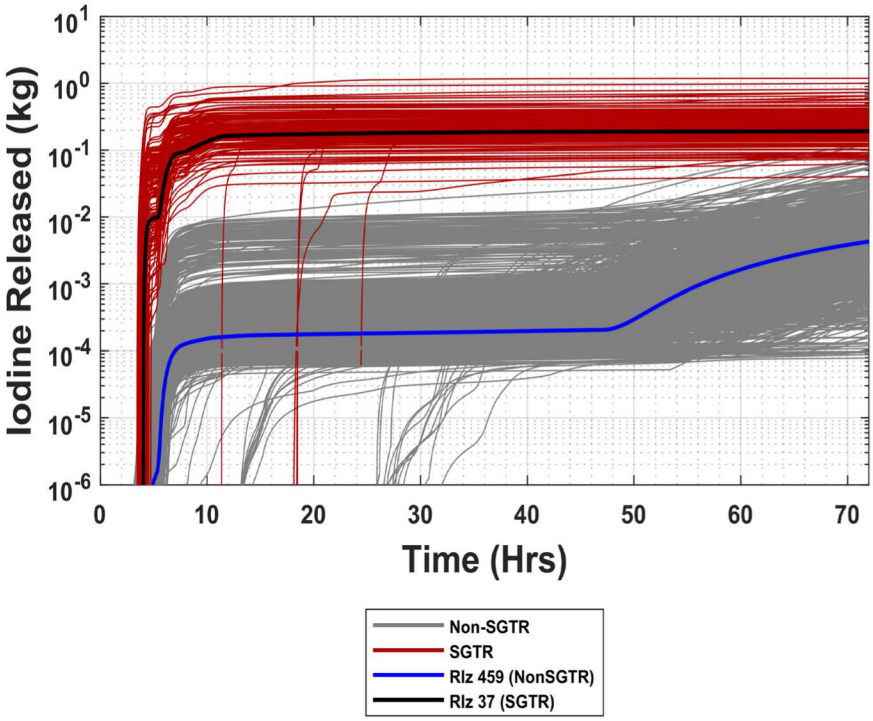

Figure 3-23. C-SGTR and non-C-SGTR iodine release masses to the environment with the corresponding reference case realizations

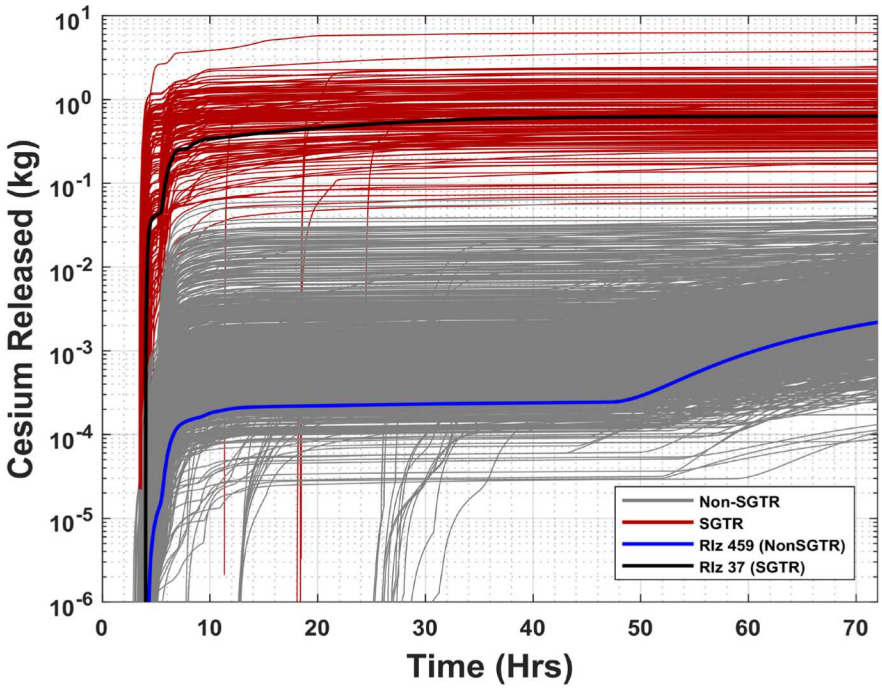

Figure 3-24. C-SGTR and non-C-SGTR cesium release masses to the environment with the corresponding reference case realizations

Detailed insights from the C-SGTR reference case

The reference C-SGTR realization was selected to give the median response for four specific attributes of interest. The attributes selected to identify the reference calculations were (a) the cesium release to the environment, (b) the iodine release to the environment, (c) the timing of the containment liner yielding (or the C-SGTR if calculated), and (d) the containment pressure at the end of the calculation. The first three parameters characterize the magnitude and the timing of the source term, which is the focus of the SOARCA. The containment pressure was included in this evaluation to reflect the median hydraulic condition for long term releases from the containment.

Some of the key attributes that apply to both reference calculations include:[18]

- No over cycling FTC SV occurred on any of the SGs.
- No over cycling FTC occurred on the pressurizer SV.
- No reactor coolant pump seal failures, which is the most likely outcome from the uncertainty distribution.
- The hot leg nozzle rupture occurred on Loop C where the pressurizer surge line connects. Loop C heated faster due to the cycling pressurizer SV, which led to the preferential failure on this loop.
- Hydrogen deflagrations occurred in containment after the hot leg failure, but they did not pose a significant over pressure challenge to the containment boundary.

[18] A reference case was also identified for a realization without a C-SGTR but not discussed further here.

- The containment design pressure and the pressure associated with liner yield were both exceeded. However, the containment pressure was below the rebar failure pressure at 72 hr, which is the most likely outcome at 72 hr.[19]
- Although the containment pressure associated with rebar yield was not reached by 72 hr, the pressure was expected to exceed this value shortly thereafter.
- The largest contributor to containment pressurization was the continuous heating of RCS coolant recast as steam in the containment (rather than addition of non-condensable gases to the atmosphere from core-concrete interaction [CCI]).
- The C-SGTR significantly increased the release to the environment. The reference realization without a C-SGTR released 0.028% and 0.003% of the iodine and cesium inventory, respectively. However, the C-SGTR reference realization released 1.42% and 0.92% of the iodine and cesium inventory, respectively.
- The concrete ablation from CCI had not slowed by the end of the MELCOR calculation at 72 hr. The concrete erosion rate and non-condensable gas generation was relatively constant after the start of the CCI.

The timing of key events is shown in Table 3-5. The C-SGTR occurs after the start of core damage, which is identified by the first fission product release. There is 16 min between the C-SGTR and the subsequent hot leg failure, which terminates the high flow leakage. As noted above, the reference C-SGTR calculation approximated the median C-SGTR cesium and iodine release to the environment. In contrast, the realization with the largest release to the environment was a rare calculation that experienced two C-SGTRs. The multiple C-SGTRs led to a depressurization of the primary system that delayed the hot leg failure until 1 hr 27 min after the first C-SGTR, which was at the 86th percentile for high-flow C-SGTR duration.

The rate of gas leakage from the C-SGTR and the containment is shown in Figure 3-25. The C-SGTR occurs at 4 hr 1 min and begins leaking at 4700 scfm from the primary system to the secondary side of the SG and then past the MSIV. After the hot leg failure, the C-SGTR leakage decreases by two orders of magnitude and follows the containment pressure response. The fission product releases that are released after the hot leg creep failure primarily flow to the containment through the large hot leg failure rather than out the C-SGTR. After vessel lower head failure at 9 hr 13 min and the core debris discharge into the containment, there is a natural circulation flow from the containment, through the vessel and out the failed hot leg with some small leakage out the C-SGTR pathway. Consequently, the radionuclide release through the C-SGTR after the hot leg failure is slowed due to the large reduction in flow rate and the dilution from entering the containment through the hot leg failure and mixing with the containment air. The containment liner yield occurs at 57 hr 55 min and increases to 175 scfm at 72 hr, which becomes the secondary source of leakage (i.e., the primary leakage location in non-C-SGTR outcomes).

Figure 3-26 illustrates the creep damage accumulation in the three various tube locations of the three SGs. The accumulated creep is a function of the tube temperature, the differential pressure across the tube, and the flaw depth. The C-SGTR reference realization had a severe flaw depth in the cold tube region of SG A. The creep accumulation increased much faster in this tube than the other monitored locations until its failure at 4 hr 1 min. No other tube is close to failure prior to the hot

[19] There were 1,091 liner failures and 16 rebar failures within 72 hr. There were 56 calculations with a 0.5 day time in the cycle where no containment failure was occurred within 72 hr.

leg nozzle rupture 16 min later, emphasizing the importance and requirement of a severe flaw for a C-SGTR.

The SGs are cluttered with thousands of SG tubes, seven levels of grid spacers, steam separators, and steam dryers. The complex deposition of aerosols released to the SG was prescribed using insights and results from the ARTIST (AeRosol Trapping In a Steam generaTor) experiments [3]. The uncertainty in the aerosol retention in the secondary side of the SG was varied by sampling the location and number of SG tube grids supports between the C-SGTR and the exit of the SG boiler section. The grids are a dominate retention location and especially effective at capturing larger aerosols.

Figure 3-27 shows the calculated time-dependent aerosol sectional decontamination factors in SG A following the C-SGTR. The MELCOR model discretizes the aerosols into size ranges called sections. The ten sections are uniformly spaced logarithmic intervals from a minimum of 0.1 microns to a maximum of 50 microns. The larger aerosols in Sections 5 through 10 have very large decontamination factors and are effectively retained in the SG. Large aerosols are more likely to deposit on the surrounding tubes and be captured in the tube grid spacers. However, the smaller aerosols in Sections 1 through 4 more closely follow the gas streamlines through the tube region and out the MSIV leakage pathway.

The integral SG decontamination factors of key chemical groups exiting through the C-SGTR are shown in Figure 3-28. The retention of the noble gases (i.e., characterized by the xenon radionuclide class) and the elemental iodine gas are contrasted with the predominantly aerosol release of the cesium iodide and the other cesium compounds.[20] There is no retention of the noble and iodine gases passing through the steam generator tube bundle and exiting out the MSIV leak path. In contrast, the total iodine (i.e., the sum of the gaseous and aerosol components) and the cesium decontamination factors trend towards 1.5 and 1.9 at 5 hr, respectively.

Of the total cesium and iodine released to the environment, 99.9% and 99.8% comes through the C-SGTR pathway versus containment leakage. However, the C-SGTR leakage during the high flow rate phase prior to the hot leg failure and primary system depressurization is not the dominant release phase to the environment. For example, only 2.7% and 5.0% of the total cesium and iodine is released via the C-SGTR to the environment by 5 hr (see Figure 3-29). The bulk of the release to the environment (i.e., 97.3% and 95% of the cesium and iodine released to the environment) occurs after 5 hr. This was primarily due to more significant releases from the fuel occurring during the second fuel heatup after the hot leg failure and accumulator discharge at 4.3 hr. The dominant C-SGTR releases of 69% and 62% of the total cesium and iodine release to the environment, respectively, occurs by vessel failure at 9.2 hr. Nevertheless, the C-SGTR persists as an important pathway after vessel failure (i.e., accounting for >30% of the total iodine and cesium release), which is somewhat disguised on a semi-log scale (e.g., see Figure 3-23 and Figure 3-24).

The Surry UA modeled 100% of the elemental iodine in the gap between the fuel and the cladding. The iodine gas is released in a puff following the cladding failures in the various rings. Due to the rapid and complete release of the elemental iodine, 57% of the total environmental release occurs by 5 hr. In contrast, most of the xenon gas is tied up in the fuel matrix, which releases over time as the fuel heats and degrades. The percentage of the xenon gas released to the environment is only 29% at

[20] The total cesium decontamination factor includes all forms of cesium including cesium hydroxide, cesium molybdate, and cesium iodide. The total iodine decontamination factor includes the two forms of iodine, which are elemental iodine (i.e., gas) and cesium iodide.

vessel failure. The subsequent release occurs very slowly as xenon flows back into the RCS from the containment and out the C-SGTR leakage pathway. The long-term shape of the xenon release via the C-SGTR is driven by the steady containment pressurization.

Table 3-5. Key event timing in the Reference STSBO calculation with a C-SGTR

Event	Time (hh:mm)
STSBO – loss of all AC and DC electrical power, auxiliary feedwater (AFW) unavailable	00:00
Reactor trips Main steam isolation valves (MISVs) close RCP seal leakage initiates at 21 gpm/pump	00:00
SG dryout	01:32
PRT rupture disk breaks	02:16
RPV water level reduces to TAF	02:16
First fission product gap release	03:43
C-SGTR in SG A in the cold region	04:01
Release of elemental iodine to the environment exceeds 1%	04:06
Loop C hot leg nozzle rupture	04:17
Accumulators begin discharging	04:18
Accumulators empty	04:19
Release of noble gases to the environment exceeds 1%	05:37
Core debris mass exceeds 5%	05:46
1st hydrogen burn	06:09
Initial core plate failure	06:36
RPV lower head breach	09:13
End of containment hydrogen burns	10:12
Containment pressure reaches design (45 psig)	32:15
Containment liner yields	57:55
End of calculation	72:00

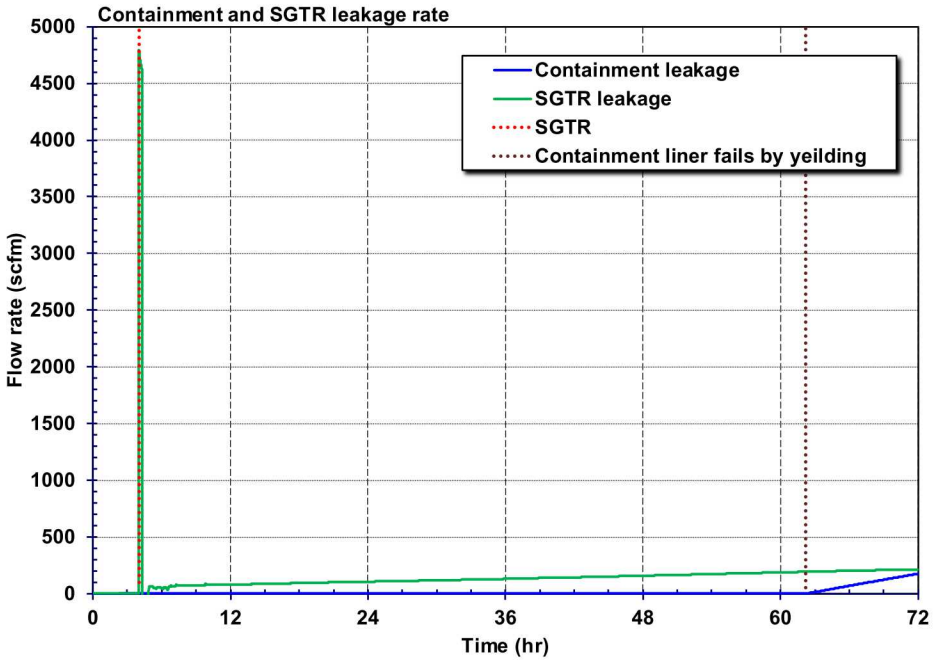

Figure 3-25. Containment and C-SGTR leakage rate (C-SGTR Reference Case)

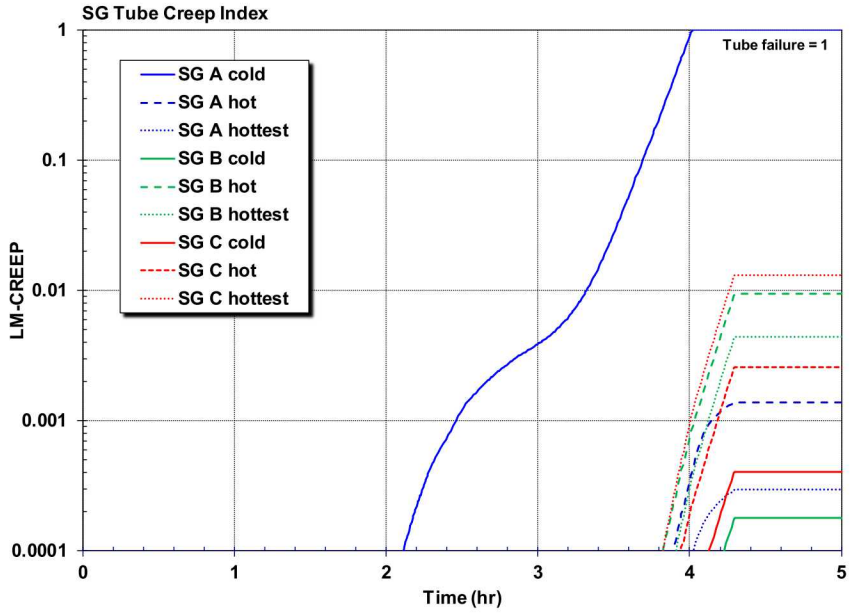

Figure 3-26. SG tube creep damage accumulation (C-SGTR Reference Case)

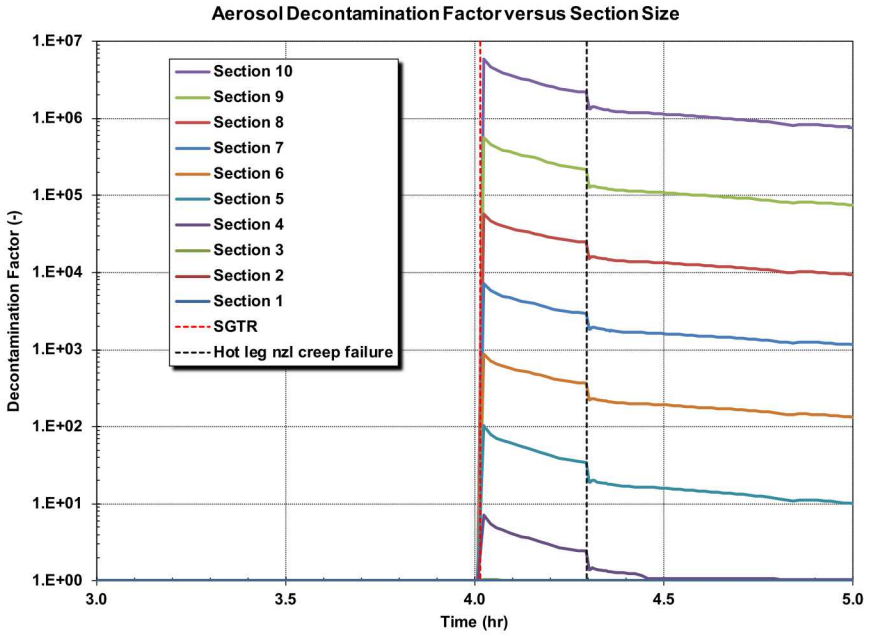

Figure 3-27. Integral aerosol decontamination in the SG secondary following the C-SGTR (C-SGTR Reference case)[21]

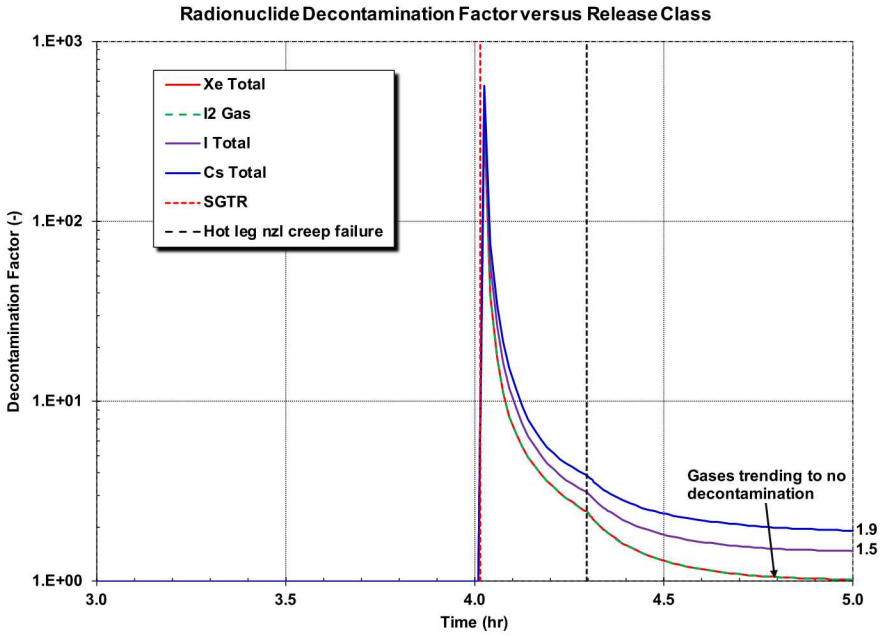

Figure 3-28. Comparison of the short-term xenon, iodine gas, total iodine, and total cesium integral decontamination factor in the SG (C-SGTR Reference Case)

[21] After the hot leg failure at 4.25 hr, the secondary side of the steam generator temporarily leaks inward to the primary system and outward through the MSIV leak path until fully depressurized. Since the integral decontamination factor (DF) is the $Mass_{entering\ SG} / Mass_{leaving\ SG}$, the $Mass_{entering}$ takes an abrupt decrease, which lowers the DF.

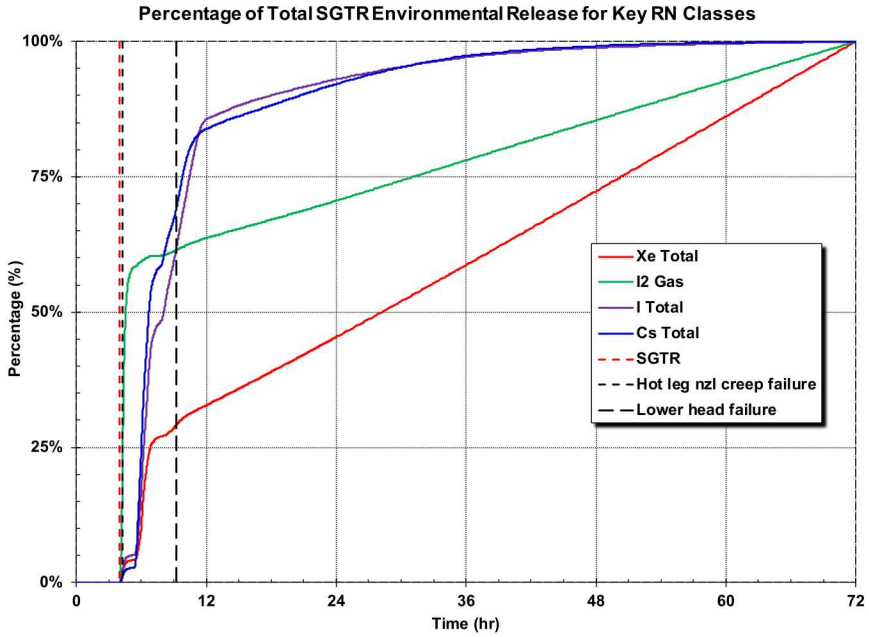

Figure 3-29. Percentage of xenon, iodine gas, total iodine, and total cesium environmental release as a function of time (C-SGTR Reference Case)

Impact of multiple steam generator tube ruptures

A sensitivity analysis was performed in the draft Surry UA to understand the effects of the multiple SG tube failures.[22] A reduced set of parameters judged to be most important to variations in C-SGTR behavior were selected and varied (i.e., the number of tubes, C-SGTR location, secondary SV open fraction, and primary SV open fraction). The distribution sampled the failure of 1 to 5 tubes, and 97 realizations finished to completion. The sensitivity study included other specified boundary conditions that ensured a C-SGTR (i.e., severely flawed tube[s] are located in the hot plume region of the SG). It also included some assumptions not used in the final Surry UA, which specified a pressurizer and MSS SV FTC after 45 cycles. The MSS SV FTC would promote a high radionuclide release by venting the radionuclides more quickly to the environment. The pressurizer SV FTC after 45 cycles helped delay a hot leg failure and promote a longer release.

The fractional releases of iodine and cesium to the environment are shown on Figure 3-30 and Figure 3-31. The horsetails were color-coded to identify the number of failed tubes. Additional tube failures led to higher releases. With a couple overlapping exceptions, the releases for 2 tubes are higher than 1 tube, and the releases for 3 tubes are higher than 2 tubes. However, the releases for 3 to 5 tubes show no clear differences and seem to randomly overlap. While the leakage rate of radionuclides through the C-SGTR was limited by the tube flow rate with less than 3 failed tubes, there was adequate flow above 3 failed tubes to pressurize the SG. The leakage rate is controlled by the MSL leakage rate rather than the C-SGTR flowrate.

[22] The C-SGTR modeling was substantially changed for the final Surry UA, which included plant-specific data for tube flaws, monitoring of multiple locations, and an improved characterization of the highest temperature location in the SG. Other than this multiple steam generator tube sensitivity study, the draft Surry UA was also constrained to one tube failure per steam generator\, which prompted this sensitivity study.

The single tube C-SGTR realizations have an initial puff release that is followed by a gradual increase over the next 10 hr. This trend is seen to a lesser extent with 2 tubes. In contrast, there is a large initial release at the time of 3 or more C-SGTRs, which ends within 6 hr. At the time of the C-SGTR, the radionuclide releases from the fuel were with rapidly increasing but the fuel and cladding has not yet collapsed (i.e., intact geometry). A larger number of failed tubes overwhelms any hot leg natural circulation patterns and redirects radionuclide filled gases towards the failed C-SGTRs.

A limited regression analysis was conducted for the multiple tube C-SGTR sensitivity study. The number of tubes dominated results, with none of the other 3 sampled parameters having a significant additional impact. A large factor in the magnitude of the environmental release is the timing of hot leg creep relative to the C-SGTR. The variability in the timing is impacted by the primary system depressurization rate, based on the number of tubes failing and exacerbated by the primary SV open fraction. One realization, with 5 tubes failing, had no hot leg creep and led to the highest release fractions.

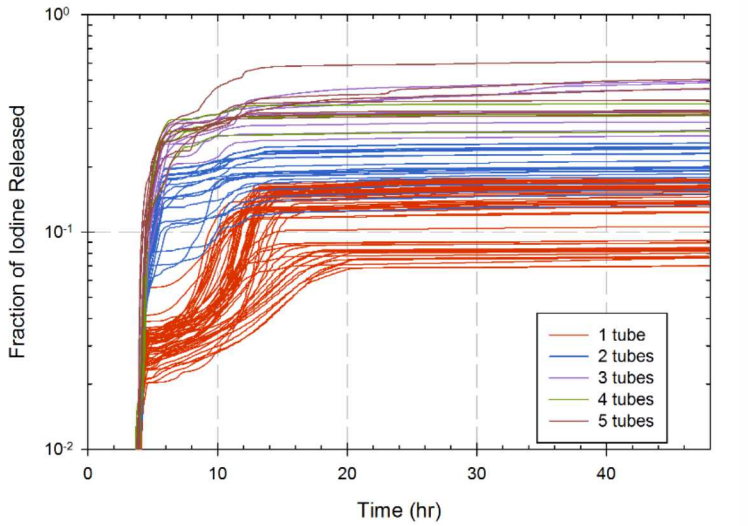

Figure 3-30. Iodine environmental release fraction versus number of tubes failed

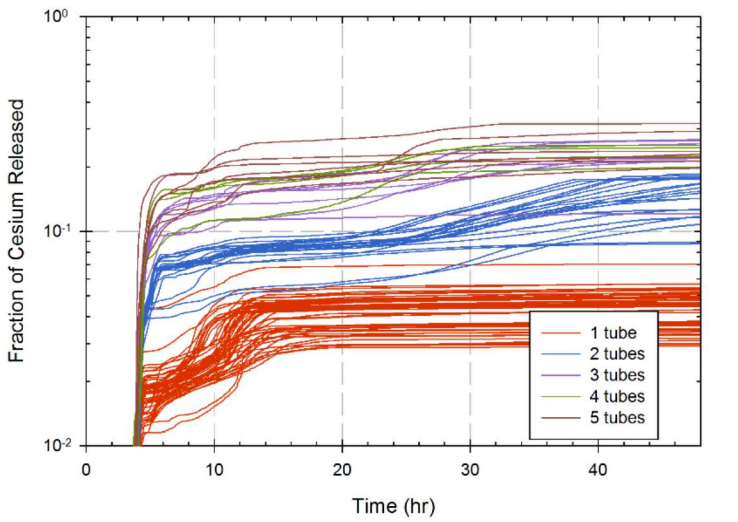

Figure 3-31. Cesium environmental release fraction versus number of tubes failed

3.2.3.2. Implications for Other Plants

The prediction of a C-SGTR includes modeling natural circulation flows to the SG and thermal-mechanical stress calculations. The natural circulation flows are unique to the plant design. The geometry of the B&W NSSS plant with its once-through SGs is not supportive of a natural circulation flow. These plants include Arkansas Nuclear One, Unit 1 in Arkansas, Davis-Besse in Ohio, and Oconee Units 1, 2, and 3 in South Carolina. The remaining PWR nuclear power plants use a U-tube SG design. These plants were designed by CE and Westinghouse. A C-SGTR is not applicable to BWRs, which do not have SG tubes.

Natural circulation for Westinghouse plants

The technical basis for the Surry natural circulation flows was developed from experiments and computational fluid dynamics (CFD) modeling. The NRC and industry performed 1/7th scale experimental tests to characterize the natural circulation flows between the vessel and the SG [22][23]. The tests were studied using CFD techniques [24]. The CFD benchmark to the 1/7th-scale showed very close agreement to measured values and provided confidence in the code and modeling approach. The CFD techniques were subsequently scaled to full-scale from the 1/7th-scale using the geometry and severe accident conditions. The CFD modeling scale-up to a full-scale SG with the geometry of the 1/7th-scale facility shows similar mixing and entrainment in the inlet plenum as the experiment.

However, a full-scale model of the 1/7th-scale was not prototypical of a Westinghouse SG. The 1/7th-scale facility has a hot leg oriented in a vertical plane normal to the divider plate that separates the inlet and outlet plenums. This orientation of the hot leg makes the SG symmetric. The hot leg nozzle of the Westinghouse Model 44 SG is oriented approximately 30 degrees from a vertical plane normal to the divider plate. Consequently, a second set of predictions was performed for a prototypic Westinghouse Model 44 SG [25], which also has a shallower inlet plenum than the 1/7th-scale model. The Westinghouse Model 44 SG calculations were specified in a similar manner to the scale-up, which provided a direct indication of the effect of the geometric differences on the inlet

plenum mixing parameters. The Model 44 predictions indicated significant variations in the plume intensity and location versus the scale-up geometry.

The final CFD recommendations that guided the Surry natural circulation modeling are presented in NUREG-1922 [26]. The NUREG-1922 results extend earlier predictions of SG inlet plenum mixing with the inclusion of the entire natural circulation loop between the reactor vessel upper plenum and the SG. The Model 51 H geometry is used as the basis for the new CFD calculations. The CFD predictions are utilized as a numerical experiment to improve the basis for simplified models used in the MELCOR Surry model. NUREG-1922 provided specific recommendations for (a) the hot leg discharge coefficient, (b) the SG mixing fraction, (c) the ratio of the hot leg flow to the SG recirculation flow, (d) the percentage of tubes involved in up-flow versus the circulatory return flow ratio, (e) the bounding normalized temperature of the hottest tube, and (f) the hot and cold stream flow split into the surge line. The insights from the CFD work were also used to select the variability in the peak plume temperature as an uncertain parameter for the Surry UA.

Applicability to Westinghouse plants

The insights from the NUREG-1922 natural circulation work and its implications for C-SGTR were uniquely developed for a Westinghouse design with Model 51 SGs. Surry uses Model 51 H SGs, which are consistent with this geometry. However, Reference [25] noted that the primary side dimensions of a Model 44 SG are very similar to the dimensions of the Westinghouse Model 51 designs. Consequently, guidance provided in NUREG-1922 is judged to be applicable to all Westinghouse plants using these SG designs. Westinghouse has other SG designs that were not assessed. A comparison of the other Westinghouse model geometries would be needed to assess the direct applicability of NUREG-1922 recommendations. The similarity of the hot leg and inlet plenum dimensions are identified in the CFD work as most important.

New AP1000 nuclear reactors are being built at the Vogtle site in Georgia. The AP1000 SGs are significantly different than the other operating Westinghouse plants. The AP1000 plant is rated at 3626 MW and uses only two large SGs (i.e., 1813 MW/SG). In contrast, the Surry plant is rated at 2587 MW and uses three SGs (862 MW/SG). The large two-loop AP1000 is expected to be more similar to the Combustion Engineering (CE) SG design.

The flaw distribution is the key second component for predicting a C-SGTR. The Surry UA flaw distribution was developed from a combination of generic data from SGs with Alloy 600 tubes and plant specific ISI data. Surry has a very long ISI history (circa 1980). However, the recorded occurrences of tubes with severe flaws was impacted by loose parts damage and inadvertent damage by a lancing machine while removing sludge at the bottom of the SG. The corresponding flaw frequency and severity damage may be atypical of other plants.

The generic data used in the Surry UA flaw distribution was for Alloy 600 tubes from NUREG-2195 [18]. However, guidance is provided for both Alloy 600 and Alloy 690 tubes. The correlation for the flaw distribution used in the Surry UA is based on the effective full-power years (EFPYs) of operation, which was defined uniquely for the Surry plant. Consequently, this would generate conservative results for almost all other plants (i.e., Surry had the first SG replacements of the older plants with Alloy 600 tubes).[23]

[23] Westinghouse subsequently shifted to Alloy 690 tubes, which have superior performance to Alloy 600 tubes. Of the 577,070 thermally treated Alloy 690 steam generator tubes placed in service, only 333 tubes (0.06 %) have been plugged after approximately 173 calendar years of operation [52].

The Surry UA and other NRC research for Westinghouse plants show that a flaw is required for a C-SGTR. Although the research is not exhaustive for all SG designs and every accident sequence, the research is very comprehensive (e.g., see analysis in [18][27][3]). Therefore, the flaw distribution is very important. The assumptions in the Surry UA include the long EFPYs of operation. The analysis in the Surry UA also shows that the historical frequency of deep flaws is consistent with the larger generic data of all Alloy 600 tubes [18]). In summary, the Surry UA C-SGTR insights are applicable for Westinghouse plants with SGs similar to the Model 51 SG, which includes the Model 44 SG.

Applicability to Combustion Engineering plants

NRC has also done research on C-SGTRs in CE plants. CE plant designs only have two SGs, which are larger than the Westinghouse Model 51 SGs and have a different inlet plenum geometry. The two CE hot legs are also much larger to accommodate the large 2-SG design. For example, a Westinghouse Model 51 SG plant has a 29-inch hot leg and 3388 tubes. A CE SG has a 42-inch hot leg and 8471 tubes [28]. The larger dimensions allow less mixing in the hot leg as the hot plume enters the SG plenum. The CE SG plenum is wider and shallower, which results in less mixing and a hotter plume that enters the SG tubes. The CFD results show a small portion of the flow from the vessel enters the SG tube bundle with very little mixing. The smaller amount of mixing in the SG inlet plenum is attributed the large hot leg positioned relatively close to the tube bundle entrance. Whereas the peak normalized hot plume temperature[24] in the Westinghouse plants is 0.43, the value in the CE plants is between 0.95 to 1.0 [28]. T_n =1.0 means the hottest portion of the plume enters the SG tubes without mixing or cooling, which places higher thermal stresses on the tubes.

NUREG-2195 performed MELCOR analyses using the CFD CE-specific guidance from Reference [28]. Similar to the Westinghouse plants, the analyses did not predict a C-SGTR in an unflawed tube prior to the hot leg failure. The study also noted that any radionuclide releases from a C-SGTR without a failure of an MSS SV are expected to be small, as indicated by the MELCOR runs.

NUREG-2195 developed probabilistic risk assessment (PRA) tools for predicting the occurrence of a C-SGTR. The study found that the conditional probability of a C-SGTR in core damage scenarios with a high primary pressure and a low secondary pressure without secondary water is about a factor of 10 larger for plants with a shallow inlet SG plenum (e.g., the selected CE plant) than the plants with a deep inlet SG plenum (e.g., the example Westinghouse plant). The observations on the flaw depth for a C-SGTR from the Surry UA would suggest less severe flaws will fail tubes in a CE plant. Consequently, the Surry UA quantitative insights on flaw depth would not be conservative for a CE plant or other SG designs with large, shallow SG inlet plenums.

NUREG-2195 also evaluated other locations along the natural circulation pathway for thermally-induced failures (e.g., the SG primary manway, the resistance temperature detector, the power-operated relief valve). The detailed thermal analyses indicated that the upper half of the hot leg will fail much earlier than the other RCS regions.

[24] The normalized hot plume temperature is defined as, $T_n = {(T - T_{ct})}/{(T_h - T_{ct})}$, where T_n is the normalized hot plume temperature, T_{ct} is the cold return tube temperature, and T_h is the hot plume temperature leaving the vessel.

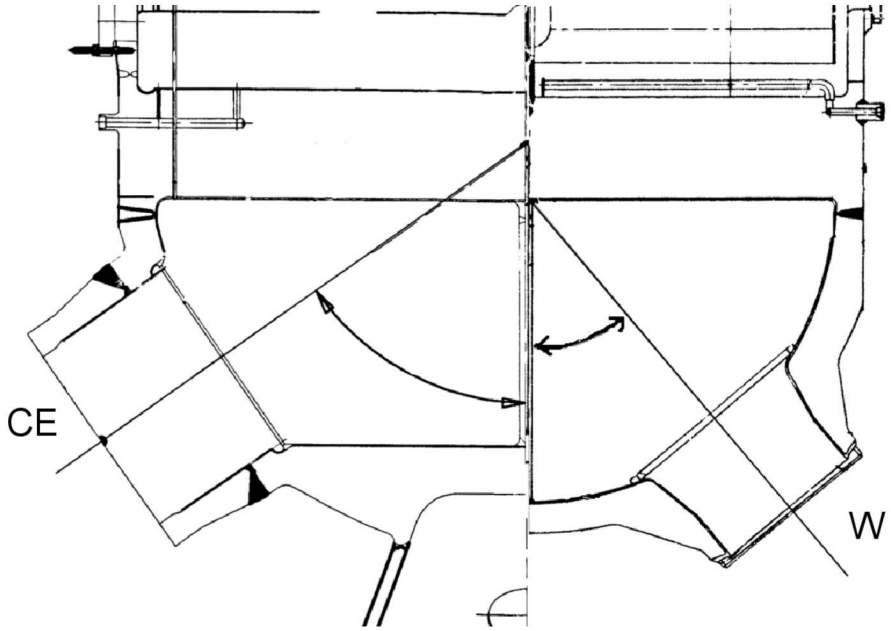

Figure 3-32. Comparison of the CE and Westinghouse Model 51 steam generator inlet plenums

3.2.4. Hydrogen Behavior

The onset of the hydrogen release and total in-vessel production are indicators of the start and magnitude of the fuel damage, respectively. The release of hydrogen is also an indicator for radionuclide releases as these occur during the fuel damage progression. The amount of hydrogen produced in-vessel, along with the ex-vessel production of hydrogen and other non-condensable gases during ex-vessel core-concrete interactions (CCI), are also the primary influences on whether combustible conditions are reached in containment (i.e., for PWRs and BWR Mark III containments) and contribute to the containment pressurization (i.e., all designs). The prediction of hydrogen combustion in PWRs is important for the pressure increases that augment containment leakage and fission product releases to the environment and possibly challenge the containment integrity.

The in-vessel hydrogen production was identified as a key figure of merit (FOM) in all the UAs. The in-vessel hydrogen production is primarily due to oxidation reactions of the zircaloy fuel cladding, although there is also some hydrogen produced by oxidation of stainless steel structures. The cladding oxidation continues at rapid rate until the Zircaloy interior of the zirconium oxide shell melts, breaks through the oxide layer, and relocates downward to cooler surfaces. Eventually, the fuel rods collapse, which creates a debris bed. The amount of in-vessel zircaloy oxidation rate is relatively low following the core collapse and relocation due to the inability of steam to flow freely into the debris bed and reduced amount of open surface area.

The magnitude of the in-vessel hydrogen production is impacted by variations in the time-in-the- cycle (i.e., discussed in Section 3.2.1), uncertainties in the valve performance (i.e., discussed in Section 3.2.1), and uncertain core degradation behavior.

The insights on hydrogen behavior from the Surry UA is described in Section 3.2.4.1, which is typical of a PWR with a steel-reinforced concrete containment. The Surry UA included several uncertain parameters to investigate hydrogen combustion loads. The insights on hydrogen behavior from the Sequoyah UA is described in Section 3.2.4.2, which is typical of an ice-condenser PWR

with a free-standing steel containment. A focus of the Sequoyah UA was the evaluation of parameters contributing to an early containment failure due to a hydrogen burn. The implications of the insights from the PWR UAs for other plants is discussed in Section 3.2.4.3.

3.2.4.1. Surry UA

Significant modeling effort was made in the draft and final Surry UA to examine the potential for a large hydrogen burn to over-pressurize the containment. The relatively large Surry containment only experienced localized burns following the hot leg failure before becoming steam-inerted. No persistent or large burns challenged the containment integrity. Following vessel failure, the heating from the ex-vessel core debris evaporated the water on the containment floor from the RCP seal leakage, water flashing and spillage after the PRT rupture disk opening, and the hot leg failure. The leaked water evaporated and contributed to the high steam concentration to prevent hydrogen burns.

The modeling related to investigating hydrogen combustion included an uncertain parameter on the containment wall heat transfer and condensation rate, uncertainty sampling on the oxidation kinetics for in-vessel hydrogen production, and uncertainty sampling for ignition that spanned to the lower flammability limit for hydrogen-air mixtures.

Figure 3-33 shows the containment pressure response in the Surry UA reference case without a C-SGTR. The key events related to the hydrogen behavior include rapid pressure rise when the hot leg nozzle on Loop C ruptures. The hot leg failure immediately depressurizes the RCS and discharges water, steam, hydrogen, and radionuclides to the containment. There was relatively little hydrogen produced at the time of the hot leg failure, so the first burn does not occur until roughly 2 hr later at 6 hr. Some small burns are evident in the pressure trace between 6 to 10 hr. The last burn propagated to the containment dome and shows the largest hydrogen-induced pressure spike.

The ex-vessel debris appears after 9 hr and is considered a persistent ignition source for combustion. The energy produced by deflagrations in containment and the room steam concentrations are illustrated in Figure 3-34. There are two periods of large deflagrations, two large burns at 2 hr after hot leg nozzle creep failure and another large burn at 1 hr after lower head failure. The second burn is larger because it propagates to the dome. The steam concentrations throughout the containment are included on the figure, which show two step increases. The first one occurs when the PRT rupture disk opens at 2 hr 16 min. The second sharp increase occurs when the hot leg creep ruptures at 4 hr 17 min. Most of the containment is steam-inerted after the hot leg failure until 6 hr. However, condensation on the cooler walls briefly drops the steam concentration below the inerting limit by 6 hr, which leads to the first combustion. The final large burn occurred at 10 hr when the oxygen concentration in the cavity region increased to the combustible threshold. The burn in the cavity propagated into the other regions of the containment.

After this period of hydrogen burns, the containment slowly pressurized due to the heating and concrete ablation gases generated from the ex-vessel debris until the containment liner yield at 47 hr. The steel liner is imbedded in the concrete containment but functions as the leak-tight barrier to retain fission products. The liner yield increases the leakage rate from the containment above the 0.1%/day design rate to 1% per day (i.e., not a catastrophic increase). The leakage slowly increases to 10%/day at 8.0 bar (101.5 psig) when the rebar yields and the leakage starts to increase more rapidly.

The reference case response is typical of the other realizations. As shown in Figure 3-6, the peak pressure from a hydrogen burn in time interval where a hydrogen burn was possible (i.e., ~4 hr to

12 hr) never exceeded about ~5 bar (~73 psia), which is well below the median containment failure pressure of 6 bar (i.e., 87 psia shown on Figure 3-33). The lowest sampled containment pressure was 4.3 bar (64 psia), which is within the range of the peak pressurizations. However, no realizations had an early rebar yield due to a hydrogen burn. A liner yield at less than 5 bar was judged possible but assigned a very lower likelihood (see Section 3.2.5.2, the earliest liner yield was >30 hr). If the containment had failed, then the leakage rate only increased to 1%/day, which was at the upper bound of the sampled design leakage rate. Consequently, the impact of an earlier increase in the containment leakage to 1% was considered using the uncertainty parameter for the design leakage multiplier.

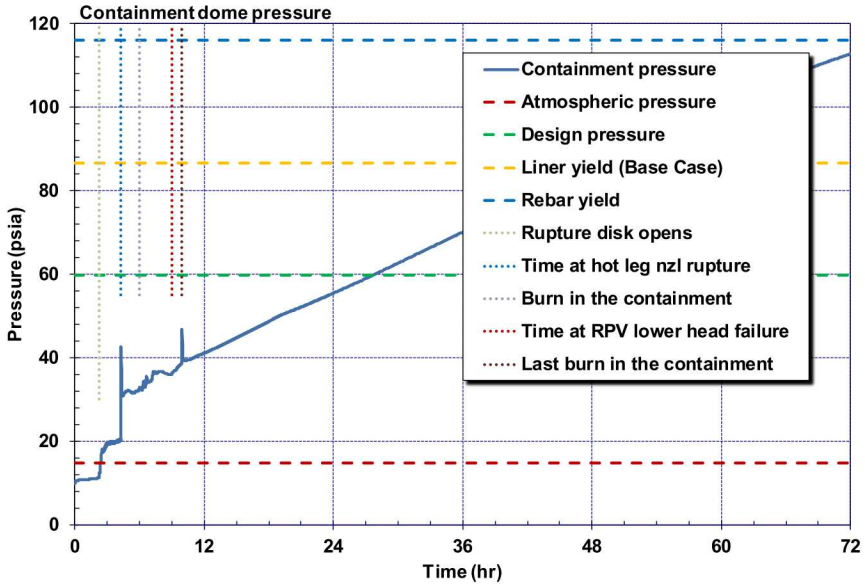

Figure 3-33. Containment pressure (Non-C-SGTR Reference Case)

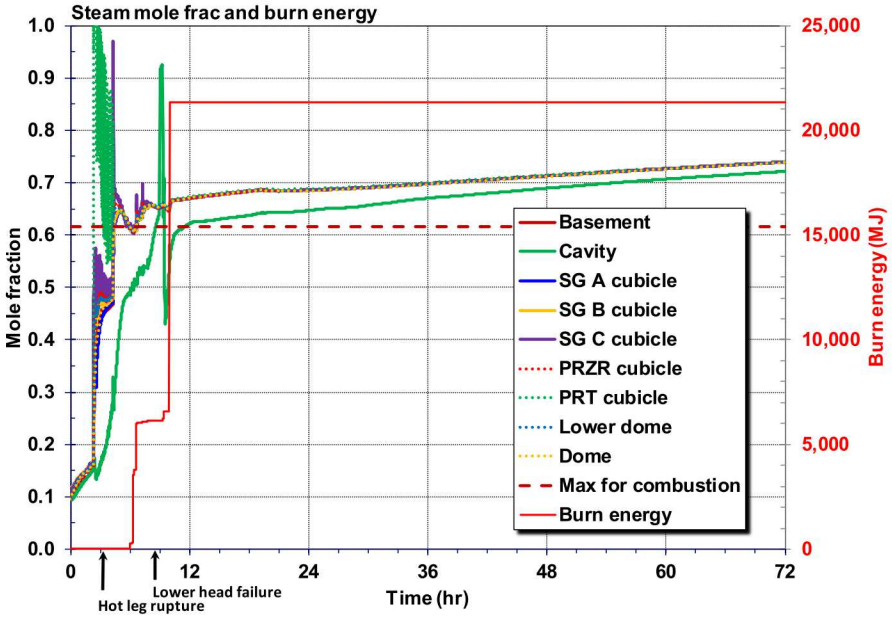

Figure 3-34. Containment steam mole fraction and energy produced by deflagrations (Non-C-SGTR Reference Case)

3.2.4.2. Sequoyah UA

In the Sequoyah UA, the in-vessel hydrogen is generally on the order of 300 kg. The ex-vessel hydrogen, which follows after lower head failure and initiation of CCI, is significantly larger as it continues to increase above 1000 kg by 72 hr. The ex-vessel CCI also generates very large amounts of carbon-monoxide, which is also combustible. However, the most important factor to early containment failure is the release and distribution of the hydrogen generated in-vessel prior to the first ignition source. If there is not a containment failure with the first burn, then smaller burns occur until the local oxygen concentration drops below 5% in the lower containment (i.e., the location of the ignition sources).

The Sequoyah UA only rarely predicted an early containment failure due to a large hydrogen deflagration. In the four realizations with an early containment failure, a large hydrogen deflagration initiated in the lower compartments of the containment that propagates to the large containment dome volume. Figure 3-35 shows containment rupture time across the full set of realizations. The four early (i.e., near the time of core damage) containment ruptures are colored red. The common elements of the four early containment failure realizations were a relatively high in-vessel hydrogen production (Figure 3-36), a pressurizer FTC with a large open area that vented a large quantity of hydrogen to the containment via the PRT (Figure 3-37), and significant migration of the hydrogen to the large containment dome prior to the first burn (Figure 3-38). In no realization did a burn subsequent to the first burn result in containment rupture.

In order to generate the large hydrogen burn conditions described above, the pressurizer SV must fail and have a fractional open greater than 0.3, which is the necessary but not sufficient condition for early containment failure. Of the 85 realizations with a pressurizer FTC, only 23 realizations had a fractional area >0.3. The ignition source for two of the realizations was hot gases above the

hydrogen autoignition temperature entering the containment from the PRT; and the other two resulted from hot gases entering the containment after the hot leg failure.

The relationship of the number of pressurizer cycles to an FTC on early containment failure

The failure area of the SV together with failure cycle were identified to strongly influence whether an early containment failure is possible. In the draft Sequoyah UA [29], a correlation was observed between the number of pressurizer SV cycles versus the SV failure area needed for an early containment failure. Most of the realizations with >46 cycles and <0.3 SV failure area progressed to a late containment failure. These two factors combined to identify high pressure sequences during the core damage phase. The progression of events in these sequences includes a hot leg failure from high primary system pressure followed by a rapid discharge of the accumulators into the degraded core. There is less hydrogen in the lower containment at the moment of the RPV breach. The discharge of gas through the hot leg failure includes a concentration of steam, which is immediately followed by a large steam source from the accumulator water quenching the degraded core. The large and rapid accumulator water source into the core also eliminated the ignition source at the hot leg (i.e., the gases exiting the hot leg no longer satisfied the auto-ignition temperature criterion). The lower containment remained steam inerted and/or without an active ignition source and always progressed to an oxygen deficient state.

The other realizations with fewer SV cycles prior to a failure (i.e., 1 to 45 cycles) and larger failure areas (>0.3) vented more hydrogen to the containment prior to the first ignition source (e.g., a hot leg failure). There were more complicated factors that contributed to whether there was an early or late containment failure (i.e., see the results of the focused pressurizer SV study at the end of this section).

The realizations with an early containment failure had the highest source terms in the Sequoyah UA. An early containment failure permitted a rapid release of airborne radionuclides during core degradation phase prior to any significant benefit from settling. Consequently, it was expected that early containment failures with <45 pressurizer SV cycles would correlate with a higher release. The regressions for the cesium and iodine environmental releases showed that the primary SV cycles parameter has high interaction effects (identified from non-linear regression techniques). As shown in Figure 3-39, the highest iodine releases resulted from early containment failures (i.e., the four iodine releases $\geq$0.08). However, the number of early containment failure realizations was too limited to make meaningful correlations, which is discussed next in the focused pressurizer SV study. With regards to the magnitude of the environmental release, no other parameters were identified as having significant main effects on cesium or iodine.

Differences in the draft Sequoyah UA hydrogen modeling

The draft Sequoyah UA had a number of significant modeling differences from the final Sequoyah UA. A few of the key differences in the draft UA were (a) a higher likelihood for SV FTC, (b) a uniform SV failure area distribution, (c) only one oxidation model (i.e., only the Urbanic-Heidrick model), and (d) the potential for spontaneous ignition. The most important differences were the SV FTC and SV failure area distributions (see Section 3.2.2.1). Due to the changes in the SV modeling, the majority of the cases in the final UA (89%) result in no FTC of the SVs. The no FTC outcome in the final UA was four times more likely than in the draft UA. Furthermore with the changes in the SV failure area distribution, there are far fewer cases (4%) of SV FTC with an open area fraction greater than 0.3 compared to the draft UA (62%) [2]. The draft UA showed that this is a necessary (but not sufficient) condition for an early containment failure (i.e., hydrogen that is produced in-

vessel moves more readily from the RCS to the containment through the PRT as the system is depressurized).

A comparative analysis between the draft and final UAs showed the trends hydrogen production prior to the first burn were consistent but with each study more densely populating different outcomes. In the cases with the system depressurization through SV FTC (i.e., especially realizations with an early SV FTC and a fractional area >0.3), the timing for the start of the hydrogen production is generally accelerated. However, the accumulation of creep damage to the hot leg and the heat transfer from the core to the hot leg are less efficient at low pressure. The combined effects of these factors lead to a longer amount of time from the start of core damage to the first deflagration and a larger amount of hydrogen production. Finally, the higher rate of hydrogen discharge to the containment and lower retention in the vessel also significantly increases the amount of hydrogen in the containment at the time of the first deflagration. These cases (i.e., more likely in the draft UA) generally had much more severe burns that challenged the containment integrity. In both the final and the draft UA, only realizations with an SV FTC and area fraction greater than approximately 0.3 had early containment failure. The higher SV open area fraction led to an accident progression that would allow more time for hydrogen to be produced and transported to the dome.

The comparative analysis showed some distinct differences in the amount of hydrogen generated by the various oxidation models. The effect of oxidation kinetic model is pronounced for the SV with no FTC. In the final UA, three oxidation models are used as compared to only the Urbanic-Heidrich (UH) in the draft UA. The Leistikov-Schanz/Prater-Courtright (LS/PC) model produces less hydrogen at low temperatures as compared to the other models, which leads to lower hydrogen generation. The Catchart-Pawel/Urbanic-Heidrick (CP/UH) and UH models had successively higher hydrogen oxidation rates at low to mid temperatures that led to successively higher hydrogen generation amounts prior to the first deflagration, respectively.

Both the draft and the current UAs also capture the decrease in the time to hot leg failure with increasing hydrogen production. Both UAs show a downward trend in the hydrogen production to the timing of the first burn. The higher oxidation rates cause a faster accident progression that accelerates the heating of the RCS pressure boundaries including the hot leg. This trend resulted in shorter timings from the start of hydrogen generation to the hot leg creep rupture and the first deflagration.

Finally, the draft UA investigated two mechanisms for ignition, (a) ignition with a well-defined source and (b) random ignition. Ignition from a well-defined source is modeled based on hot gases exiting the RCS hot leg failure location above the hydrogen auto-ignition temperature or ex-vessel debris with vigorous concrete ablation. These two conditions are assumed to provide well-defined ignition sources throughout the lower containment. The random ignition, when activated, randomly provides a 1 second ignition source every 30 minutes at a specific location inside the containment. For combustion to occur when an active or random ignition source is present, the local gas concentration must satisfy the combustibility limits based on combustion research; however, the combustibility limits from this research were varied.

Separate uncertainty studies were performed in the draft UA with and without the presence of random ignition sources. It was observed that random sparks trigger ignition prior to the reactor coolant system breach, which made the accident progression much less likely to proceed to early containment failure. Consequently, the inclusion of random sparks was less conservative relative to the early containment failure probability. Figure 3-40 shows the cumulative distribution of the

containment failure timing for the two studies. Other than a lower likelihood of an early containment failure, the distribution of the failure timings was similar. Furthermore, the potential for a random spark in the dome did not increase the likelihood of an early containment failure. As discussed previously, all the late containment failures (i.e., after 22 hr on Figure 3-40) were caused by heating and gas generation from ex-vessel CCI rather than burns. The random ignition was dropped for the final UA. The final UA also included hot gases exiting the PRT rupture disk opening as an additional active ignition source.

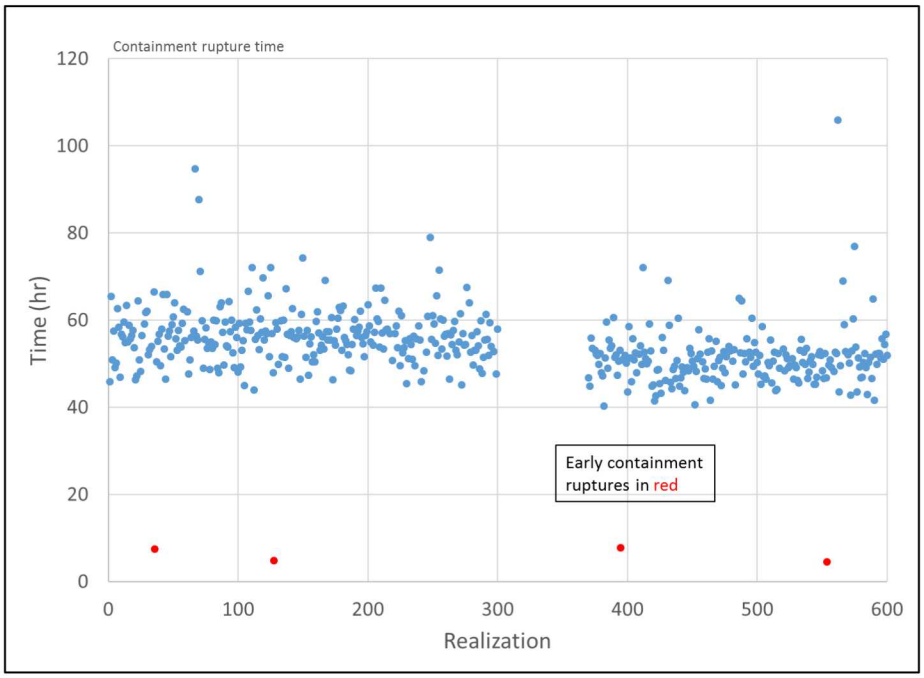

Figure 3-35. Containment rupture timing across in the Sequoyah UA

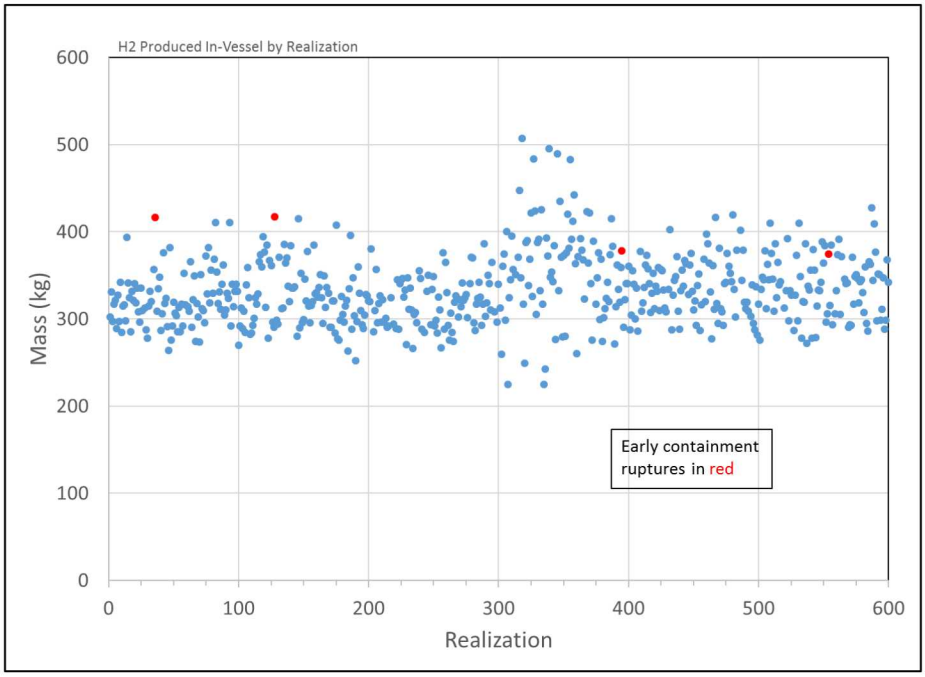

Figure 3-36. In-vessel hydrogen production across the full set in the Sequoyah UA

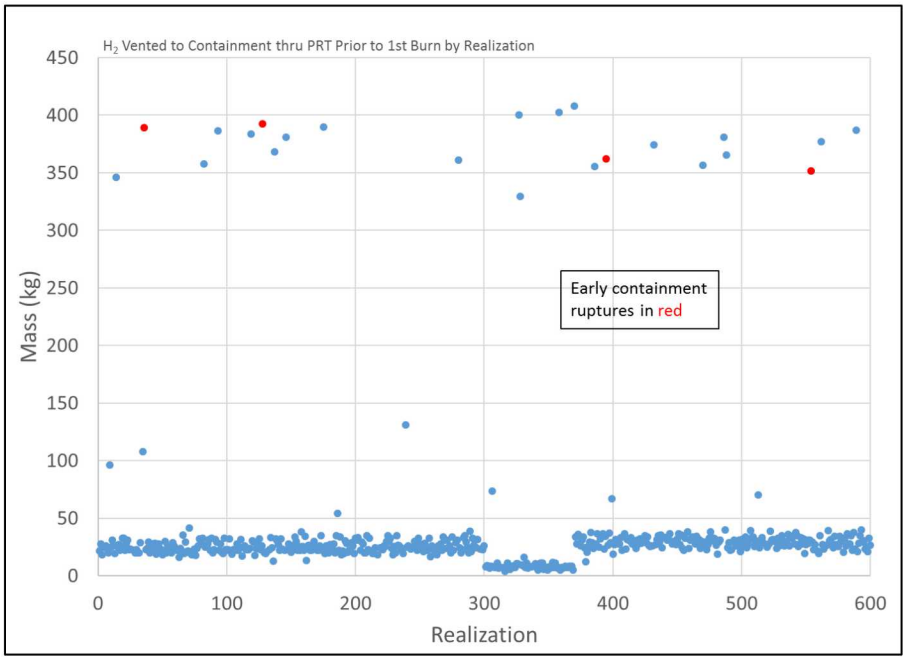

Figure 3-37. Hydrogen vented from the primary system to containment through the PRT by the time of the first burn in the Sequoyah UA

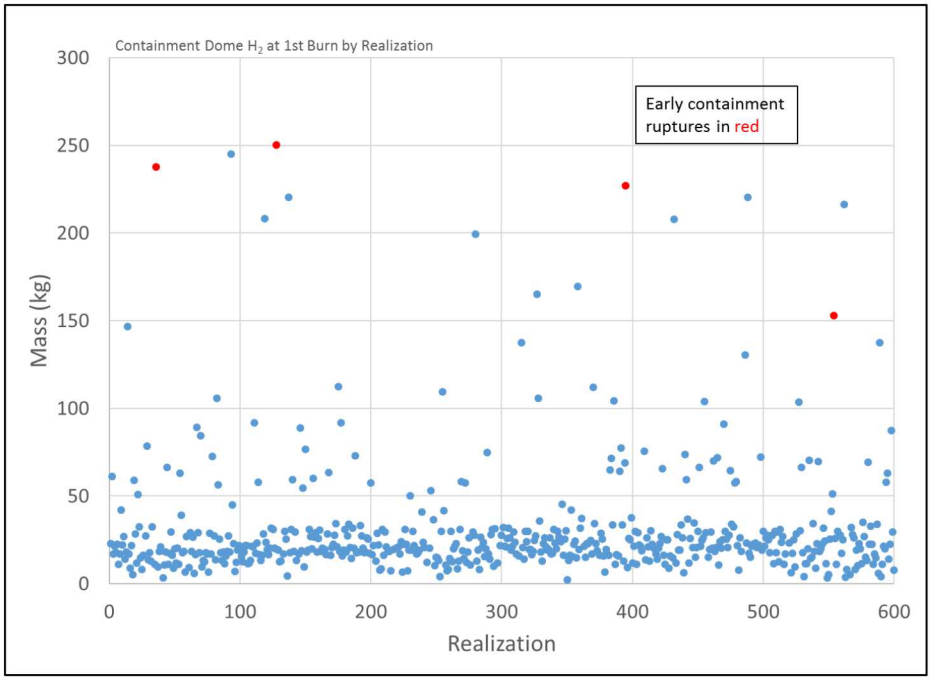

Figure 3-38. Hydrogen in the containment dome by the time of the first burn in the Sequoyah UA

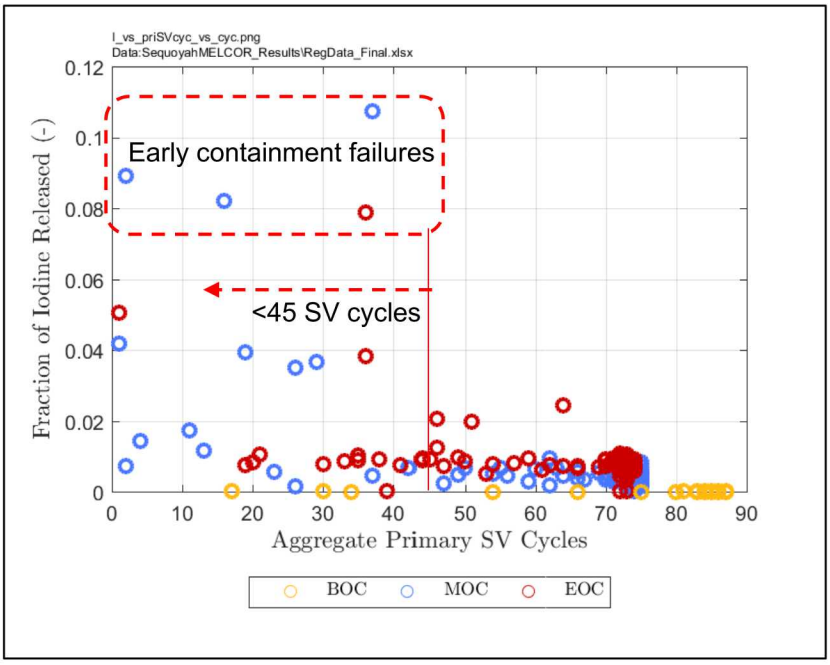

Figure 3-39. Scatterplot of iodine environmental release fraction versus the number of pressurizer SV cycles in Sequoyah UA

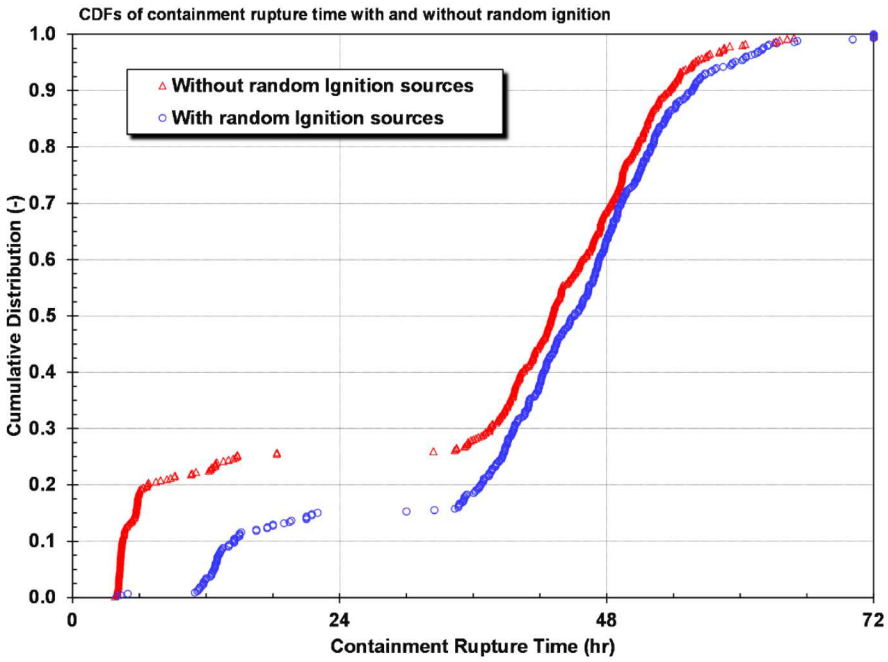

Figure 3-40. Comparison of containment failure timing as a function with or without random ignition sources from eth draft Sequoyah UA

Overview of focused pressurizer SV study

The Sequoyah UA only included four realizations with an early containment failure, which was in sharp contrast to the draft UA results [29] that resulted in early containment failure for 25% of the realizations. The key differences are primarily attributable to changes to the pressurizer SV failure characteristics noted in Section 3.2.2.1. A detailed discussion of all differences is presented in the Sequoyah UA report [2]. The Sequoyah UA included a focused pressurizer SV study to better understand conditions leading to an early containment failure. The focused pressurizer SV study was performed limiting the range of the pressurizer FTC to 1 to 65 cycles and the failure area to 0.3 to 1.0, respectively. These ranges created conditions for a pressurizer FTC prior to the hot leg failure with a large flow area to discharge the hydrogen into the containment before the first ignition source.

Approximately 17% of the 361 completed realizations had a containment failure occurring in less than 15 hr. The 17% early containment failure rate in this study compares well with the 17% failure rate in the full study (i.e., 4 early containment failures out of 23 realizations with the same attributes as the focused SV study). The focused SV study also shows the potential for early containment failure at the BOC, which was not calculated in the full UA.

Within the focused constraints of the FTC distribution and failure area sampling, the regression results show the failure pressure (Rupture) as the most important factor effecting early containment failure timing. An examination of the results shows that almost all the sampled rupture pressures leading to early containment failure were less than the mode of the failure pressure (see Figure 3-41). The number of pressurizer SV cycles (i.e., priSVcycles) is the next strongest correlation. An increase in the number pressurizer SV cycles leads to later containment failure, which is consistent with full UA results.

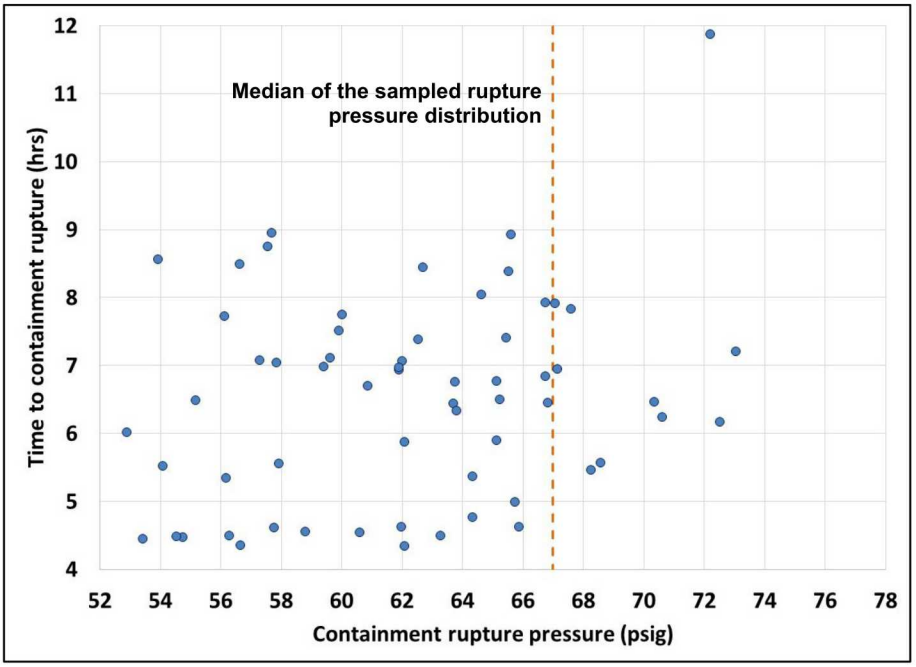

Figure 3-41. Time to containment failure plotted against the sampled containment rupture pressure[25]

The focused pressurizer SV study also provided a better understanding of the source term from the realizations that included pressurizer SV failures. All the realizations with an early containment failure were rerun and the simulation time was extended to 72 hr. In addition to the early containment failure realizations, 57 other randomly selected realizations were also extended to 72 hr. The average cesium and iodine release fractions at 72 hr for successful realizations with early containment rupture were 0.022 and 0.063, respectively. The highest release fractions were 0.058 and 0.15 for cesium and iodine, respectively. The lowest releases were 0.01 and 0.025 for cesium and iodine, respectively. The average values from the focused study confirm the four early containment failure results in the full UA. However, the focused pressurizer SV study provide new insights into a broader range of results.

Although the early containment failure realizations from this study have higher iodine and cesium releases than the late containment failure realizations, there is some overlap as shown in Figure 3-42. There was little overlap in the full UA where, in the early containment failure, cesium and iodine releases were well above the 95th percentile (i.e., only one late containment failure realization was above the lowest early containment failure's cesium and iodine releases). In contrast, this study has many late failure realizations that overlap the early containment failure results. It is important to note that the late containment failure results presented in Figure 3-42 are limited to realizations with a pressurizer SV failure prior the hot leg failure. Consequently, it is only a partial description of the full spectrum of results considered in the full UA. The results show that the magnitude of the maximum releases from the late containment failure are within the range of results from the early containment failure realizations.

[25] Only the realizations with an early containment failure are shown in Figure 3-41.

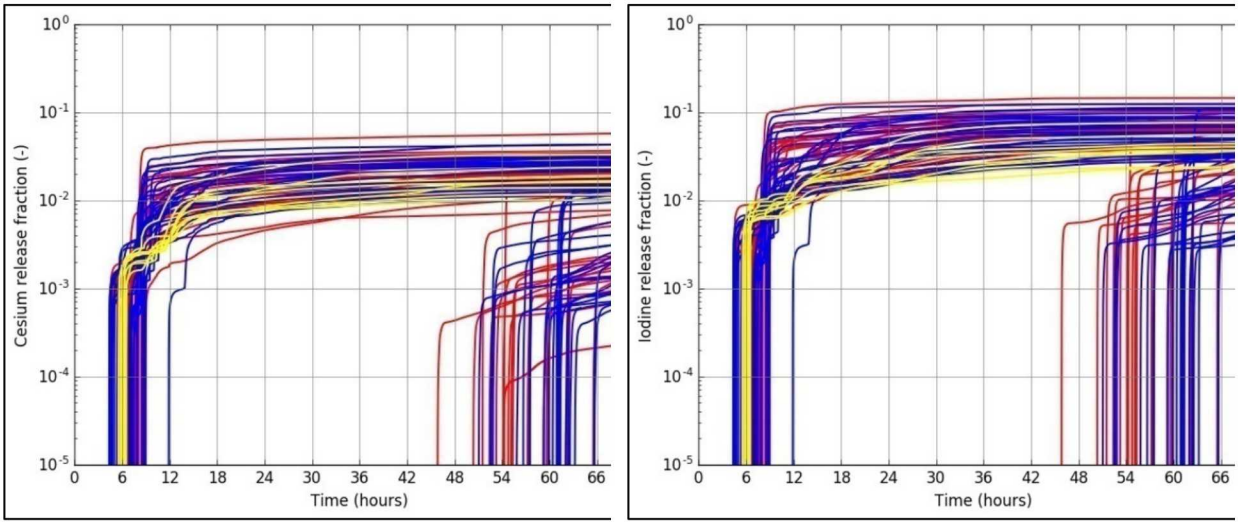

Figure 3-42. Cesium release fraction (left) and iodine release fraction (right) to the environment (yellow=BOC, blue=MOC, red=EOC)

Kinetics model importance

Realizations in the Sequoyah UA used one of three sampled oxidation models: (1) Urbanic-Heidrich, (2) Catchart-Pawel/Urbanic-Heidrich, or (3) Leistikov-Schanz/Prater-Courtright. Compared to the Leistikov-Schanz/Prater-Courtright model, the Urbanic-Heidrich and Catchart-Pawel/Urbanic-Heidrich models estimate a faster rate of oxidation at low to mid temperatures. Realizations without an SV FTC that used the Urbanic-Heidrich and Catchart-Pawel/Urbanic-Heidrich predicted more hydrogen generation prior to the first burn. The result was somewhat surprising. Although the high temperature Prater-Courtright correlation specified the fastest oxidation rate at high temperatures, it was the lower temperature oxidation (i.e., <1900 K) kinetics that generated the highest in-vessel hydrogen quantities.

Long-term ex-vessel hydrogen production

More hydrogen and other combustible gases are generated from molten core concrete interactions (MCCI) than through in-vessel zirconium and steel oxidation. Because the Sequoyah UA treated molten debris ejected from the RPV as a persistent ignition source, the first burn always happened at or before the start of CCI. As such, the hydrogen from CCI did not have an impact on whether containment failed early.

Unlike early containment failures, the late containment failures were caused by a slow over-pressurization and not pressure spikes from deflagrations. If a containment survived the first burn, then the subsequent deflagrations were never energetic enough to rupture the containment. The burns after the first ignition were generally from hydrogen produced from hot CCI gases and aerosols igniting hydrogen in the cavity region. The containment eventually became oxygen-inerted from the oxygen consumption during the burns and the lower relative oxygen partial pressure from the build-up of steam and CCI gases. The late containment pressurization occurred due to the generation of hot non-condensable gases from CCI and the evaporation of water on the lower containment floor.

Hydrogen igniter sensitivity study

The Sequoyah UA did not include emergency operator actions to restore the hydrogen igniter system. Without AC power, the hydrogen igniters must be powered by a small generator, which requires operator actions to start and align the generator to the hydrogen igniters. The emergency generator and associated procedures are part of the required post-Fukushima Dai-chi upgrades to Sequoyah.

The Sequoyah MELCOR model includes igniters that will burn hydrogen when the concentration exceeds approximately 7%. The igniters are spatially distributed throughout the containment per the Sequoyah design. The hydrogen mitigation sensitivity analysis showed that the igniters prevented early containment failure by preventing hydrogen buildup and circulation into the dome prior to the first burn. The igniters burned the hydrogen at a concentration of 7% in the lower containment, which prevented large severe burns in the large upper containment dome (i.e., a large burn in the upper containment was necessary to fail the containment). The recovery of the hydrogen mitigation system must take place by 3 hr to prevent the potentially rapid flow of hydrogen in the containment.

Long-term SBO hydrogen insights

A series of LTSBO simulations were performed to evaluate the changes in response and source term from the STSBO in the Sequoyah UAs [2]. The LTSBO calculations investigated the uncertainty of hot gases exiting the PRT as an ignition source. The hot gases exiting the PRT was identified as a potential ignition source after the draft Sequoyah UA, which had more early containment failures [29]. A sensitivity study was performed that only allowed an ignition when the hot leg failure gases exceeded the hydrogen autoignition temperature or when ex-vessel core debris was present. When the hot gases exiting the PRT ignition source was disabled from consideration in the combustion logic, the hydrogen continued to build up in the containment for 1.7 hr longer until the hot leg rupture created a hot jet ignition source. The peak pressure from the delayed burn increased from 3.88 bar (~56 psia) in LTSBO-1 to 5.83 bar (~85 psia) in LTSBO-1a, which ruptured the containment at 24.5 hr (see Figure 3-43). Also included in Figure 3-43 is the impact of the igniters (green curve). The recovery of the igniter system prior to significant hydrogen production (<21 hr) burned the hydrogen at a lower concentration to prevent a containment over-pressurization from a hydrogen burn. A characteristic of the long-term SBO was significantly later core damage and containment failures due to the initial availability of the auxiliary feedwater injection to the SGs.

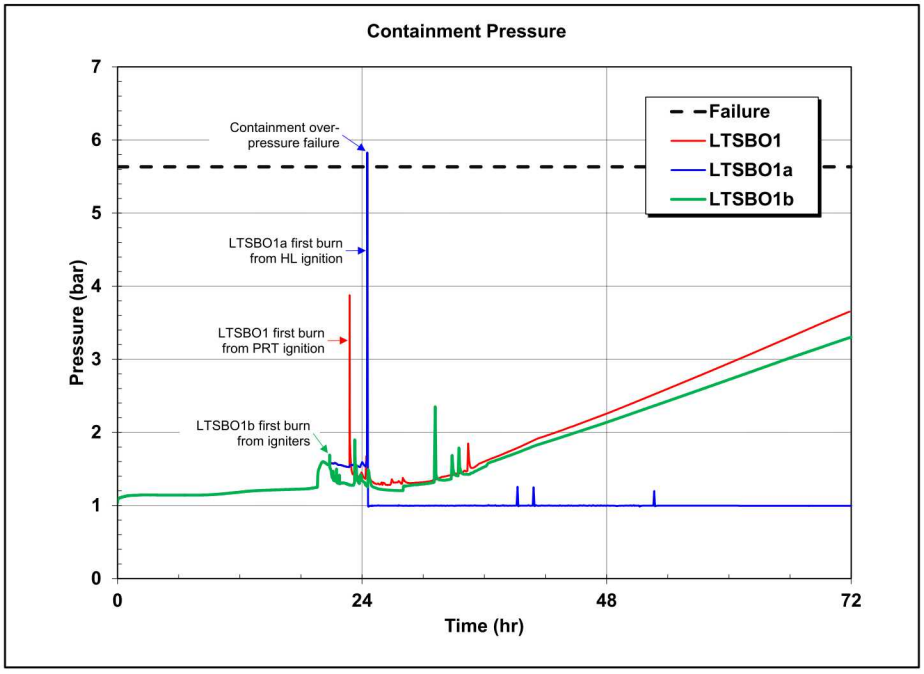

Figure 3-43. Comparison of LTSBO ignition sensitivity containment pressure responses

3.2.4.3. Peach Bottom UA

The Peach Bottom containment is inerted and therefore not susceptible to hydrogen burns. However, hydrogen burns occurred in the Peach Bottom reactor building after the containment failure. The reactor building offers some retention for radionuclides released from the containment but is impacted by hydrogen burns that push radionuclides into the environment and cause structural failures (e.g., consider the destruction to the Fukushima Dai-chi reactor buildings). The impact of the reactor building response was investigated through several uncertain parameters including the minimum concentration for a spontaneous ignition in the reactor building and differential pressure criteria to fail the large rail doors.

The BWR reactor building is not a containment and has a high leakage rate relatively to a containment. It includes blowout panels near the roof that open at small over-pressure that further increase the leakage. A large hydrogen burn can fail the large railroad doors at the grade level of the reactor building. The opening of the railroad doors creates a robust natural circulation pattern through the building that further diminishes any retention.

Neither the iodine nor the cesium release to the environment regressions showed the reactor building hydrogen ignition threshold as an important parameter explaining the magnitude of the releases. The differential pressure criteria for the railroad doors had a low secondary importance. The relatively low retention in the reactor building and its fragility to a wide range of hydrogen burns contributed to the low importance of the hydrogen behavior. Instead, the SRV and MSL failures had the most significant importance, which is discussed in Section 3.2.2.3.

Other secondary BWR regression parameters impacting hydrogen production

The regression analysis for hydrogen production identifies the stochastic SRV FTC cycle uncertainty parameter as the most important parameter (see Section 3.2.2.3). Key secondary parameters influencing the total in-vessel hydrogen production included the zircaloy melt breakout temperature and the molten clad drainage rate as important parameters. The zircaloy melt breakout temperature

specifies the release criterion of the molten zircaloy. The release of the molten zircaloy from behind the outer cladding oxide shell ends the rapid hydrogen production phase. The regression shows less in-vessel hydrogen at lower zircaloy melt breakout temperatures. Similarly, the molten clad drain rate impacts the rate that the molten zircaloy drains to regions less supportive of oxidation. The faster that the zircaloy drains, the less time for oxidation.

3.2.4.4. Implications for Other Plants

The implications of the hydrogen behavior observed in the Surry UA are expected to be applicable to other large PWR containments with a steel-reinforced concrete containment. The STSBO severe accident releases steam and water to the containment via RCP seal leakage, SV venting, and primary system failures (e.g., hot leg and vessel lower head). Consequently, the water inventory of the primary system is transferred to the containment. In addition, saturated water will spill into the containment when the PRT rupture disk opens. Following the start of the ex-vessel CCI, the decay heat evaporates the spilled water to make high steam concentrations that limit or preclude hydrogen burning. The containment pressurization due to evaporating water and ex-vessel gases eventually reduces the relative oxygen concentration below the amount needed to sustain a burn. The hydrogen behavior observed in the Surry UA is expected to be consistent with other PWRs with the same containment design.

Surry uses an initial subatmospheric pressure to reduce the size of the containment relative to other PWRs without an initial subatmospheric pressure (i.e., most PWRs). With all other factors being similar, a subatmospheric containment has higher hydrogen concentrations and pressurizes more quickly than a larger non-subatmospheric containment. A smaller containment also benefits from higher steam concentrations for the same amount of evaporated water. These factors are expected to have some impact on the hydrogen behavior but not judged to be significant. The accident progressions in other PWRs are expected to include the ignition sources from the ex-vessel debris, the hot gases exiting the PRT (i.e., with a pressurizer SV FTC), and possibly hot gases exiting through the pump seals, instrument tubes, or penetrations (e.g., see analysis in [16]). The hydrogen released from the vessel was identified to ignite during the core degradation without reaching high concentrations. CE and Westinghouse plants are expected to have the same hot jets above the hydrogen auto-ignition temperature from a hot leg creep rupture failure (i.e., not expected in B&W plants).

The Sequoyah plant has a relatively small ice condenser containment. The ice condenser containment design is different than other PWRs because it: (1) has ice that condenses steam, (2) is relatively small, (3) has a lower design pressure rating, and (4) fails abruptly from an over-pressurization through a tear in the steel liner. The Sequoyah containment is similar to eight of the other 10 ice condenser units in the U.S. The insights from the Sequoyah UA on the conditions leading to larger releases of hydrogen to the containment prior to an identifiable ignition source will be qualitatively consistent with all PWRs. The insights on the likelihood and conditions for an early containment from the hydrogen burn is expected to be qualitatively similar in the eight ice condensers plants with free-standing steel containments. Although the qualitative response and insights are applicable to this type of containment, the quantitative results are dependent on the containment failure pressure (i.e., the most important parameter in the focused pressurizer SV UA). The benefits of well-placed igniters in other ice condensers is expected to be the same as observed in the Sequoyah sensitivity results (i.e., burns at lower concentrations that limit widespread hydrogen distribution in the containment and any associated buildup).

The hydrogen impact on the source term for the Sequoyah UA was foremost tied to containment failure timing. However, the focused study provided more insights into the range and uncertainty in the releases for conditions that promote an early containment failure, which is expected to be applicable to the other ice condenser plants. The focused study included both early and late containment failures but with some late containment failure source terms that overlapped the magnitude of the early containment failure results (i.e., not shown in the base UA due to the lack of realizations with these pressurizer FTC attributes). Although the magnitude of the cesium and iodine source term in the late containment failure results can reach the magnitude of the early containment releases, the median result was lower (see Figure 3-42). The applicability of this insight to other ice condenser plants can be qualitatively informed by results in the Sequoyah UA and the focused study. Ice condenser plants with a lower containment failure pressure than Sequoyah would be more susceptible to an early containment failure, although this result is not likely based on the Sequoyah UA results.[26] However, the range of uncertainty in the cesium and iodine source term from a late containment failure with a pressurizer SV FTC includes releases as large as some of the early containment failure results, albeit significantly later in time (e.g., >46 hr versus <12 hr for Sequoyah).

The BWR Mark III has similar characteristics to the ice condenser (i.e., a small containment filled with air), a relatively low failure pressure, and a design attribute that can condense steam (i.e., water in the wetwell instead of ice). The failure of an SRV is similar to a pressurizer SV FTC but the subsequent distribution of hydrogen and radionuclides through the containment would be different than the ice condenser containment. The ice condenser ice chest doors open relatively easily to condense steam and capture aerosols. The Mark III wetwell vents require to distribute hydrogen steam throughout the containment and remove the steam for a large burn, and the response of mechanisms for propagation are expected to be significantly different. Consequently, it is difficult to assess the containment vulnerability to hydrogen burns using insights from the Sequoyah UA. Similarly, the over-pressure failure characteristics are expected to be different than the Sequoyah PWR containment. Nevertheless, the benefit of well-placed igniters is expected to be the same as observed in the Sequoyah sensitivity results (i.e., burns at lower concentrations that limit widespread hydrogen distribution in the containment and any associated buildup).

3.2.5. Containment Failure Insights

The key FOM in the UAs was the source term to the environment. As the last barrier to radionuclide release to the environment, the integrity of the containment was a first-order parameter affecting the iodine and cesium release to the environment. In particular, the UAs investigated uncertain parameters judged to impact the timing of the containment failure. Each UA had unique insights that are described in Sections 3.2.5.1 through 3.2.5.3. The implications for other plants are discussed in Section 3.2.5.4. A C-SGTR, while not a containment failure, is a containment bypass and equally as important. The insights on C-SGTR are discussed separately in Section 3.2.3.

[26] The ice condenser plants with a free-standing steel containment are similar but not identical. The assessment of the failure pressure could be influenced by plant-specific differences. Furthermore, the failure pressure assessment has uncertainties that are likely as large as the plant-specific differences. Any evaluation of the containment failure pressures uncertainties was beyond the scope of this report. Nevertheless, the results of the Sequoyah UA and the focused study suggest a low likelihood of an early containment failure and the potential of a late containment failure source term as large as some of the early containment failure source terms.

3.2.5.1. Peach Bottom UA

BWR containment failure timing insights

There were two key modes of containment failure in the Peach Bottom UA: (a) drywell head leakage and (b) drywell liner melt-through. The drywell head leakage occurred as the bolts retaining the drywell head stretched to form a gap when the containment reached high pressure. The exact criteria for the bolt stretching was sampled using uncertain parameters. The drywell liner melt-through also included uncertain parameters for debris movement criteria from the reactor pedestal to the drywell. The radionuclides that escape the containment have some limited retention in the reactor building. Two other uncertain variables explored the hydrogen ignition criteria and the over-pressure opening criteria for the large railroad doors.

Every realization in the Peach Bottom UA experienced a drywell liner melt-through. In order to better understand what affects the timing of radionuclide release from the containment, a regression was performed on the timing when the fraction of iodine released to the environment reaches 0.001 (i.e., 0.1% of the iodine inventory).[27] This metric served as an indication of when fission product releases to the environment were increasing above design leakage values and directly related to the timing of the containment failure.

The regression analyses indicate that the battery duration is the most influential parameter, which would be expected. The battery duration has an obvious influence on release timing in that RCIC functions keep the reactor cool as long as DC power is available. It isn't until DC power is lost that the operators lose control of RCIC and its water delivery increases, overfilling the vessel and flooding the steam lines. The drive turbine on the RCIC pump is assumed to fail when the steam lines flood.

The number of cycles to SRV failure and the open fraction of an SRV after thermal seizure were also important to release timing because they are important to whether or not an MSL rupture occurs. When an MSL rupture occurs, containment over pressurizes and leaks past the drywell head flange, which results in an early release. The role of the valve and MSL failure is more thoroughly discussed in Section 3.2.2.

After the DC battery duration and the valve cycle parameters, no other parameters had a significant impact to the timing of the containment failure. In particular, the uncertain parameters for the drywell head leakage, the ex-vessel debris movement to the drywell liner, or reactor building leakage or failure were not important factors to the timing of the iodine release.

The regressions on the magnitude of the iodine and cesium release, rather than the timing of the radionuclide release, provide a few more insights on the influences of the uncertain parameters related to the containment and reactor building failure. The magnitude of the iodine release shows some small influence of the drywell liner failure area, and the railroad door opening pressure. Both parameters appear as small contributors to the magnitude of the cesium release to the environment. Consequently, there is no strong impact of the containment or reactor building uncertainty parameters on either the timing or the magnitude of the releases to the environment.

[27] The 0.1% iodine regression is used as a surrogate for containment failure timing insights to assess whether the various uncertain parameters on the mode of containment failure or reactor building failure were important.

Secondary parameters important for the source term

The independent regression analyses for each of the failure modes (SRV stochastic, SRV thermal seizure, or SRV thermal seizure with MLS creep rupture) in the Peach Bottom UA identified additional important parameters and phenomena (see Section 3.2.2.3). For realizations with only a stochastic SRV failure, the releases of iodine and cesium are also sensitive to drywell liner failure flow area. There is a correlation between the uncertainty in the drywell liner breach size and whether a surge of water from the wetwell occurs (see Figure 3-44). Larger breach sizes cause stronger containment depressurizations. The surged water from the wetwell spreads across the core debris on the drywell floor and evaporates. The evaporating water creates steam that increases the leakage rate from the containment that promotes the release of the airborne radionuclides. Any radionuclides in the water that surges into the drywell will be released into the drywell atmosphere where they can leak to the environment. Due to the larger releases with a thermal seizure of the SRV, with or without an MSL creep rupture, the influence of drywell liner area was not important for these failure modes.

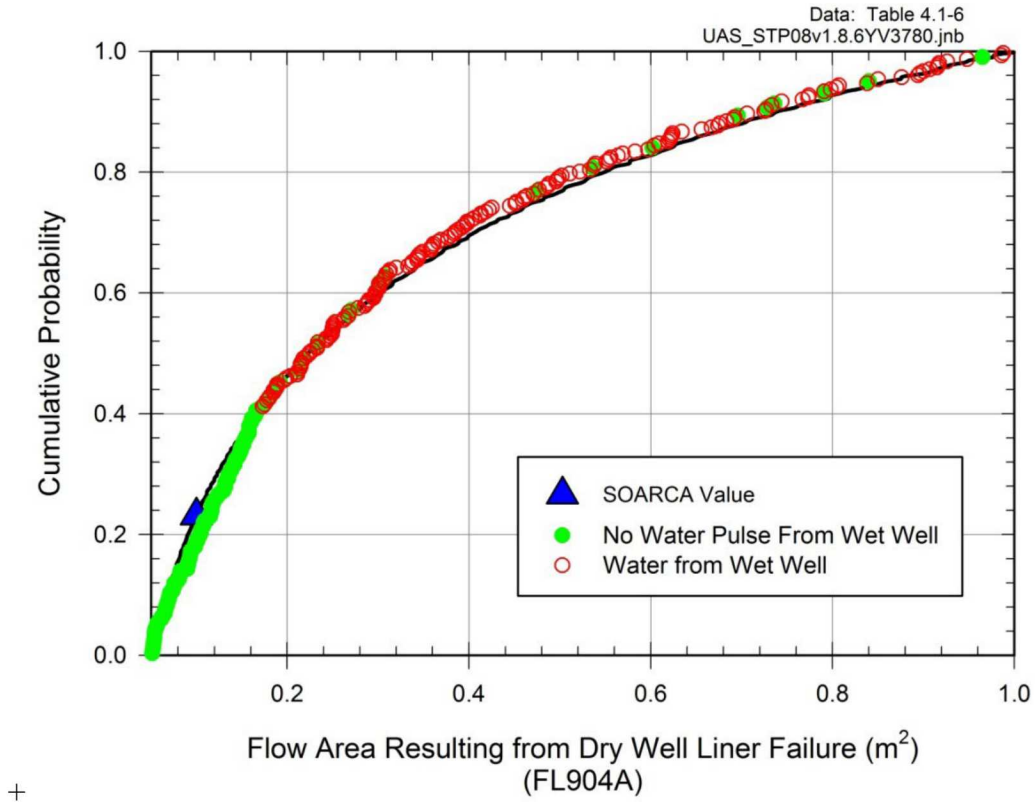

Figure 3-44. Cumulative distribution function for the flow area resulting from drywell liner failure with an indication of a water pulse from the wetwell to the drywell

Impact of an earlier RPV penetration failure

The investigation into failing RPV lower head penetrations yielded outcomes where core debris made its way to the containment floor generally earlier than in the UA calculations, which were constrained to only failing the RPV lower head in a gross manner. The uncertainties in the number of penetrations that might fail and the temperature that might be associated with failure were addressed by performing sensitivity calculations. The specific vulnerabilities of the drain line/valve

at the low-point of the lower head to failure were not addressed. The earlier relocation of core debris to the containment floor in the failed-penetration calculations led to an earlier onset of fission product releases from containment and hence larger I and Cs releases to the environment by 48 hr.

Insights from the updated Peach Bottom model using MELCOR 2.2

Since the Peach Bottom UA was completed using the MELCOR 1.8.6 code, the two PWR UAs were performed. The two PWR UAs incrementally updated the approach and methodology, including using MELCOR Version 2.2. A small number of Peach Bottom reference calculations were performed using the updated model and MELCOR 2.2 to assess the changes since the Peach Bottom UA [30].

The updated Peach Bottom input model includes input corrections and enhancements. It also includes changes to the uncertainty parameters and the distributions. The new model was compared to three reference calculations from the Peach Bottom UA. Some differences are expected due to changes in the code versions and changes in the input. In addition, the severe accident models have inherent variabilities due to complex numerical and physical interactions. Consequently, some variations are expected as subtle interactions accumulate and change model responses.

The three reference calculations included examples of the three important outcomes: (1) a stochastic failure of an SRV prior to significant core degradation in ~50% of the realizations, (2) a thermal failure of a SRV after the start of core degradation with a failure of the MSL in 33% of the realizations, and (3) a thermal failure of a SRV and a thermal failure of the MSL after the significant core degradation in 17% of the realizations. The Peach Bottom UA insights relative to the valve behavior are further discussed in Section 3.2.2.3, which are the dominant uncertain parameters influencing these three accident categories. However, the comparisons of Peach Bottom UA results with the updated Peach bottom model and MELCOR 2.2 provide new insights on the role of the two containment failure modes.

Reference Realization 51 with a stochastically-failed SRV

Realization 51 from the original Peach Bottom UA[28] was selected as one of the reference case comparisons with new Peach Bottom deck using MELCOR 2.2. It included a stochastically-failed SRV. As specified in the uncertain valve parameters, an SRV stochastically failed open on the 224th valve cycle, which defined the accident progression. The new MELCOR 2.2 model included the following key differences that impacted the progression of events,

- The new MELCOR 2.2 calculations included pump seal leakage that pressurized the containment early and left a pool of water in the drywell. In contrast, Peach Bottom UA did not consider pump seal leakage.
- The new MELCOR 2.2 calculations used the new ex-vessel models for melt spreading and water ingression heat transfer. The Peach Bottom UA calculations used a simple empirical model for the melt spreading rate and a multiplier for the enhanced debris surface to water heat transfer.

The early drywell pressure comparison shows an initially higher pressurization from the pump seal leakage. The pump seal leakage in the MELCOR 2.2 calculation accelerated the timing to the reactor vessel lower head failure (i.e., 20.0 hr versus 21.6 hr). The ex-vessel debris in the Peach Bottom UA calculation immediately flowed to the drywell liner, which failed 0.2 hr after LHF. In the new MELCOR 2.2 calculation, the ex-vessel debris initially cooled in the pool of water in the drywell.

[28] The MELCOR Version 1.8.6 calculation documented in NUREG/CR-7155 is identified as the Peach Bottom UA. The updated MELCOR 2.2 calculation is identified as MELCOR 2.2.

The steam production from the ex-vessel debris-water in the MELCOR 2.2 calculation is evident as a drywell pressurization above ~4.8 bar (70 psia) from ~20 hr to 25.1 hr.

Figure 3-46 shows the debris heated and moved to the liner at 25 hr in the MELCOR 2.2 calculation, which was~5 hr after the lower head failed and when debris started relocating to the containment (i.e., versus 0.2 hr in Peach Bottom UA). After the drywell liner melt-through, the containment depressurized, and the leakage hole was the dominant release pathway. However, while the containment was pressurized from 20 hr versus 25.1 hr prior to the liner melt-through, there was high leakage through the drywell head seal as shown in Figure 3-47. In contrast, the Peach Bottom UA calculation shows a much lower leakage with a short-term increase for 0.2 hr after reactor vessel failure.

The most interesting insight from the changes in the containment response is the impact on the release of the xenon, cesium, and iodine release to the environment (see Figure 3-48 through Figure 3-50, respectively). The release of the xenon gas is slower due to the smaller leakage area through the drywell head seal in the MELCOR 2.2 calculation relative to the drywell liner failure. About 50% of the gas is released prior to the drywell liner failure at 25 hr. However, the MELCOR 2.2 calculation quickly increases to >500 kg after the drywell liner failure to the Peach Bottom UA value.

In contrast to the differences in the xenon gas comparison, the total cesium and iodine releases increase slowly after the start of the drywell head leakage and are not significantly impacted by the drywell liner failure. Xenon is a non-condensable gas that is initially retained in the gas space above the wetwell pool, in the drywell, and in the reactor. The sharp depressurization at the drywell liner failure allows the gas to be rapidly released from the containment. Unlike xenon, cesium and iodine predominantly exist as aerosols that are released due to their airborne or revaporized concentrations in the drywell. Although there are some differences in the timing and trends, there is relatively little difference in the integral release to the environment at 48 hr for the xenon, cesium, and iodine radionuclides. The timing is primarily due to modeling changes for the recirculation pump leakage. However, the results from the new MELCOR 2.2 calculations show higher releases from the drywell head leakage prior to the drywell liner leakage that compensates for the later drywell liner failure.

There are several insights on the containment performance from these comparisons:

- First, the radionuclide release from the drywell head leakage in the MELCOR 2.2 calculation with a delayed drywell liner melt-through is almost as large as the Peach Bottom UA result with a rapid liner failure. The integral radionuclide release of xenon, cesium, and iodine at 48 hr are approximately the same.
    - Approximately 50% of the xenon gas is retained in the wetwell gas space until the rapid containment depressurization after the drywell liner failure.
    - The airborne cesium and iodine in the drywell releases at approximately the same rate through the drywell head in the MELCOR 2.2 calculation as the Peach Bottom UA leakage through the drywell liner.
- The inclusion of recirculation pump leakage creates a pool in the drywell that initially cools the debris. The ex-vessel debris evaporates the water in the drywell and then re-heats. The debris incrementally spreads for 5 hr after vessel failure until the delayed drywell liner.

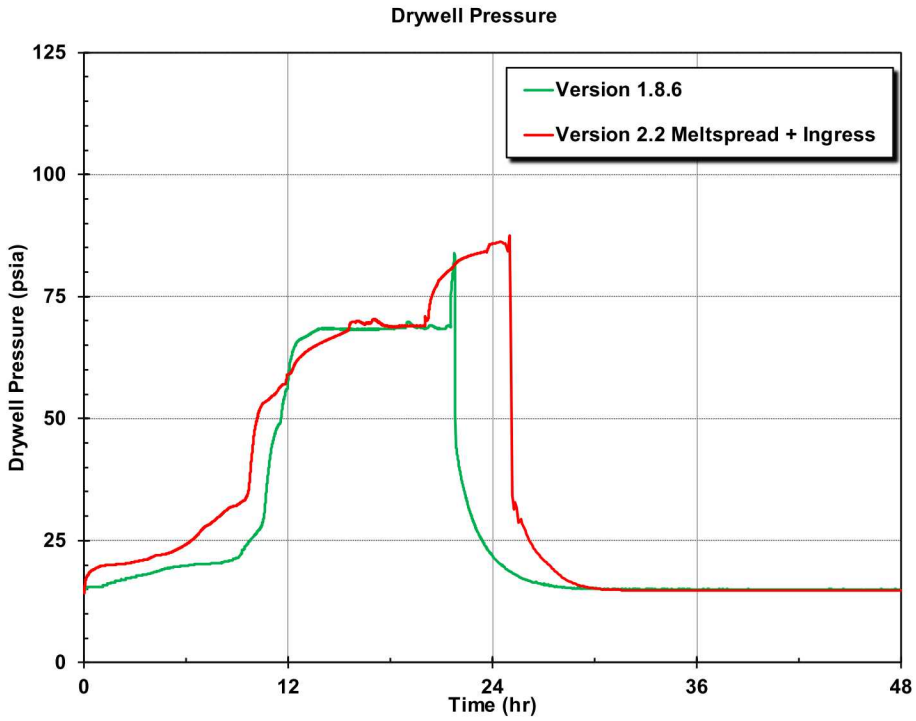

Figure 3-45. Comparison of the drywell pressure from the Peach Bottom UA and MELCOR 2.2 for Realization 51 with a stochastically-failed SRV

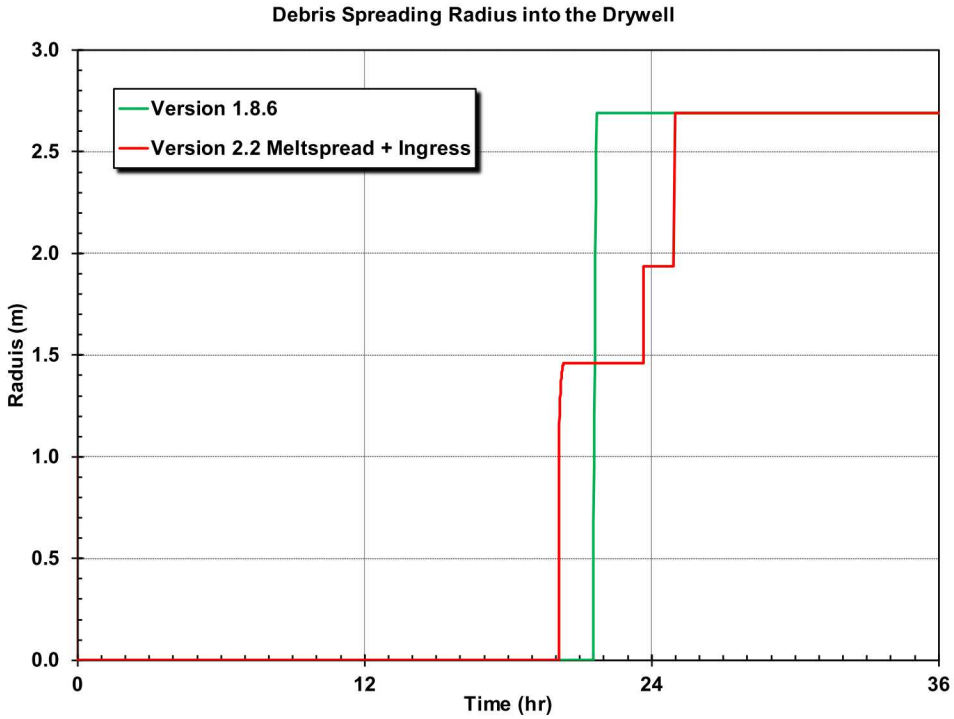

Figure 3-46. Comparison of the debris spreading radius into the drywell from the Peach Bottom UA and MELCOR 2.2 for Realization 51 with a stochastically-failed SRV

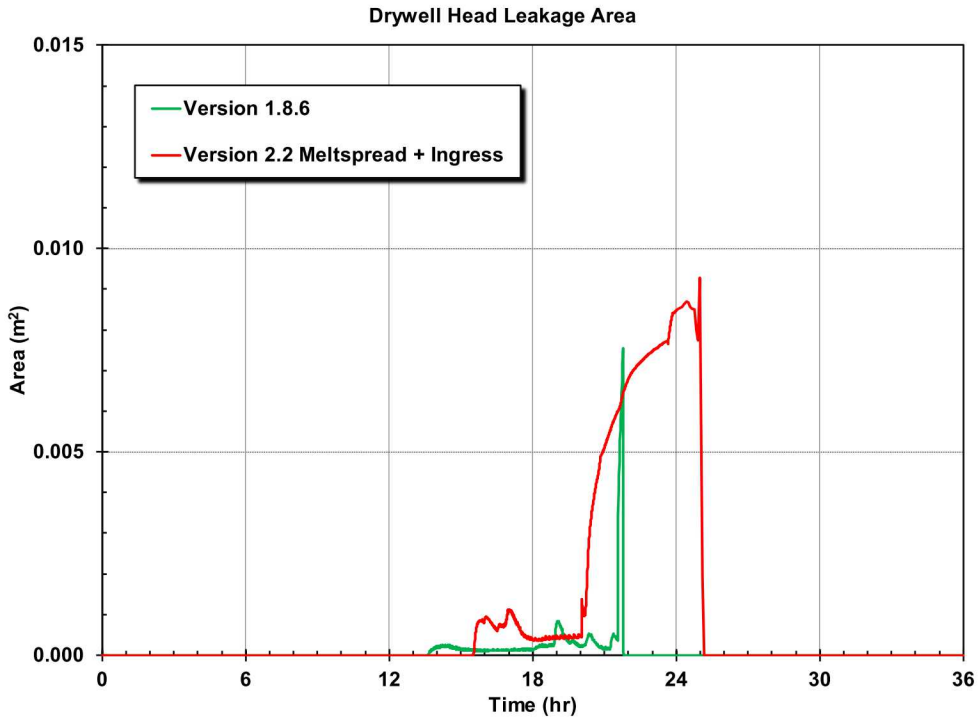

Figure 3-47. Comparison of the drywell head leakage area from the Peach Bottom UA and MELCOR 2.2 for Realization 51 with a stochastically-failed SRV

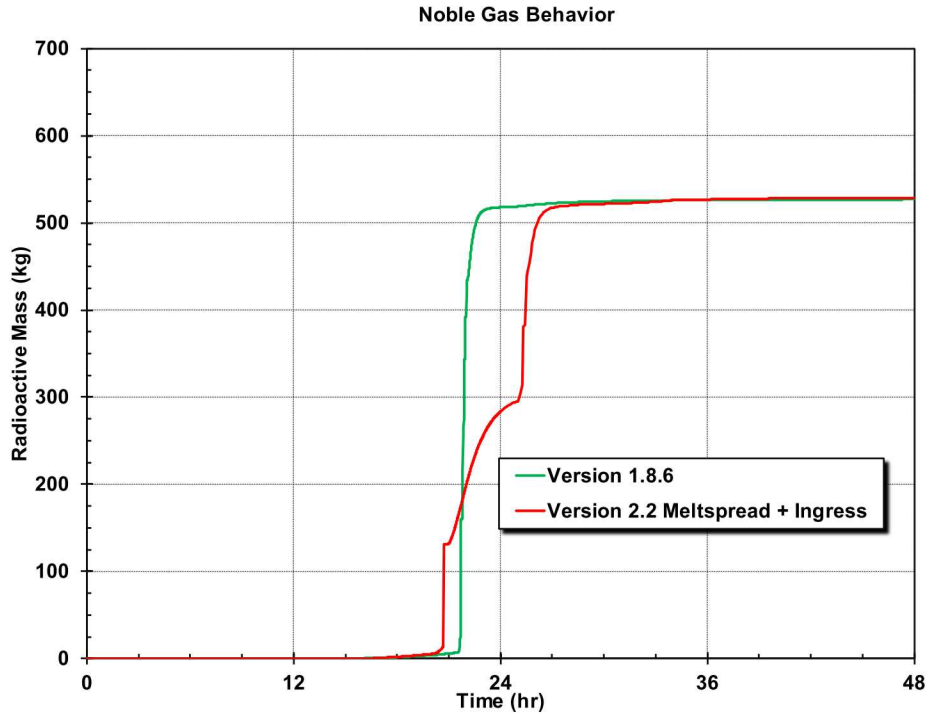

Figure 3-48 Comparison of the xenon release to the environment from the Peach Bottom UA and MELCOR 2.2 for Realization 51 with a stochastically-failed SRV

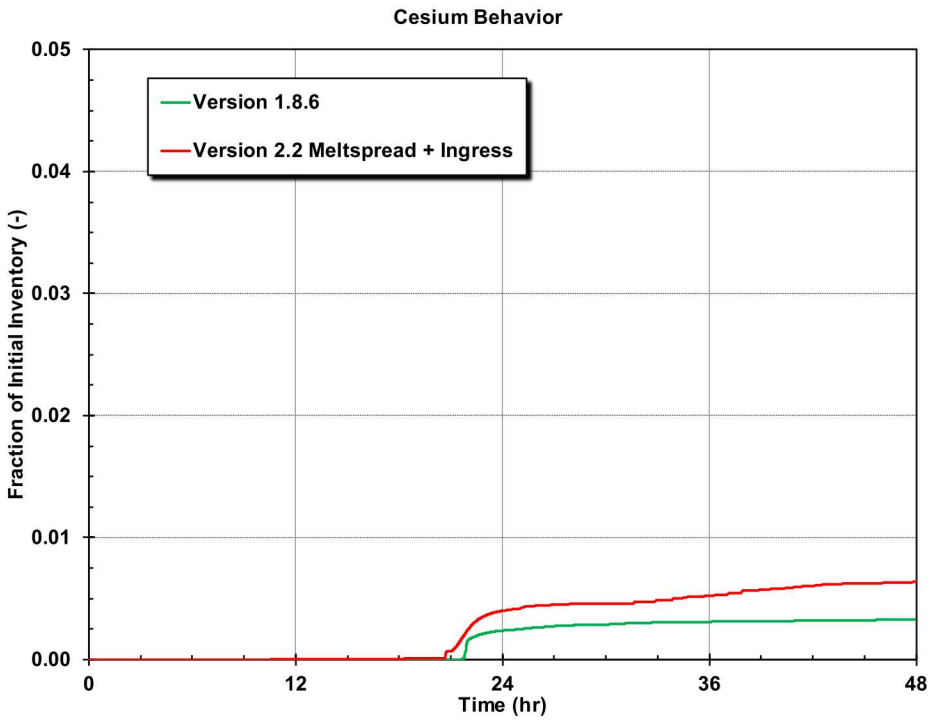

Figure 3-49. Comparison of the cesium release to the environment from the Peach Bottom UA and MELCOR 2.2 for Realization 51 with a stochastically-failed SRV

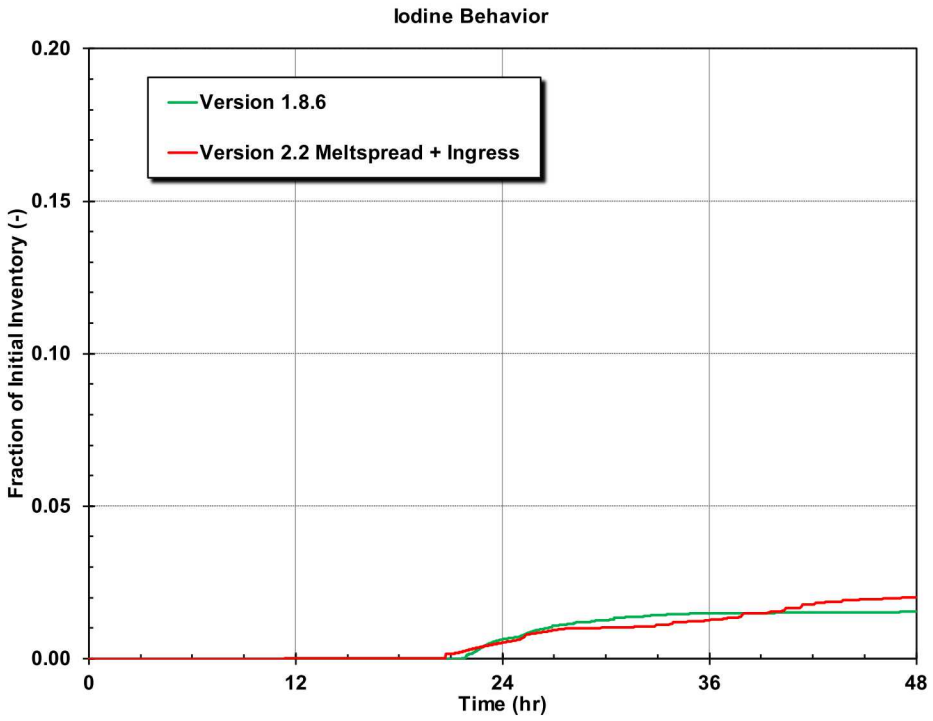

Figure 3-50. Comparison of the iodine release to the environment from the Peach Bottom UA and MELCOR 2.2 for Realization 51 with a stochastically-failed SRV

Reference Realization 18 with a thermally-failed SRV

The comparison of Realization 18 further illustrates some of the differences in the accident progression noted in the Realization 51. Realization 18 included a thermally-failed SRV with a relatively large failure area (i.e., non-dimensional area = 0.687) that pressurized the RPV.

Similar to Realization 51, the early drywell pressure comparison shows an initially higher pressurization from the recirculation pump seal leakage. The recirculation pump seal leakage in the MELCOR 2.2 calculation accelerated the timing to core damage. The timing of fuel-cladding gap release and the SRV thermal failure occurred about 1.4 hr earlier. Similarly, the timing of the LHF occurred earlier in the MELCOR 2.2 calculation (~3 hr earlier). The ex-vessel debris in the Peach Bottom UA calculation immediately flowed to the drywell liner, which failed 0.2 hr after vessel failure. In the MELCOR 2.2 calculation, a small amount of debris started to flow out of the pedestal region but was rapidly cooled by the pool of water. As more debris ejected from the RPV into the pedestal and heated, it slowly flowed into the drywell. The debris from the pedestal spread into the drywell in successive increments and reached the drywell liner at 22.3 hr. The drywell liner failed shortly after at 22.7 hr, or 4.5 hr after LHF.

After the debris arrived in the containment, the drywell pressure remained high in the MELCOR 2.2 calculation until 22.7 hr when drywell liner failed and depressurized the containment (i.e., see Figure 3-52). The boiling water in the drywell caused the drywell pressure to increase until the drywell head leakage balanced the steam production. The drywell head leakage, shown in Figure 3-53, follows the drywell pressure response. The drywell leakage goes to near atmospheric pressure once the drywell liner fails.

The impact on the source term for the diverse leakage paths in the two calculations is shown in the xenon, cesium, and iodine releases (see Figure 3-54 through Figure 3-56, respectively). The release of the xenon gas is slower due to the smaller leakage area through the drywell head seal in the MELCOR 2.2 calculation relative to the drywell liner failure. The xenon release is increasing but over 40% of the xenon gas is retained in the wetwell air space, the drywell, and the reactor vessel at 48 hr. The xenon in the wetwell airspace will remain trapped until the depressurization at the drywell liner opens the vacuum breaker between the wetwell and the drywell.

The total cesium and iodine releases increase after the start of the drywell head leakage and look somewhat similar whether the liner had failed (i.e., the Peach Bottom UA calculation) or remained intact (i.e., the MELCOR 2.2 calculation). In particular, the cesium releases are very similar between the two calculations. Following the drywell liner failure at 24.7 hr, the iodine releases are higher in the MELCOR 2.2. The new MELCOR 2.2 results were higher than the Peach Bottom UA results but not significantly considering the variations noted in NUREG/CR-7155 for results with a thermally-failed valve. The MELCOR 2.2 cases included a surge of water from the wetwell that was not calculated in the original calculation. The higher release in the Version 2.2 calculations is partially attributed to the surge of radionuclides from the wetwell water that boiled away on the drywell debris and revaporization of cesium iodine in the drywell. The pump seal leakage pathway also contributed to the higher cesium and iodine leakage into the drywell rather than exclusively to the wetwell prior to the RPV LHF. For example, there was ~15 kg of cesium and iodine leaked to the drywell in the Version 2.2 calculation versus essentially none in the Version 2.2 calculation with no RP leakage. The cesium and iodine released to the drywell contributed to an increase in the source term as the drywell water evaporated and lofted the radionuclides.

The comparisons for Realization 18 had the following insights that generally confirm the Realization 51 results.

- The delayed drywell liner failure slowed the release of the xenon, which initially occurred through the drywell head leakage. However, once the drywell liner failed, the remaining xenon was released.
- The integral radionuclide release of cesium and iodine at 48 hr was higher than the Peach Bottom UA. The differences were attributed to the recirculation pump seal leakage, the surge of water from the wetwell. However, the differences were not significantly large considering the variations noted in NUREG/CR-7155 for results with a thermally-failed valve.

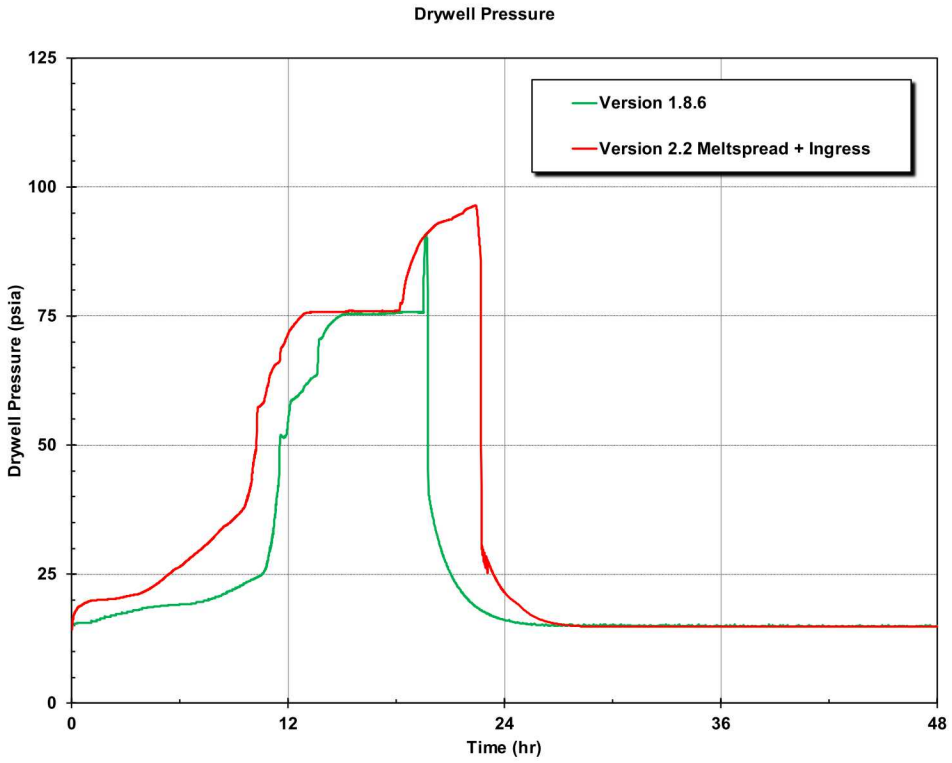

Figure 3-51. Comparison of the drywell pressure from the Peach Bottom UA and MELCOR 2.2 for Realization 18 with a thermally-failed SRV.

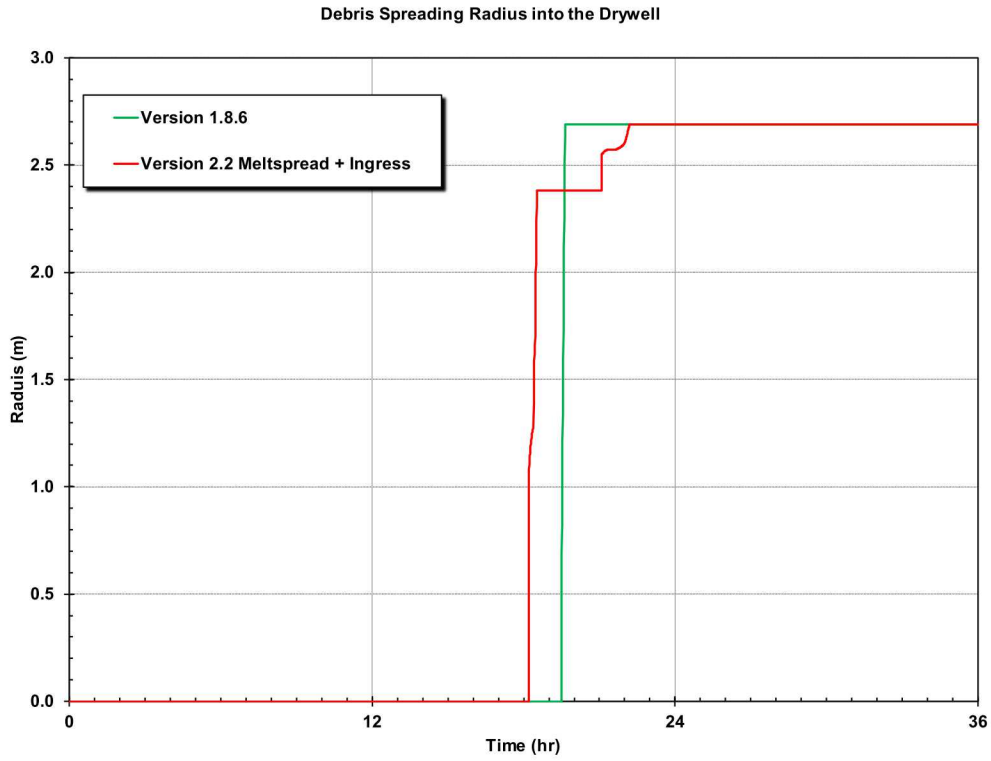

Figure 3-52. Comparison of the debris temperature and debris radius in the drywell from the Peach Bottom UA and MELCOR 2.2 for Realization 18 with a thermally-failed SRV.

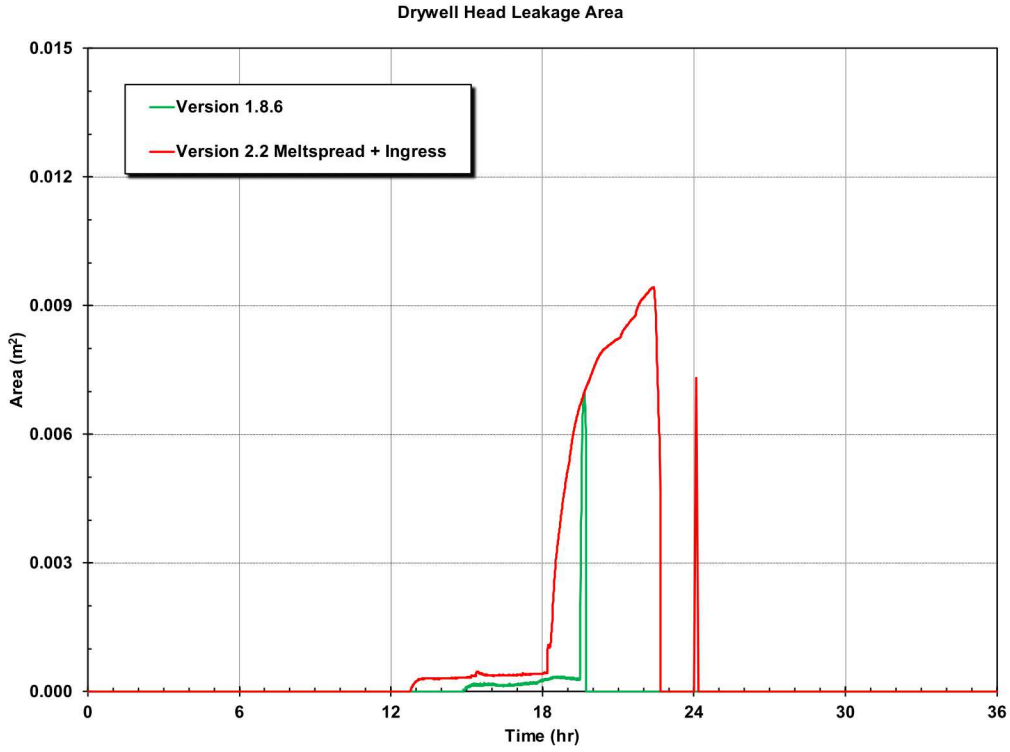

Figure 3-53. Comparison of the drywell head leakage area from the Peach Bottom UA and MELCOR 2.2 for Realization 18 with a thermally-failed SRV.

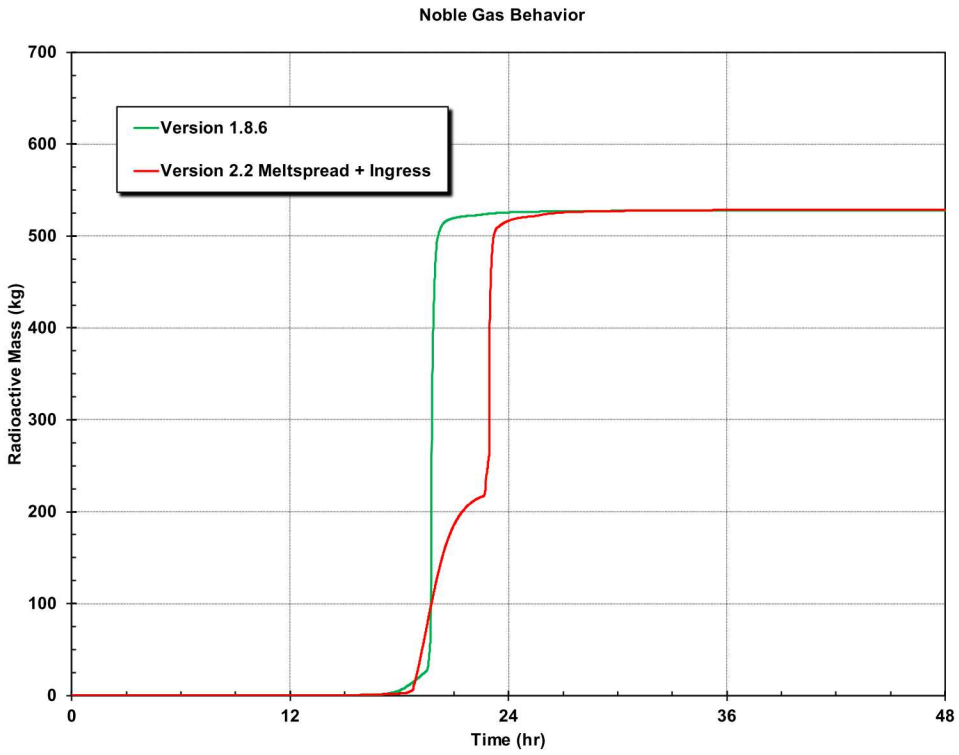

Figure 3-54. Comparison of the xenon release to the environment from the Peach Bottom UA and MELCOR 2.2 for Realization 18 with a thermally-failed SRV.

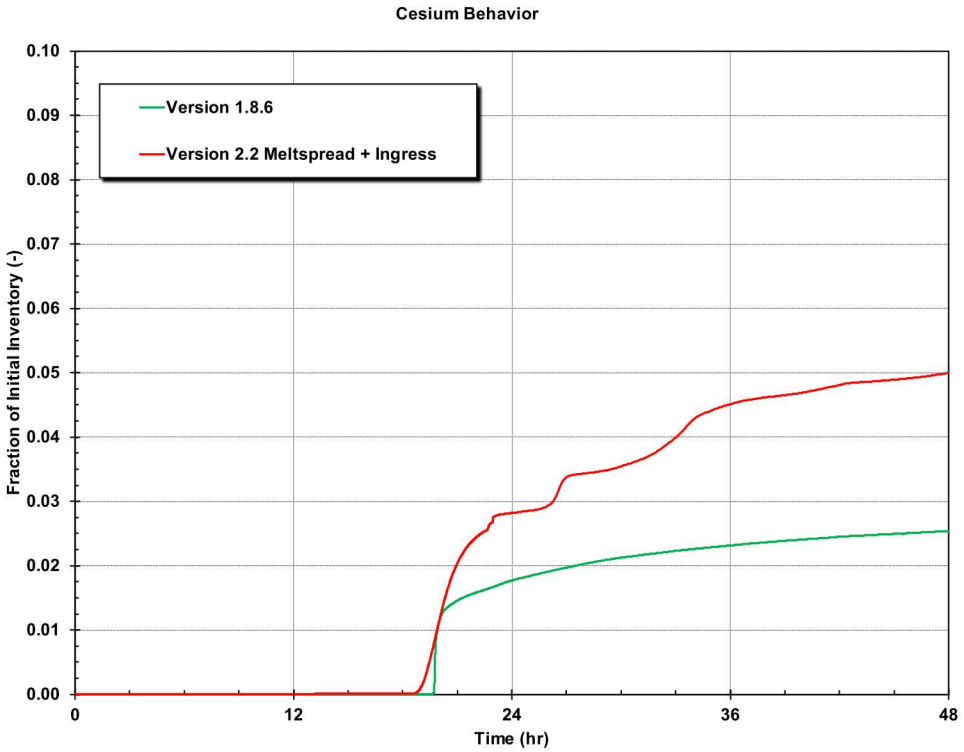

Figure 3-55. Comparison of the cesium release to the environment from the Peach Bottom UA and MELCOR 2.2 for Realization 18 with a thermally-failed SRV.

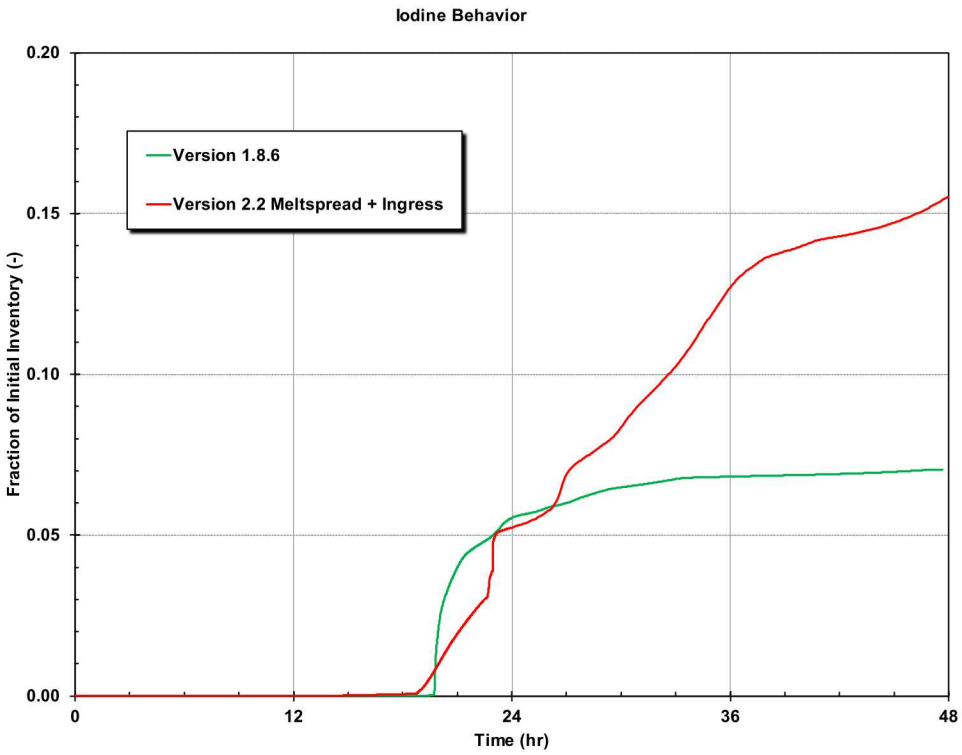

Figure 3-56. Comparison of the iodine release to the environment from the Peach Bottom UA and MELCOR 2.2 for Realization 18 with a thermally-failed SRV.

Rapid drywell depressurization

An important finding in the Peach Bottom UA was that water containing radionuclides can surge up from the wetwell to the drywell floor following core debris melting through the drywell liner. The potential for water surging depended on the sampled drywell liner breach size. Breach sizes greater than 0.2 m^2 resulted in rapid containment depressurization and water flashing in the wetwell. This pressure differential and flashing generated a large differential pressure that overwhelmed the vacuum breakers between the wetwell and drywell. As a result, water containing scrubbed radionuclides surged into the drywell and also flowed into the reactor building through the drywell breach.

3.2.5.2. Surry UA

A primary goal of the Surry UA was to investigate parameters leading to an early containment failure from a C-SGTR. A C-SGTR, though not a containment failure, is a containment bypass and equally as important. Accordingly, Surry UA sequence end states had the following outcomes:

- Late over-pressurization from steam and non-condensable gases generated from CCI (95.1%),
  - Liner failure only (81.2%)
  - Liner failure and C-SGTR (12.6%)
  - Liner and rebar failure (1.4%)
- No containment failure prior to the end of the 72 hr simulation time (4.9%).

Table 3-6 and Figure 3-57 present the timing of the failures. All the failures resulted from gradual monotonic pressurizations of containment (i.e., there were no containment ruptures immediately

following a hydrogen deflagration). Most (92.8%) of the realizations reached the liner yield criteria, which was sampled between 1.09 times the design pressure (P_{design})and 2.03 times P_{design} using a Beta distribution informed with insights from Sandia's scale containment testing program, assessments of containment performance in severe accidents, and assessments of degraded containment conditions [31][32][33][34].

The Surry containment pressure versus leakage curve is shown in Figure 3-58. The value for the lowest point (i.e., the liner plate yield) is sampled as an uncertain variable. The median value for the liner plate yield pressure is shown in Figure 3-58. When the liner plate yields, the leakage increases to 1% volume/day. The leakage rate due to the liner yield slowly increases to 10% volume/day until the rebar yield pressure. If the pressure reaches 2.25 times the design pressure, then the rebar is expected to yield, which starts an increased leakage rate. The rebar yield pressure was only exceeded in 1.4% of the realizations within 72 hr and was not sampled as an uncertain variable in the Surry UA. The trend shown on Figure 3-59 suggests other cases would exceed the rebar yield pressure after 72 hr.

The realizations with a containment failure within 72 hr are attributed to the 0.5 day time in the cycle calculations. The 0.5 day are cases very early in core life (i.e., shortly after refueling). The decay heat power at 0.5 days was too low to generate a significant containment pressurization.

As discussed in Section 3.2.4.1, the hydrogen deflagrations were common in the calculations but were not threatening for a containment over-pressure failure (i.e., see spikes on Figure 3-59 and the discussion in Section 3.2.4.1). A C-SGTR decreased the rate of containment pressurization as evidenced in the horsetails in Figure 3-57. The lower pressurization rate is discussed in Section 3.2.3.1 and is attributable to the additional containment leakage pathway afforded by a tube rupture.

Table 3-6. Containment failure timing

	Liner failure time (hr)
Mean	50.8
Median	50.1
Min	34.5
Max	71.9

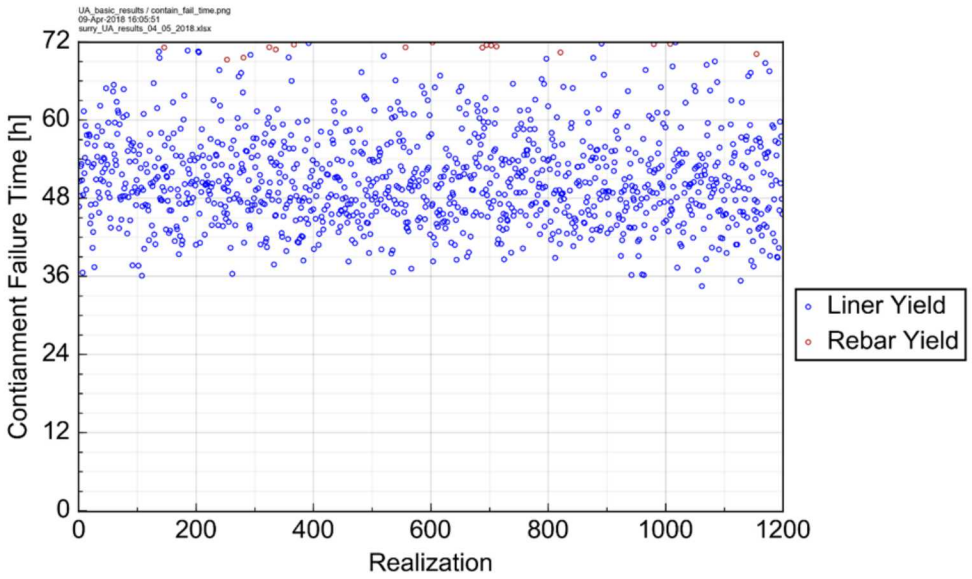

Figure 3-57. Containment failure timing by realization

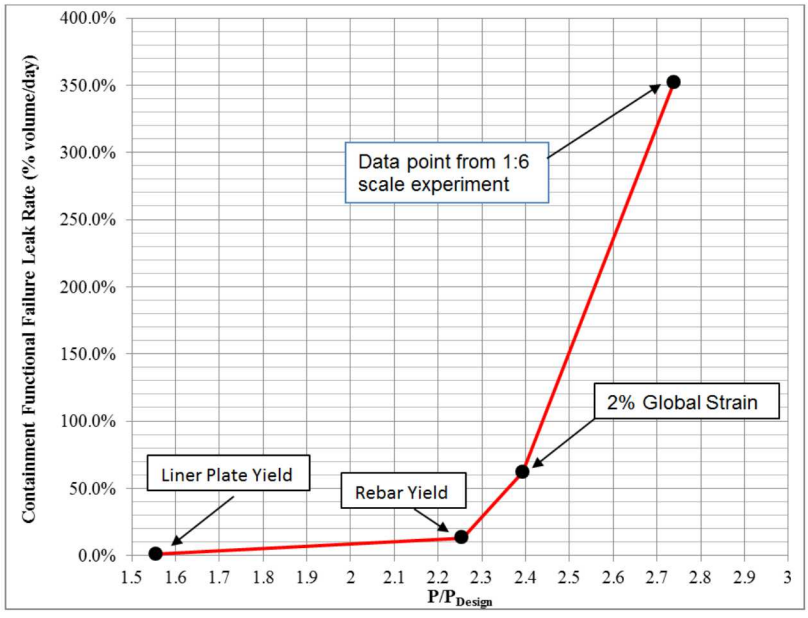

Figure 3-58. Containment functional failure leakage [3]

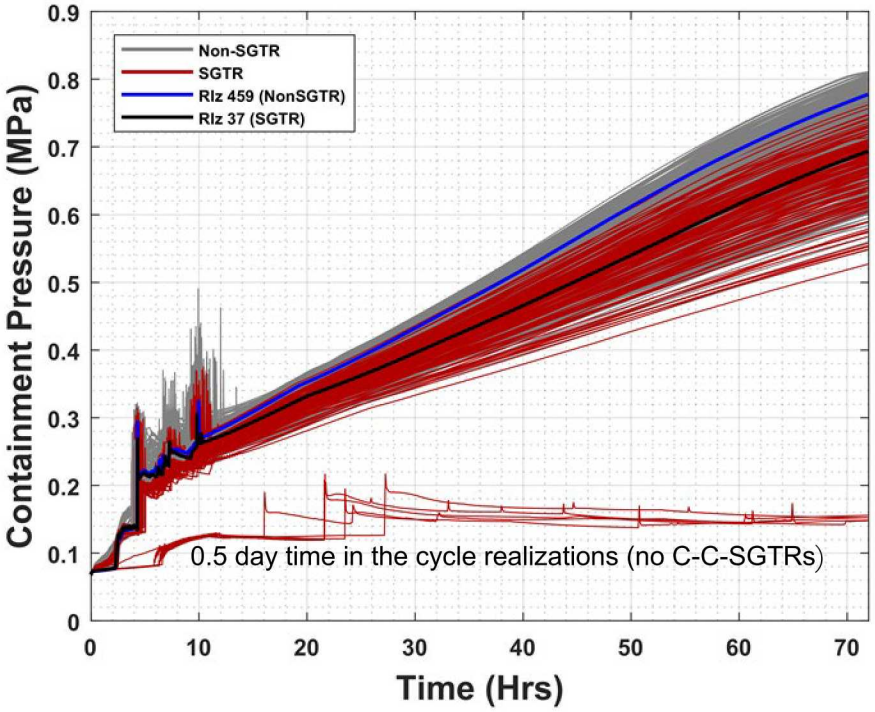

Figure 3-59. Containment Pressure by C-SGTR/Non-C-SGTR[29]

[29] Note that due to a plotting error, the low horsetails were mischaracterized as C-C-SGTR cases. None of the low horsetails had a C-SGTR. These were the 0.5 day time in the cycle realizations. Not all realizations are shown in the figure to improve the definition on the individual pressure curves.

Impact of the reactor cavity concrete composition on containment failure timing

The original Surry SOARCA MELCOR analyses specified a limestone-based aggregate for the containment concrete. However, subsequent information confirmed Surry has a basaltic aggregate concrete in the reactor cavity. Two sensitivity MELCOR calculations were performed that varied the concrete type. The basaltic concrete shows more ablation of the concrete than with limestone concrete. However, the limestone concrete has approximately 30% greater release of non-condensable gases. These results are in line with previous EPRI analyses that show an inverse relationship between the downward heat transfer coefficient to the effective decomposition enthalpy. Although there is a higher ablation rate for basaltic concrete (Figure 3-60), the non-condensable generation rate is lower due to the increased cooling effect of the higher ablation rate on the corium.

Most of the pressure in containment is attributable to the partial pressure of steam (Figure 3-62). The partial pressures of non-condensable gases generated by molten core concrete interaction (MCCI) do not contribute much to the overall pressure, so differences in the amounts of gas generated do not either. Instead, the containment pressure increase over the long term is due to continued heating of the containment atmosphere by decay heat generated in the core debris residue on the containment floor.

A sensitivity study was also performed to assess the impact of the rebar mass in the concrete. The rebar mass was changed from to zero and 30% (i.e., the base value was 17%). The total containment pressure for the no rebar and 30% rebar cases is 1% greater and 2% less, respectively, when compared to the base case. Additionally, the containment temperature differences response between the three cases is small. However, the amount of rebar does have a secondary effect for hydrogen response after hot leg failure. A high rebar content increases hydrogen and carbon monoxide production from MCCI (i.e., iron within the rebar reacts with water and carbon dioxide to generate iron oxide and hydrogen and carbon monoxide, respectively). The impact is a slightly larger hydrogen burn. However, no hydrogen deflagration challenged the containment structural integrity.

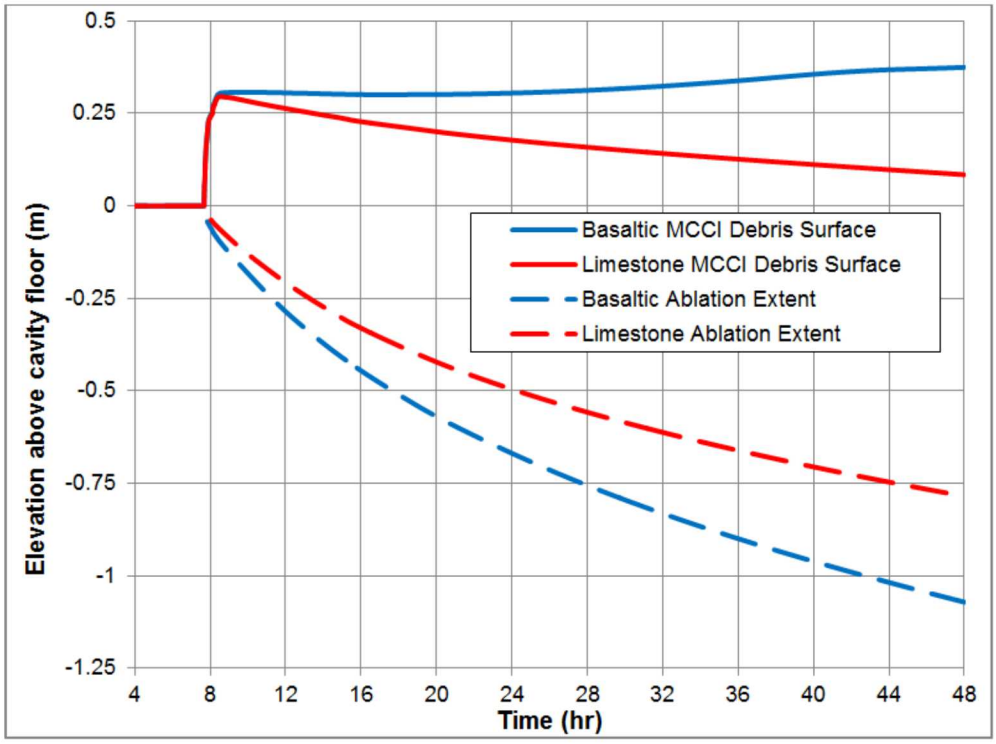

Figure 3-60. MCCI debris surface and ablation depth

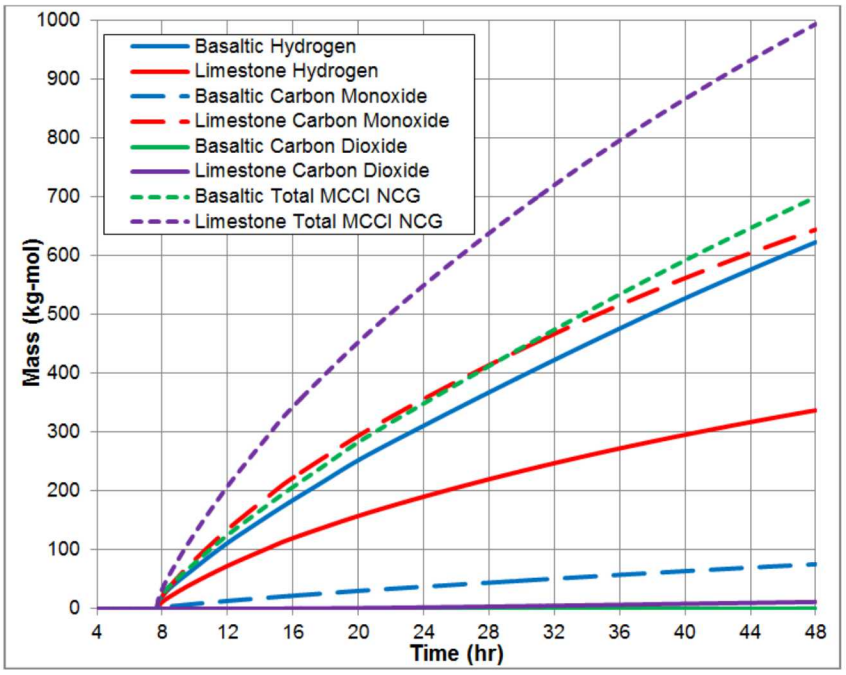

Figure 3-61. MCCI non-condensable gas contribution and sum total

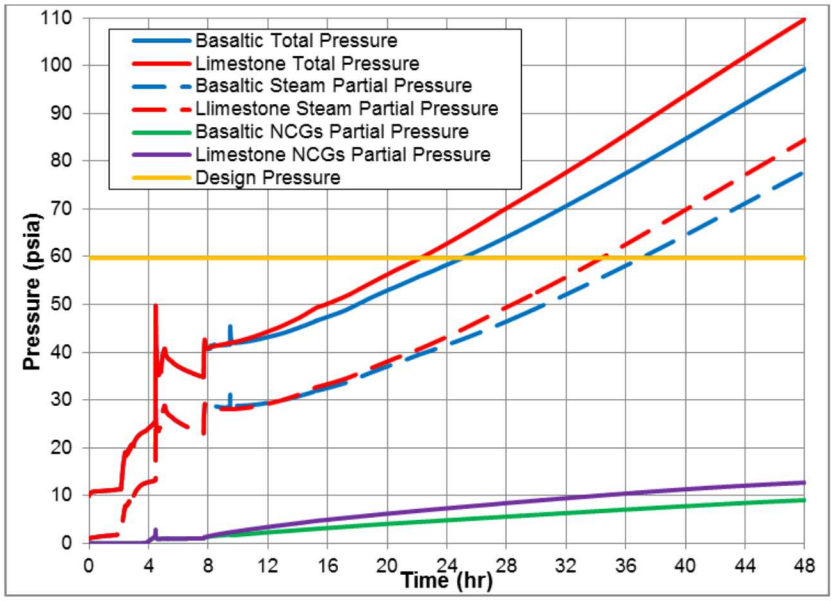

Figure 3-62. Containment pressure response

Impact of containment design leakage on the source term

The Surry UA sampled the amount of design leakage from containment. Prior to increased leakage due to a containment liner yield, the design leakage is the only release path for radionuclides to the environment, excluding bypass events like a C-SGTR. The design leakage was identified by each regression technique as the largest contributor to the uncertainty in the cesium release to the environment and the third most important contributor to the iodine release to the environment. It was less important for iodine due to late revaporization physics that also allowed iodine leakage after the containment failure. The regression was biased by the early time in the cycle results that have late or no containment liner yield, leaving this leakage as the only release pathway. The scatterplot (Figure 3-63) shows a clear trend of an increasing cesium release with an increasing design leakage rate. There is also an interesting result in that there is a clearly increasing lower bound with higher leakage. A higher design leakage allows more release of airborne aerosols before there is time for deposition in containment.

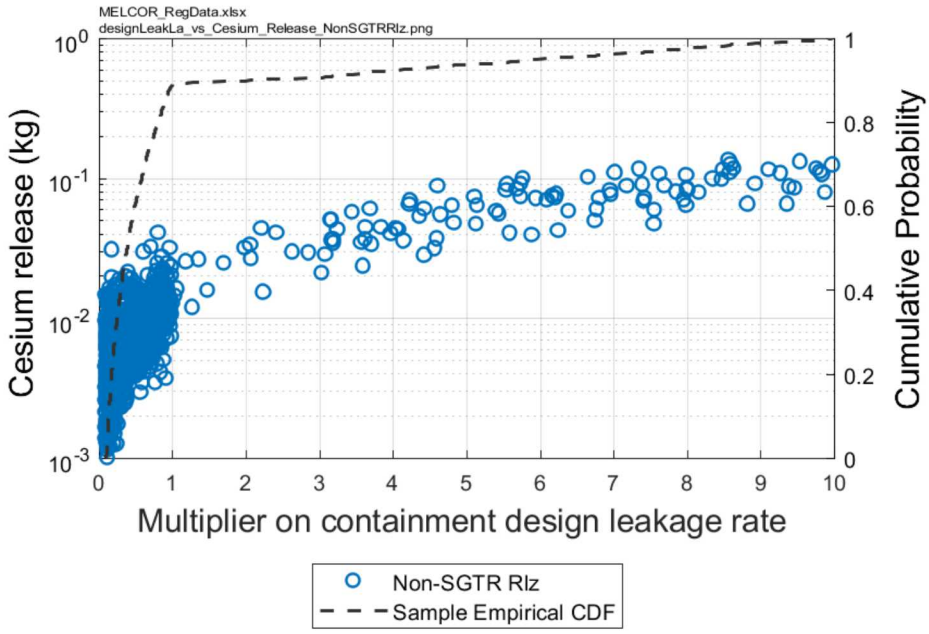

Figure 3-63. Scatterplot of cesium release fraction versus containment leakage input values

3.2.5.3. Sequoyah UA

A primary goal of the Sequoyah UA was to investigate parameters leading to an early containment failure from hydrogen deflagrations. Accordingly, containment end states had three general outcomes:

- Early containment failure from the first hydrogen combustion (i.e., 4 realizations or 0.7%),
- Late over-pressurization from steam and non-condensable gases generated from CCIs (i.e., 86.8%), and
- No containment failure prior to the end of the 72 hr simulation time (i.e., 12.5%).

The most common outcome was late containment failure. None of the BOC cases reached containment failure within 72 hr and only a very small percentage of realizations with a MOC decay heat profile (i.e., 1% of the total) did not fail the containment.

Unlike early containment failures, the late containment failures were caused by a slow over-pressurization and not pressure spikes from deflagrations. If a containment survived the first burn, then the subsequent deflagrations were never energetic enough to rupture the containment. The burns after the first ignition were generally from hydrogen produced by CCI igniting in the cavity region. The late burns (after 12 hr) are less energetic due to frequent burning of smaller quantities of combustible gases near the lower flammability limit (i.e., ignited by aerosols and hot gases from ex-vessel CCI). As the burns consume oxygen and the containment pressurizes, the oxygen concentration in containment eventually decreases to the point where it is insufficient to support further burning. Although the deflagrations cease, the containment continues to pressurize and heat up from the ex-vessel CCI non-condensable gas generation and the resulting vaporization of water from the melted ice. The pressurization is monotonic and most often pressurizes the containment to rupture prior to 72 hr (end of simulation time). However, none of the BOC (i.e., 6.25 days at cycle) realizations over-pressurized containment by 72 hr (see Section 3.2.1.1).

Focused pressurizer FTC study

The Sequoyah SOARCA pressurizer safety valve study explored the conditions that were more favorable for early containment failure. The focused pressurizer safety valve study found that:

- The containment failure pressure was the most important sampled parameter with respect to containment failure time.
- The number of pressurizer cycles-to-failure, the time-in-the-cycle, and the oxidation model were the most important sampled parameters with respect to the mass of hydrogen vented to containment.
- The number of pressurizer SV cycles to failure, eutectic melting temperature, and oxidation model were the most important sampled parameters with respect to the mass of hydrogen transported to the containment dome.

3.2.5.4. Implications for Other Plants

The insights on the various containment failure modes from the Peach Bottom UA and updated MELCOR 2.2 results are applicable to other BWR Mark Is. All BWR Mark I containments include a drywell head that is susceptible to leakage at high pressure. All the Peach Bottom UA calculations included a drywell liner melt-through. The Peach Bottom UA calculations did not include any mitigation or ex-vessel water addition. Consequently, the ex-vessel debris is expected to heat and attack the concrete. The updated calculations showed the debris movement to the liner can be delayed by the pump seal water on the drywell floor. However, the water evaporates and allows the continued movement to the drywell shell. The ex-vessel debris behavior in other Mark I design will be affected by the size of the in-pedestal sump, the doorway opening to the drywell floor, and the exposure of the steel shell near the drywell floor.

The insights being formed from the Fukushima Dai-chi accidents, which were complicated by emergency water addition and debris interaction with the structures below the vessel lower head, illustrate additional complications not included or considered in the Peach Bottom UA. Consequently, the drywell failure by spreading likely has larger uncertainties than illustrated in the Peach Bottom UA. However, a key insight from the new MELCOR 2.2 calculations showed that drywell head seal leakage replaces the drywell liner leakage as a comparable radionuclide leakage pathway. Consequently, the limitations in current abilities to model ex-vessel debris behavior had an unexpectedly low impact on the magnitude of the source term.

Each Mark II design is different, with significantly different reactor pedestal designs (e.g., see NUREG/CR-5528 [35]). The drywell liner is not directly vulnerable in the Mark II containments in the same manner as the Mark I containments. The three basic variations include: (1) a flat floor cavity with no in-pedestal downcomers (Susquehanna and Limerick), (2) a deep cavity below the drywell floor (Columbia and La Salle), and (3) cavities with in-pedestal downcomers (Nine Mile Point, Unit 2). Any ex-vessel debris may not reach the drywell liner due to the location of the pedestal relative to the drywell floor (i.e., design 2) or the presence of downcomers in the pedestal and drywell regions (i.e., design 1) or downcomers in the drywell (i.e., design 1).

The Mark II drywell head is similar to the Mark I design and expected to leak at high pressure. However, the pressure response of the Mark II will be different due to its large size and variations and uncertainties on debris movement into the wetwell. Consequently, it is difficult to extrapolate the Peach Bottom UA containment failure dynamics directly to the Mark II design.

Some of the other insights from the Peach Bottom UA are expected to be applicable to all BWRs. Operation of RCIC will delay the timing of the containment failure. All BWRs include RPV penetrations (e.g., a drain line at the bottom of the lower head) that could be susceptible to an earlier failure than predicted in the Peach Bottom UA. The impact would be an earlier and more protracted release of debris to the containment. Due to the limited sensitivity investigations, any extrapolation to containment failure conditions for other designs would be limited and qualitative (i.e., likely less important to Mark II and Mark III designs). Finally, the reactor building is not expected to provide significant retention of released radionuclides for any BWR. The hydrogen burns in the reactor building will cause failures and increased leakage that limits their retention in unmitigated severe accidents.

The PWR UAs provided somewhat consistent insights on the containment performance. The most likely outcome is a slow, monotonic pressurization to an over-pressure condition. In a free-standing steel ice condenser containment, the failure mode is expected to be a rupture. The insights on the timing and mode of the containment failure will be qualitatively similar for eight of the 10 ice condenser plants. The susceptibility of the ice condenser plant to an early failure from a hydrogen burn is discussed in Section 3.2.4.2 and the role of the pressurizer SVs in a large early burn is discussed in Section 3.2.2.2.

Most of the PWRs have steel reinforced concrete containments. The slow pressurization to an over-pressure failure identified in the Surry UA is qualitatively applicable to all PWRs with similar containments. The Surry containment is a small, subatmospheric design. The insight of a low challenge of an early containment over-pressurization from a hydrogen burn is expected to be representative of most plants. The mode of a gradual over-pressure failure from the liner yield to rebar yield is also expected to be characteristic of most PWRs with steel-reinforced concrete containments.

The insights on design leakage impacting the timing and early magnitude of the release is expected to be applicable to all BWR and PWR plants. Nuclear power plant control of containment leak tightness is governed by the Code of Federal Regulations Appendix J. Since NRC implemented an initiative to allow performance-based requirements to replace prescriptive requirements of Appendix J, EPRI reports that the industry response to the risk-informed testing approach has been very successful. The program reports 75 successful Integrated Leakage Rate Tests (ILRTs) from the adoption of performance-based testing and no failures (i.e., leakage is below the design limits) [37]. Nevertheless, severe accidents without power may present challenges to isolate all penetrations to the containment. Consequently, the trends observed in the Surry UA from lower aerosol (cesium) source term with low leakage to a higher aerosol source term for high leakage above the design limits is expected to be applicable for all reactor types.

Finally, an inadvertent mistake in the concrete specification for the Surry containment illustrated the impact of the concrete type on the containment pressurization rate from the CCI [38]. CCI with basaltic concrete shows more ablation of the concrete than with limestone concrete. However, the limestone concrete has approximately 30% greater release of non-condensable gases. The most important factor contributing to the higher releases in the original SOARCA calculation is the faster pressurization rate due to the limestone concrete and the earlier transition to a rebar yield failure at 25.5 hr. In contrast, most liner failures occurred after 48 hr in the Surry UA simulations (e.g., primarily due to the lower smaller gas generation from the basaltic concrete) [3]. The qualitative insights on the concrete type are expected to be applicable to CCI in all plants (i.e., higher change due to erosion with basaltic concrete and higher pressurization with limestone concrete).

A sensitivity study was also performed in the *draft* Surry UA to assess the impact of the rebar mass in the concrete. There was very little difference in the containment pressurization during CCI or the temperature response (i.e., a 3% impact on pressure over a 30% rebar variation). A high rebar content increases hydrogen and carbon monoxide production from MCCI (i.e., iron within the rebar reacts with water and carbon dioxide to generate iron oxide and hydrogen and carbon monoxide, respectively). The impact is a slightly larger hydrogen burn. The qualitative insight on rebar variations (or uncertainty) is expected to be applicable to all nuclear designs.

3.2.6. Primary System Pump Leakage

Both BWRs and PWRs use seals that minimize leakage around the recirculation pump shafts. When AC power is available, the pumps inject water through the seal into the primary system fluid or the RPV for a BWR. Following the loss of power, the seal pumps stop and the flow in the seal reverses and leaks from the pump. Early in the accident, the pump seal leakage is important for the accelerated inventory loss from the primary system. It also impacts the system pressure response and requirements for SV or SRV demands. Late in the accident, hot gases exiting the seals can be an ignition source, which was identified as an important ignition source in the Sequoyah UA (see Section 3.2.4.2). Finally, the updated Peach Bottom model showed its impact on the early containment pressurization and slowing debris movement towards the drywell shell (see Section 3.2.5.1). The PWR and BWR insights are further discussed in Sections 3.2.6.1 and 3.2.6.2, respectively. The implications for other plants are discussed in Section 3.2.6.3.

3.2.6.1. PWR Pump Seal Leakage Insights

The PWR owners group estimates the seal cavity will fill with the primary system water in approximately 13 minutes. The high temperature water heats the seals and also flashes to steam as it is released. The consequences range from continued leakage through intact seals to failures of the various seals in the pump. Failure of the seal components increases the leakage rate, which impacts the timing to the core uncovery. The nominal PWR leakage is 21 gpm/pump with a potential for 480 gpm/pump at the full system pressure following a complete seal system failure.

The issue evolved to a NRC Generic Safety Issue, which was resolved in 1999 as not warranting generic cost-beneficial safety enhancements [39]. However, PWRs have systematically replaced their seals with improved materials that are less susceptible to thermal degradation. More recently, some plants, including Surry, have upgraded to leak resistant seals, which are advertised to have fail-safe redundancy and negligible leakage [40].

Although Surry has updated their seals, the pump seal leakage was retained as an uncertain parameter for insights to other plants without the upgrade. The Sequoyah UA included the nominal amount of seal leakage (21gpm), which did not vary. The Surry UA did not identify seal leakage as an uncertain parameter important to the iodine and cesium source term to the environment. It showed up as weakly impacting the magnitude of the in-vessel hydrogen production. An increase in pump seal leakage limits pressurizer cycles for an FTC and allows the accident progression to proceed at higher pressure. As discussed in Section 3.2.2.3, multiple seal failures would offset other system failures if all pressurizer SVs FTO.

A review of the Sequoyah containment isolation documents indicates that the containment isolation system, which is assumed to survive a seismic initiating event causing an SBO, will respond to Phase A isolation signal first [2]. This will result in automatic closure of Phase A isolation valves. The operators are expected to ensure closure of RCP cooling water seal return and master valves in

30 minutes, which is suggested in PWR SAMGs. Consequently, operator actions exist to terminate the seal leakage. However, the operator action was not credited in the UAs.

Sequoyah STSBO Sensitivity study

In the Sequoyah UA calculations, the RCP seal leakage occurred at a nominal rate of 21 gpm per pump at full reactor pressure. Two sensitivity calculations were also performed to investigate the impact of a seal failure that forms a small loss-of-coolant accident (SLOCA) through the reactor coolant pump (RCP). The seal failures increased the nominal leakage to a nominal leakage value of 182 gpm per RCP. The two realizations were selected to include pressurizer SV attributes that promoted either an early containment failure or a late containment failure. In particular, one realization had pressurizer SV failure attributes that led to late containment failure (i.e., a large sampled FTC value that resulted in no failure of the pressurizer SV). Conversely, the second realization had pressurizer SV failure attributes that have the potential to promote an early containment failure (i.e., the pressurizer SV failure on the first cycle with a relatively large SV failure area).

The inclusion of higher RCP leakage only had a small effect on the realization with attributes for a late containment failure. Both calculations had a hot leg failure from high primary system pressure and a late containment failure. As shown in Figure 3-64, the seal leakage impacts the early primary system response until the hot leg creep rupture failure at ~4 hr. After the hot leg failure, the RCP leakage was very small and did not impact the accident progression. There was only a small impact on the timing of the containment failure (see Figure 3-65). Overall, the timing of the key events and the source term to the environment were similar.

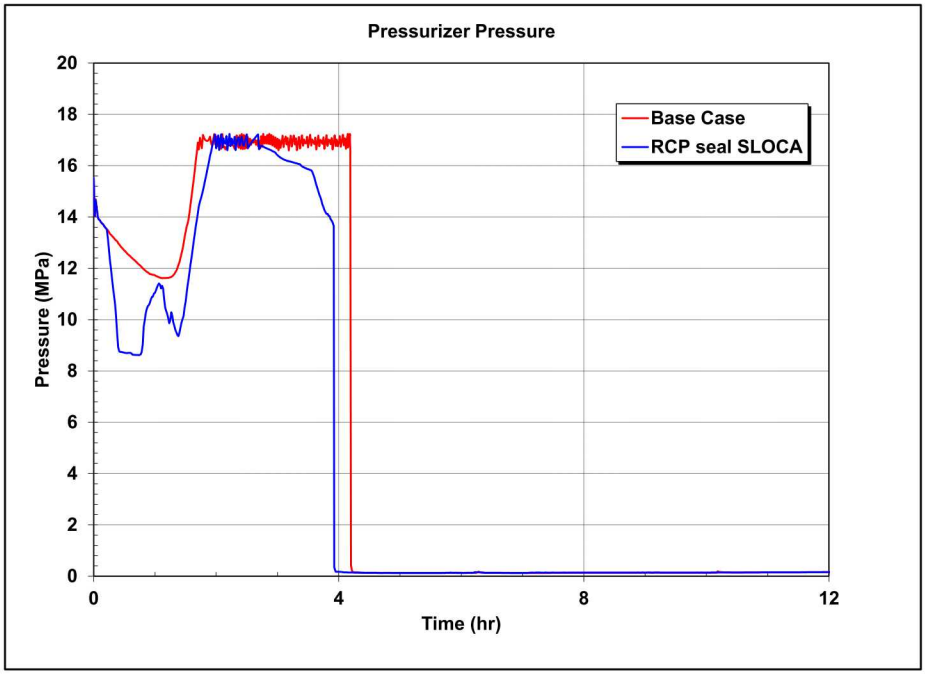

Figure 3-64. Impact of higher RCP leakage on the primary system pressures for a STSBO realization with attributes for a late containment failure

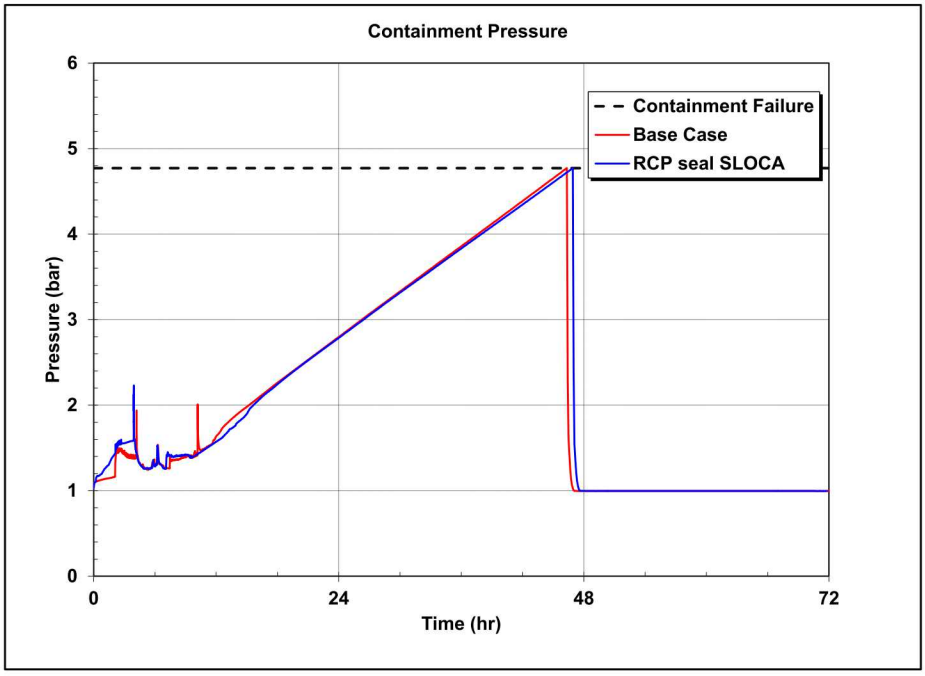

Figure 3-65. Impact of higher RCP leakage on the containment pressures for a STSBO realization with attributes for a late containment failure

In contrast, the inclusion of higher RCP leakage in the realization with attributes for an early containment failure (i.e., an early pressurizer SV FTC) caused large timing differences. Although both the base case and the RCP leakage sensitivity case had an early containment failure, the timing was 4 hr different. In both cases, the stuck-open pressurizer SV is the dominant release pathway of hydrogen to the containment prior to the first ignition source. The higher RCP seal leakage delayed the early containment failure due to complex interactions between the accumulator injection and the core melt progression. Although the base case had a hot leg failure and the sensitivity case did not, the in-vessel hydrogen production and the subsequent hydrogen release to the containment prior to the first ignition source were comparable. The pressurizations from the burn following the first ignition source were also very similar.

The high RCP leakage calculation in the early containment failure case shifted some of the hydrogen leakage from the pressurizer SV to the RCP seal loss-of-coolant accident (LOCA). However, the total leakage from the SV and the RCP seals was approximately the same. Even for this extreme condition of four RCP seal failures, the total leakage through the stuck-open SV was nearly three times larger than the RCP seal leakage. Consequently, the magnitude of the hydrogen leakage through the RCP seals alone was an insufficient amount to challenge the containment integrity in a burn. The addition of RCP seal LOCAs is only expected to have a secondary impact on the conditions necessary for an early containment failure.

The gas leaking from the RCP seals was identified as an ignition source. However, a hot gas auto-ignition source would be expected to be more important with an RCP seal LOCA due to the faster inventory loss from the recirculation loop. The progression of events in late containment failure calculations showed that any hot gas auto-ignition source from the RCP seals would not occur until after hot leg failure. However, the accident progression for realization with attributes for an early containment failure showed the gases exiting the RCP seal could be an important ignition

source. In the high RCP seal leakage sensitivity calculation, the hot gas temperature exiting the RCP seals briefly exceeded the auto ignition threshold at 3 hr 35 min (see Figure 3-66). The amount of hydrogen discharged to the containment from all sources was 338 kg at the time of the first ignition source. Although there was a similar amount of hydrogen in the containment at 3 hr 35 min versus 8 hr 10 min, the amount of hydrogen in the upper dome was significantly different. Consequently, a burn at 3 hr 35 min that propagated into the dome (i.e., a 5.1% hydrogen concentration) would not likely generate a peak pressure that would fail the containment. Over the next 4 hr, the hydrogen dome mass and concentration slowly increased to 213 kg and 10%, respectively, which did cause a large burn that failed the containment.

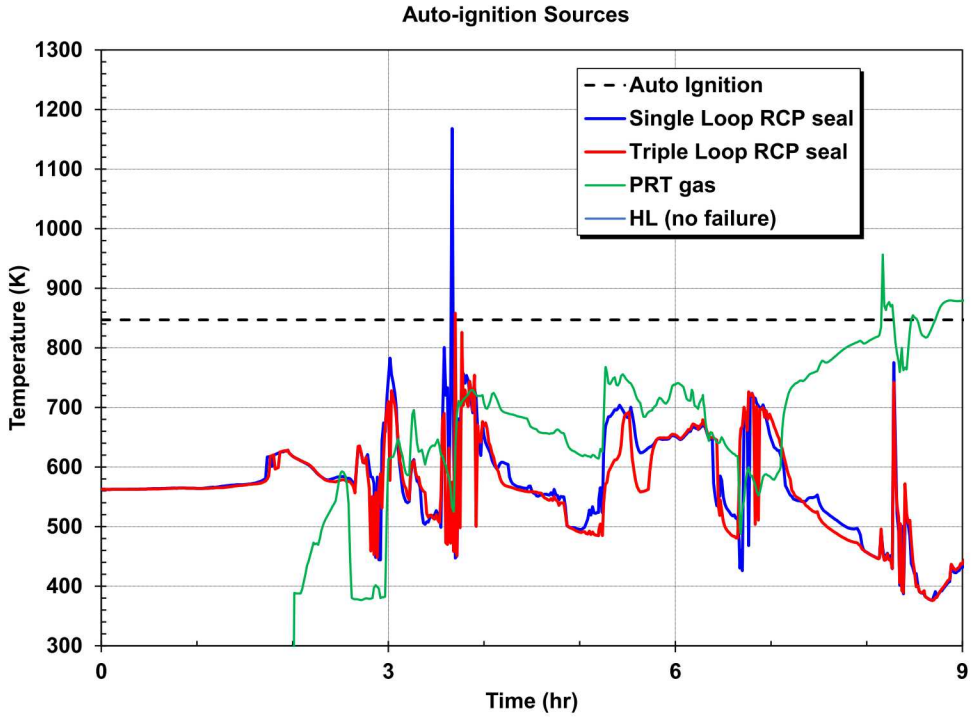

Figure 3-66. Comparison of the potential hot gas auto-ignition source in the containment for the RCP seal leakage sensitivity study

Sequoyah LTSBO Sensitivity study

A sensitivity calculation was also performed to investigate the impact of a seal failure that forms a small loss-of-coolant accident (SLOCA) through the RCP seal on a LTSBO. The other Sequoyah LTSBO calculations assumed that the RCP seal leakage occurred at a nominal rate of 21 gpm per pump at full reactor pressure. Unlike an STSBO, long-term RCP leakage led to a significant loss of the primary system inventory prior to the loss of the auxiliary feedwater injection to the secondary side of the reactor coolant system. The LTSBO included pressurizer SV attributes to promote an early containment failure by a hydrogen burn (i.e., pressurizer SV fails on the first demand).

The first ignition sources in the containment are at 22.8 hr and 15.7 hr in the base and sensitivity cases, respectively. The initial ignition source in the base case is the hot gases exiting the PRT. In the base case, a significant amount of the released fission products flowed into the PRT through the stuck-open SV. The decay heat from the radionuclides boiled the PRT empty and heated the exiting gas above the hydrogen auto-ignition temperature. In contrast, the pressurizer SV in the sensitivity

case never opened (see Figure 3-67); therefore, no steam or radionuclides went to the PRT. The first ignition source was the hot primary system gases exiting the hot leg after it failed.

The containment pressure responses (see Figure 3-68) reflect the variations in the first ignition source and the timing of the debris discharge into the containment from the vessel lower head failure. The peak containment pressures with the initial burn were 3.88 bar and 4.02 bar in the base and sensitivity calculations, which were below the median (5.62 bar) and the minimum (4.58 bar) containment failure pressures from the uncertainty distribution. The ex-vessel CCI began at 28.1 hr and 18.6 hr, respectively, in the base and sensitivity calculations. The non-condensable gas generation and heating from the CCI causes the long-term containment pressurization. The earlier pressurization of the sensitivity case reflects the timing difference of the start of the CCI. Both calculations were below the median containment failure pressure at 72 hr (i.e., 5.62 bar).

In summary, the RCP seal SLOCAs changed the progression of the LTSBO to have the attributes of a SLOCA. The primary system response was substantially different due to the large inventory loss through the SLOCA. Unlike the LTSBO calculations with the nominal RCP seal leakage (21 gpm), the primary system became thermally decoupled from the secondary system, which would disable most combinations of the SV failures investigated in the UA.

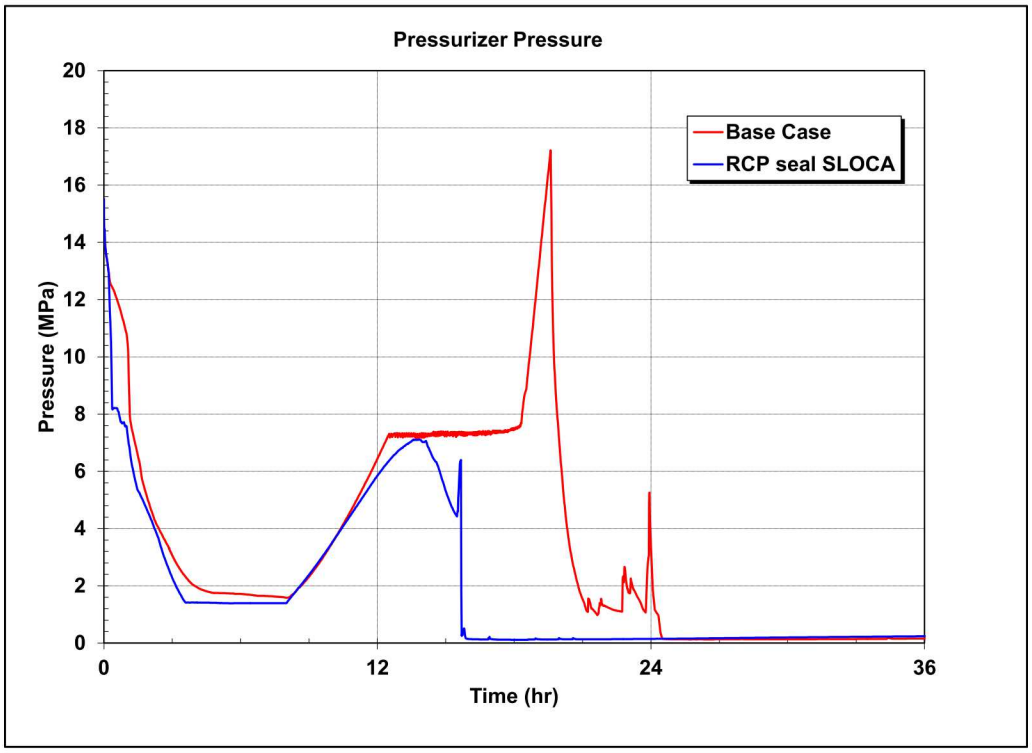

Figure 3-67. Impact of higher RCP leakage on the primary system pressures for a LTSBO realization with attributes for an early containment failure

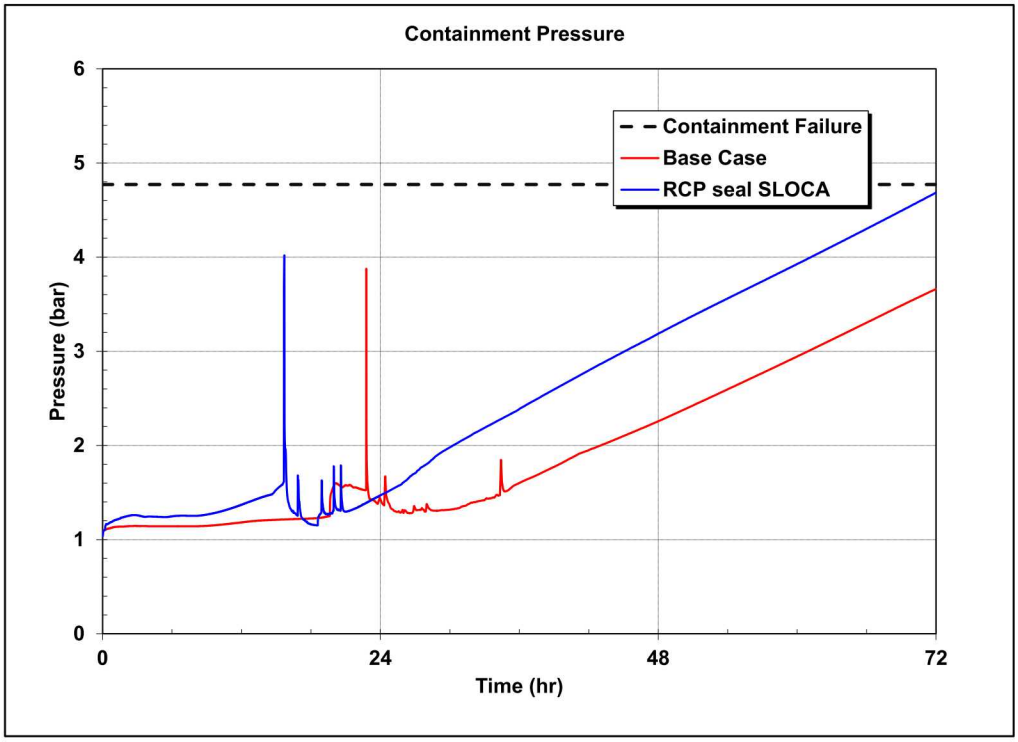

Figure 3-68. Impact of higher RCP leakage on the containment pressures for a LTSBO realization with attributes for an early containment failure

3.2.6.2. Peach Bottom Pump Seal Leakage Insights

The Peach Bottom UA did not consider pump leakage. However, it was included in related Fukushima Dai-chi UA simulations [41]. The insights from this Fukushima Dai-chi research showed the coolant losses through the recirculation pump seals accelerate the accident sequence including time to fuel uncovery and damage. Furthermore, the steam leaking through the recirculation pump seals will bypass the wetwell and contribute to the early containment pressurization. The updated Peach Bottom work described in Section 3.2.5.1 confirm the Fukushima Dai-chi insights and also the importance of the leaked water to slowing ex-vessel debris movement towards the drywell liner.

3.2.6.3. Implications for Other Plants

The PWR pump seal leakage was identified as an important generic safety issue in the 1980s. The issue was resolved in 1999 as not warranting generic cost-beneficial safety enhancements [39]. However, PWRs have systematically replaced their seals with improved materials that are less susceptible to thermal degradation. The improved seal cartridges are significantly less susceptible to degradation at high fluid temperatures versus the older seals. The pump seal research is active with new seals that are advertised to be capable of sustaining 100% system pressure with fail-safe redundancy and negligible leakage, including at Surry [40]. The Surry action to upgrade to leak resistant pump seals was in response to the post-Fukushima Order Number EA-12-049. While leak resistant seals are not required for compliance with EA-12-049, Surry found it beneficial to meet the order's long-term cooling requirements as did other plants.

As shown in in the STSBO and LTSBO responses in Section 3.2.6.1, RCP seal failures can have an important impact on the progression of events, especially when the reactor remains at high pressure

without make-up (i.e., the LTSBO). Seal failures contribute to a faster inventory loss from the primary system, which accelerates the timing to core damage. While RCP seal failures are not certain in an SBO, their consequences would be important for all PWRs without leak resistant seals (e.g., the FlowServe N-Seal). Finally, leaking seals may have an impact as a potential ignition source from leaking gases above the hydrogen autoignition. This is usually a positive impact because it can burn the released hydrogen locally in the lower containment before it circulates throughout the containment (i.e., a potential for a larger burn).

The BWR seal leakage is important to cooling the ex-vessel debris and delaying the drywell liner melt-through. It is also important for (1) accelerating the inventory loss and associated core melt progression and (2) creating a steam source for containment pressurization prior to vessel failure and through water-debris interactions after vessel failure (i.e., contributes to drywell pressurization and leakage). The insights on recirculation pump seal leakage from the Peach Bottom and Fukushima Dai-chi calculations are somewhat applicable to other BWRs. The drywell liner melt-through issue is unique to BWRs with Mark I containments. The qualitative insights are expected to be similar with some variations in the effectiveness due to the sump size, and drywell wall and floor characteristics.

The acceleration of the inventory of loss and early pressurization is applicable for the other BWRs (i.e., Mark II and Mark III containments). However, the impact on ex-vessel debris behavior is expected to be different for the BWR Mark II and Mark III containment designs as described next.

Each Mark II design is different, with significantly different reactor pedestal designs (e.g., see NUREG/CR-5528 [35]. The drywell liner is not directly vulnerable in the Mark II containments in the same manner as the Mark I containments. The three basic variations include: (1) a flat floor cavity with no in-pedestal downcomers (Susquehanna and Limerick), (2) a deep cavity below the drywell floor (Columbia and La Salle), and (3) cavities with in-pedestal downcomers (Nine Mile Point, Unit 2). Any water from the pump seal leakage would not reach the ex-vessel debris for Mark II designs with a deep cavity below the drywell floor (Columbia and La Salle). In the flat floor design with no in-pedestal downcomers (Susquehanna and Limerick), the seal leakage water will be retained in the drywell and pedestal by the downcomers, which extend 18 inches above the floor. However, the downcomers may fail before challenging the drywell liner. Finally, the Nine Mile Point, Unit 2 design with downcomers in the pedestal region already benefits from debris interaction with the water following failure of the downcomers and is not as significantly impacted by the presence of seal water.

The Mark III designs may not experience much benefit from the recirculation pump leakage. However, there is no immediate danger of a liner melt-through following core debris ejection into the containment. The water that spills onto the drywell floor from the pump seal leakage cannot flow directly into the pedestal region due to the pedestal wall. However, NUREG/CR-5529 reports that the drywell drain lines could backup through the pedestal sump [36]. Consequently, the benefits of any ex-vessel cooling are expected to be limited.

3.2.7. Other Source Term Insights

Other source term insights not already covered in the proceeding sections are present in this section. The source term insights from the Peach Bottom UA are presented in Section 3.2.7.1. The insights from the Surry UA are presented in Section 3.2.7.2. The implications of these insights for other plants are discussed in Section 3.2.7.3.)

3.2.7.1. Peach Bottom UA

Chemical form of cesium

The chemical form of iodine and cesium was also identified as an influential parameter for iodine and cesium release fractions for all three failure modes in the Peach Bottom UA. The impacts relate to (1) the amount of iodine as a gas and (2) the cesium permanently deposited in the RPV via chemisorption of cesium from cesium hydroxide onto the stainless steel of reactor internals. A high ratio of cesium hydroxide to cesium molybdate in the released cesium contributed to smaller cesium releases to the environment, especially in simulations that promoted in-vessel chemisorption (e.g., the Peach Bottom realizations with delayed MSL failures). Although cesium hydroxide has a significantly higher vapor pressure and can be more mobile as vapor than Cs_2MoO_4, the cesium in the cesium hydroxide chemisorbed at a higher rate to the RPV stainless steel structures (e.g., the dryers, separators, and vessel liner). In calculations where core degradation occurred before or without failure of the lowest setpoint SRV (i.e., the vessel remained at high pressure during the core degradation phase), the potential for chemisorption was higher due to higher structural temperatures in the RPV. For simulations with cesium predominantly as cesium hydroxide, more than half of the initial cesium inventory was permanently chemisorbed and retained in the RPV. This influence is only pertinent for the realizations that have all or some of the reactor core cesium inventory present as cesium hydroxide (i.e., 62.5% of the realizations formed all excess cesium as cesium molybdate after first forming cesium iodide).

3.2.7.2. PWR UAs

Insights on the iodine gas fraction from the Surry UA

The Surry UA varied the fraction of gaseous iodine versus the time-in-the-cycle. The fraction of gaseous iodine versus an aerosol form of iodine is based on data from the Atomic Energy and Alternative Energies Commission (CEA) detailing the fraction of fission gas released to the fuel-cladding gap as a function of burnup (see Figure 3-69). The uncertainty in the measured gap gas mass (i.e., represented as a fraction of the total iodine inventory) at a particular burn-up is the sampling distribution for the gaseous iodine mass. For each of the specified times selected during the Surry fuel cycle, the range of burnup values is identified. The relevant CEA data is fit to a log-normal distribution, and the gaseous iodine fraction is sampled from that distribution.

The I_2 gas gap fraction is identified by each regression technique as explaining much of the overall variance for iodine release masses. Notably, the rank regression model ranks the time-in-the-cycle as the most important parameter (see Section 3.2.1.1) and the gas gap fraction as the second most important parameter. The gas gap fraction is also identified as having a high conjoint contribution (i.e., contributing with other parameters to have an influence). The iodine release masses for non-C-SGTR realizations increase with an increasing I_2 gas gap fraction as shown on Figure 3-70. A clustering of release masses exists around the gas gap fraction's empirical mean and the releases masses show a strong decade-for-decade relationship with the gas gap fraction in this cluster. Due to the higher mobility of gaseous iodine relative to cesium iodide, the iodine release to the environment is correlated with the specified gaseous mass.

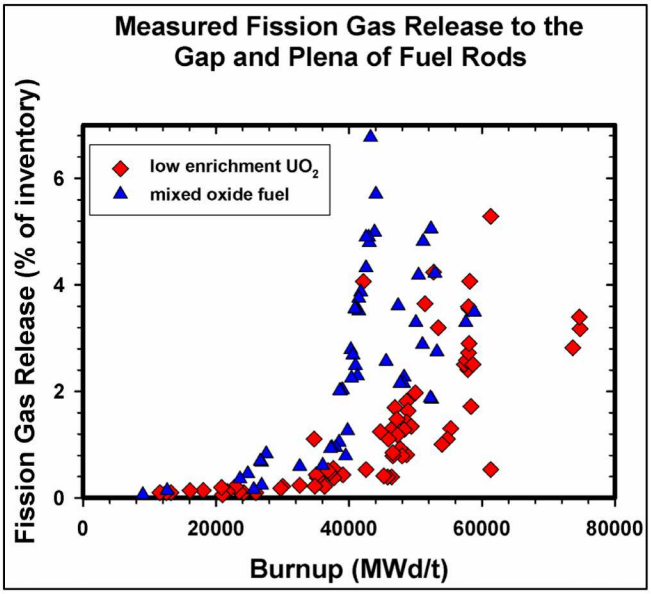

Figure 3-69. French measured fission gas release to the fuel/cladding gap

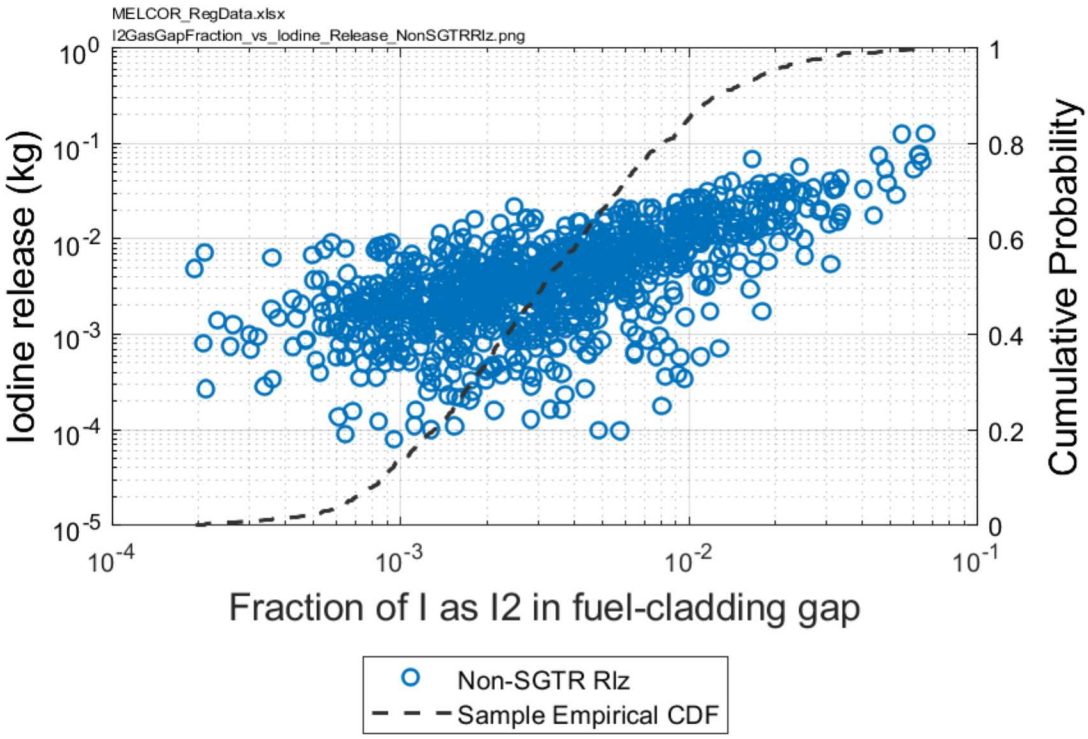

Figure 3-70. Impact of the iodine gas in the fuel-cladding gap on the total iodine release to the environment in the Surry UA

Insights on higher ex-vessel molybdenum releases

The steel in the ex-vessel debris reacts with oxygen released from the ablation of the concrete to form oxides. The steel component of Cr is oxidized first and followed by Fe and Ni. When the steel components in the melt (Ni, Cr, and Fe) are exhausted, the Gibbs free energy chemistry model in MELCOR predicts molybdenum becomes the preferred metal in the debris for oxidation by the ablation gases. The molybdenum oxide (1555°C) has much lower boiling point than the molybdenum metal (4639°C), which dramatically increase the release from the melt and to the environment. The debris change from the depletion of the steel also leads to an increase in the carbon dioxide release rate and a decrease in the carbon monoxide release rate. The timing of the transition is dependent on the concrete type (i.e., limestone or basaltic) and amount of steel in the debris and in the concrete rebar. Appendix A of the draft Surry UA shows the sensitivity of the steel oxidation and ex-vessel molybdenum release versus concrete type. It also shows the sensitivity of the ex-vessel heat balance on the timing of the failure.

The UAs did not include the molybdenum release as a figure of merit. However, the Sequoyah UA shows higher molybdenum releases in the reference calculation (i.e., Realization 266) in Table B-4 (i.e., Realizations 266 at for MACCS plumes 109 and 110). The Sequoyah calculations progressed for 72 hr after the station blackout, which allowed time for the complete oxidation of the steel in the debris.[30] The result was described in detail in Appendix A of the draft Surry UA [38]. However, the timing of complete steel oxidation is highly dependent on the duration of the ex-vessel CCI, the amount of rebar in the concrete, the dimensions of the ex-vessel cavity, and the CCI heat balance and concrete ablation rate. Nevertheless, high molybdenum releases are possible late in time.

3.2.7.3. Implications for Other Plants

The other source term insights from the BWR and PWR UAs are expected to have some generic applicability. The chemical form of the cesium is uncertain and likely variable (i.e., the chemistry forming the various forms of cesium and iodine likely change based on the accident progression for the same plant). However, the chemisorption of cesium to internal stainless structures has a higher applicability to BWRs due to the proximity and very large surface areas of the steam separators and dryers above the core. The same phenomena occur in PWRs but are less effective due to less stainless steel surface area in reactor upper plenum.

In contrast, the amount of gaseous iodine will directly impact the source term in all reactors. The gaseous iodine is highly mobile and its subsequent evolution in the containment [42][43] is complex and uncertain. The formation of iodine gas in the fuel-cladding gap used in the Surry UA shows an increasing inventory as a function of burn-up, which was the second most important uncertain parameter effecting the iodine release to the environment (i.e., more important late in the cycle as discussed in Section 3.2.1.1). The release behavior of the gas in the fuel-cladding gap and the iodine form the fuel matrix has complex uncertainties not explored in the UA (e.g., see discussion in [44] or [43]). Nevertheless, the early release of iodine gas from the gap is expected to affect the source term in all reactor types (see Figure 3-69).

[30] The timing of complete steel oxidation is highly dependent on the duration of the ex-vessel CCI, the amount of rebar in the concrete, the dimensions of the ex-vessel cavity, and the CCI heat balance and concrete ablation rate.

4. NEW EXAMPLES OF ACCIDENT PROGRESSION INSIGHTS

The SOARCA UAs were performed to understand and characterize the uncertainty in the severe accident progression, source term, and consequences. However, the SOARCA UA documentation only focused on the uncertainty in a few figures of merit (FOM). Through additional data-mining, new insights can be obtained from the wealth of results that was not previously reported. This section provides two examples.

New tools were developed that can extract any calculated variable from any number of MELCOR UA calculations. The new tools incrementally access the UA graphical results files stored on Sandia's high-performance computing cluster. The requested data are extracted and further processed using Python scripts. Section 4.1 presents the results from an application that shows the variability of key events from the Surry UA.

The second application is a comparison of the Surry UA results with the source term specifications in NUREG-1465 [9]. The NUREG-1465 source term specifications are used in nuclear safety analysis reports for regulatory compliance with NRC's reactor siting criteria. The corresponding results from the Surry UA are extracted and compared to the NUREG-1465 source term specifications. The results of the benchmark comparison are presented in Section 4.2.

4.1. Variability in Key Events

A basic methodology was developed to extract data from the Surry UA using the PyPost utility developed by Applied Programming Technology, Inc. PyPost is a Java application that can open the MELCOR binary graphical plot files (*.ptf), extract requested data into Python arrays, and write the data to a text file. The methodology has two steps. First, a Python script iterates through the Surry UA output folders to find and extract user-specified variables (e.g., pressures, temperatures, and radionuclide releases) using PyPost. The script produces a single text file per realization that contains a time column and data columns for each variable. Next, a second Python script post-processes the individual text files for the desired FOM. The process allows access to any calculated variable from any number of MELCOR UA calculations. To produce event timings that capture modeling uncertainties, basic statistics were applied to the extracted Surry UA data. The Python pandas data analysis library was used to calculate the mean, standard deviation, and 25th, 50th, and 75th -percentiles for each key event.

Table 4-1 shows the key timing statistics for 289 realizations from the Surry UA.[31] The statistics show the variability of the key event timings. Although a mean and standard deviation are given, it is important to note that the timings are not necessarily normally distributed. Other analysis presentation techniques are possible such as histograms or horsetail plots to graphically illustrate the distribution of the results and time-histories, respectively.

By including the uncertainty in the modeling and accident progression, the SOARCA UA results provide insights into the variability of the accident progression timings that can help inform emergency preparedness and accident management planning. All injections failed at the start of every transient in this data set yet there is considerable variability in event timings due to uncertainties affecting the accident progression. In contrast, the single time values from individual results do not indicate the uncertainty and possible variability in the calculated timings. For example, Table 4-2 shows an updated calculation of the original SOARCA result. With the results in

[31] The first 300 realizations were queried but the 11 realizations that did not complete were excluded from the statistical evaluations. The calculation success rate for the Surry UA was ~95%, which is reflected in this sample.

Table 4-2, a limited understanding of timings can be determined.[32] However, the results do not capture the variability and uncertainty shown in the SOARCA UAs. For example, the values in Table 4-2 could be misapplied for emergency preparedness or accident management applications. Table 4-3 shows the reactor lower head failure (i.e., an important accident progression event) occurs at 9 hr 3 min. The Surry UA results show the median timing was approximately 9 hr 12 min and the 25th to 75th range was also about 9 to 9.5 hr (i.e., rather low uncertainty and a small variation about the median). However, the fastest timing could be 7 hr 32 min and the latest could be 70 hr.

The timing to the containment liner failure (i.e., usually the start of significantly larger radionuclide releases) illustrates a more dramatic variation. The single value from Table 4-2 is 41 hr 5 min while the SOARCA UA variability is from 36 hr 4 min to >72 hr (i.e., 13 of the 289 realizations failed beyond 72 hr). For example, the requirements to re-establish containment heat removal (e.g., sprays) or complete the protective actions in the emergency planning zone is better informed by considering the range of results. The 0.1% elemental iodine timing gives other insights that incorporate C-SGTRs, which can occur as early as 3 hr 30 min. The 25th to 75th percentiles are typical of the non-C-SGTR 0.1% iodine timings while the earlier timings to 0.1% were C-SGTRs.

An additional data analysis was performed neglecting the beginning of cycle realizations, which is presented in Table 4-3. The Surry UA found that the time in the cycle had a strong influence on the accident progression. Specifically, the earliest time in the cycle realizations (i.e., the 0.5 day time in the cycle results) showed a significantly delayed accident progression as compared to all other results. Table 4-3 shows a better characterization of the more likely responses that are not biased by the significantly slower developing 0.5 day results (i.e., just the 0.5 day time in the cycle result is removed).

Generally, the SOARCA and UA timings are comparable. Except for a few events, all SOARCA timings fall within one standard deviation of the UA means. Other events, such as the 1st hydrogen burn and 0.1% iodine release, show a large difference in timing, due to model changes and enhancements made during the UA. Regardless, Table 4-1 and Table 4-3 show that there is uncertainty in severe accident timings that could be used to support emergency and accident management decision making during a severe accident.

As examples of potential applications, nuclear power plant severe accident management guidelines (SAMG) present procedural actions to mitigate the accident severity. Often the SAMG guidance must balance the merits of actions against uncertain pending events and their consequences. The SOARCA UAs provide insights into accident variability and consequences considering a range of uncertain parameters. The state-of-knowledge of severe accident progression has large uncertainties that requires an uncertainty characterization. For example, what is the range of time to restore hydrogen ignitors or should resources be allocated elsewhere? How does an apparent SV FTC impact the accident progression, timing, and consequences? How likely is a C-SGTR to impact the timing and magnitude of the radionuclide releases? What are the accident characteristics that lead to early radionuclide releases and containment failures and what is their potential range of timings? How does the time in the cycle impact timings and the accident progression?

Focused data extractions from SOARCA UA data sets or their equivalent can access hundreds of alternate accident pathways and their uncertainties to inform decisions. The UAs also provide insights into uncertain parameters that have higher importance, which can provide information to

[32] The reference case reported in the *draft* Surry UA included specifications that were close to the median response for a non-C-SGTR scenario [38].

prioritize maintenance or consider plant upgrades (e.g., leak resistant pump seal replacement, the importance of in-service SG inspections, and the importance of containment leakage testing). In summary, data-mining the UAs offers a range of possibilities to assess the importance and variability of outcomes for applications such as accident management, regulatory guidance, emergency response planning, and plant upgrades or maintenance.

Table 4-1. Event timings for Surry UA Realizations 1 to 300 including beginning-of-cycle realizations

Event	Time (hh:mm)							
					Percentile			
	n	mean	std	min	25th	50th	75th	max
First SG SV fails to close	87	00:29	00:26	00:02	00:04	00:20	00:46	01:28
SGC Dryout	289	01:27	00:17	00:25	01:27	01:28	01:31	03:24
SGA Dryout	289	01:30	00:12	00:27	01:29	01:31	01:32	02:43
SGB Dryout	289	01:30	00:16	00:26	01:29	01:30	01:32	03:29
First pressurizer SV opening	286	02:05	00:33	01:51	01:54	02:01	02:06	06:29
PRT rupture disk breaks	282	02:20	00:32	02:00	02:12	02:15	02:18	06:38
First pressurizer SV fails to close	28	02:26	00:37	01:53	01:58	02:10	02:47	04:07
First SGTR	42	03:48	00:17	03:16	03:36	03:49	04:01	04:18
First fission product gap release	289	04:01	02:54	02:43	03:29	03:40	03:44	27:21
Accumulators begin discharging	289	04:39	03:05	03:14	04:06	04:14	04:20	30:47
RCS creep failure	289	04:41	03:06	03:42	04:07	04:15	04:20	30:47
Accumulators empty	289	04:43	03:06	03:44	04:09	04:16	04:22	30:48
First failure of the core support plate	289	06:46	03:43	03:32	06:05	06:17	06:31	38:06
RPV dryout	289	08:09	02:06	05:23	07:38	07:50	08:04	27:48
1st hydrogen burn	289	08:41	03:55	03:42	06:17	09:16	09:48	38:07
Reactor lower head breach	288	10:03	06:18	07:32	08:56	09:12	09:29	70:03
Pressurizer surge tank dryout	11	10:46	02:31	08:53	09:31	09:40	10:40	17:32
Release of elemental iodine to the environment exceeds 0.1%	274	48:42	20:30	03:30	48:42	56:35	61:02	71:54
Containment liner fails	276	51:33	06:46	36:04	47:11	50:46	55:16	70:39
Containment rebar yields	3	69:59	01:00	69:15	69:25	69:34	70:21	71:08

This page left blank

Table 4-2. Key event timing in the SOARCA Surry Unmitigated STSBO[33]

Event	hh:mm
STSBO – loss of all AC and DC electrical power, auxiliary feedwater (AFW) unavailable	00:00
Reactor trips MSIVs close RCP seal leakage initiates at 21 gpm/pump	00:00
RCP seal failure (182 gpm/pump)	-
SG SV fails to close	01:11
SG dryout	01:22
First pressurizer SV opening	01:49
PRT rupture disk breaks	02:09
Start of fuel heatup	02:42
Pressurizer SV fails to close	03:00
First fission product gap release	03:22
C-SGTR	-
First failure of the core support plate	04:01
First failure of the lower support plate	04:08
Loop A hot leg nozzle rupture	04:15
1st hydrogen burn	04:15
Accumulators begin discharging	04:15
Accumulators empty	04:16
RPV dry	06:15
RPV lower head breach	09:03
Reactor cavity dry	09:09
Containment pressure reaches design (45 psig)	23:07
Pressurizer surge tank dryout	17:26
Containment liner yields	41:05
Release of elemental iodine to the environment exceeds 0.1%	Max (0.07%)
Containment rebar yields	-
End of calculation	48:00

[33] This is an updated approximation of the original SOARCA Surry unmitigated STSBO calculation presented in the draft Surry SOARCA UA report [38]. The calculation included some model updates and corrections from the original SOARCA calculation and used the MELCOR 2.1 code. It is a closer approximation to the model and code used in the Surry UA.

This page left blank

Table 4-3. Event timings for Surry UA Realizations 1 to 300 without beginning-of-cycle realizations

Event	Time (hh:mm)							
					Percentile			
	n	mean	std	min	25th	50th	75th	max
First SG SV fails to close	86	00:29	00:26	00:02	00:04	00:21	00:46	01:28
SGC Dryout	283	01:26	00:12	00:25	01:27	01:28	01:30	01:43
SGA Dryout	283	01:29	00:08	00:27	01:29	01:30	01:32	01:43
SGB Dryout	283	01:29	00:10	00:26	01:29	01:30	01:32	01:46
First pressurizer SV opening	281	02:00	00:07	01:51	01:54	01:59	02:05	02:21
PRT rupture disk breaks	277	02:15	00:05	02:00	02:12	02:15	02:18	02:48
First pressurizer SV fails to close	28	02:26	00:37	01:53	01:58	02:10	02:47	04:07
First SGTR	42	03:48	00:17	03:16	03:36	03:49	04:01	04:18
First fission product gap release	283	03:36	00:13	02:43	03:28	03:39	03:44	04:18
Accumulators begin discharging	283	04:13	00:14	03:14	04:06	04:14	04:19	04:54
RCS creep failure	283	04:15	00:10	03:42	04:07	04:15	04:20	04:54
Accumulators empty	283	04:16	00:10	03:44	04:09	04:16	04:21	04:56
First failure of the core support plate	283	06:39	00:24	03:43	06:27	06:40	06:51	07:51
RPV dryout	281	07:51	00:25	05:23	07:38	07:50	08:03	09:21
1st hydrogen burn	283	08:13	01:57	03:42	06:16	09:14	09:43	11:59
Reactor lower head breach	283	09:14	00:31	07:32	08:56	09:12	09:28	11:37
Pressurizer surge tank dryout	11	10:46	02:31	08:53	09:31	09:40	10:40	17:32
Release of elemental iodine to the environment exceeds 0.1%	274	48:42	20:30	03:30	48:42	56:35	61:02	71:54
Containment liner fails	276	51:33	06:46	36:04	47:11	50:46	55:16	70:39
Containment rebar yields	3	69:59	01:00	69:15	69:25	69:34	70:21	71:08

This page left blank

4.2. Surry UA Source Term Variability as Compared to NUREG-1465

A benchmark comparison to the historical NUREG-1465 source term characterization is another example of data-mining the existing SOARCA UA runs. The NUREG-1465 study, which was completed in 1995 [9], embodied over 30 years of research since the first regulatory source term specification (i.e., TID-14844 [45]). The updated study provided more realistic estimates of the source term for licensing considerations of containment performance following a substantial meltdown of the core. The breadth of NUREG-1465 is significant in that it considered 36 accident sequences from eight different types of PWRs and BWRs. Using this large range of results, the revised BWR and PWR regulatory source terms were developed. Consequently, the strengths of the NUREG-1465 source terms are the diversity in sequences and plant types.

The benchmark comparison presented in this section compliments the previous effort and subsequent investigations into high-burn fuels (i.e., [10][11][12]). An examination of a single SOARCA UA accident sequence from a single plant does not span the range of plants or sequences considered in the NUREG-1465 work. However, the PWR short-term station blackout (i.e., this benchmark is based on the Surry UA STSBO results) is a risk-significant and fast-progressing accident without mitigation, and therefore relevant to a regulatory source term characterization. More importantly, a benchmark to the SOARCA UA includes consideration of phenomenological uncertainties propagated over hundreds of simulations that was beyond the scope of the previous efforts. The SOARCA UA results recognize important uncertainties and their impact on one sequence to generate significant variability in the source term. Consequently, the benchmark provides insights into the uncertainty of a single sequence versus the diversity from many sequences and plants. In addition to the aforementioned differences, some other considerations for comparing the Surry UA to the NUREG-1465 source term are discussed in Section 4.2.1.

A challenge in analyzing the SOARCA UA source term results is the large number of calculations. To overcome this challenge, data analysis tools were developed to quantify the source term variability, which were described in the previous section. Section 4.2.2 discusses the specific methods used to calculate the variability of the source term in the Surry UA source term.

The results of the comparison are discussed in Section 4.2.3 and the benefits of this application are presented in Section 4.2.4.

4.2.1. Considerations for Comparing the Surry UA to NUREG-1465

The present benchmark approach is not postulated to replace a NUREG-1465-style source term characterization. Rather, the SOARCA UA results provide an alternate data source and approach to support the interpretations necessary to verify or improve the regulatory source term. Most importantly, the SOARCA UA includes consideration of important uncertainties that would impact aspects of any scenario and any plant from the diverse group considered for NUREG-1465 or the subsequent high-burn-up studies. Such an uncertainty characterization was not possible at the time these studies were performed.

Furthermore, the Surry UA is performed using MELCOR 2.2 which utilizes a significantly enhanced model versus the earlier calculations. Consequently, what the Surry UA lacks in diversity of sequences and plant types, it benefits from the current state-of the art in plant modeling and software. The efforts to perform the SOARCA UA studies included extensive ACRS and peer reviews of the model, uncertainty parameters, and results.

4.2.2. Analysis Method

NUREG-1465 [9] and the subsequent high-burn-up investigations [10][11][12] divided the accident progression into four phases after the first cladding failure (see Figure 4-1).[34] Dividing the accident into four phases allows for understanding the fission product release timings and fractions at key events in the accident progression. The key events that characterize the four phases are the first cladding failure, the significant buildup of noble gases in the containment, the reactor lower head failure, the end of ex-vessel releases, and the end of the in-vessel revaporization release. The time intervals between the key events are identified as the gap release, in-vessel release, ex-vessel release, and late in-vessel release phases. A graphical view of this timeline is given in Figure 4-1. Each phase has a characterized start time, duration, and fission product release fraction.

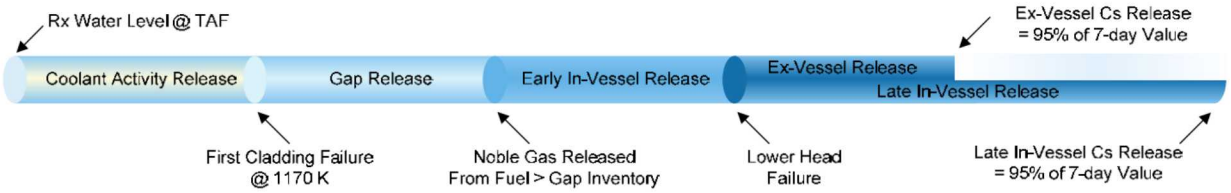

Figure 4-1. Release phase timing definitions and tie to MELCOR results [10]

The NUREG-1465 phase definitions illustrated in Figure 4-1 were used for the Surry UA benchmark. The same phase definitions were also used in the high-burn-up investigations of the regulatory source term [10][11][12]. Since the Surry UA calculations only ran through 72 hr, the end definitions of the ex-vessel and late in-vessel phases were accordingly truncated. The specifications of the start and end of the four phases used in the Surry UA example are shown in Table 4-4.

Table 4-4. Fission product release phase definition

Phases	Start Definition	End Definition
Gap Release	First Cladding Failure	5% Xe in Containment
In-Vessel Release	5% Xe in Containment	Lower head failure
Ex-Vessel Release	Lower head failure	95% of I in Containment from Cavity
Late In-Vessel Release	Lower head failure	95% of I in Containment from Remaining Sources

To complete the data analysis for the hundreds of Surry UA results, a Python script was developed to calculate the phase start times, the phase durations, and phase fission product release fractions. To do this efficiently, the required data were extracted using the PyPost software from the MELCOR graphical plot (**.ptf*) files on Sandia's high-performance server into text (**.csv*) files that could easily be imported into Python. Once the text file is loaded into Python, the start and end

[34] There is also an early activity release to the coolant from leaking fuel rods, which is not included. The early activity release is insignificant relative to the source term from the other phases and not included in the SOARCA UA and MELCOR simulations.

timings for each phase are calculated using the definitions from Table 4-4. Using the start and end timings, the magnitude of the radionuclide releases in each phase are calculated. The SOARCA UA results include the effects of design leakage from the containment and its failure. Consequently, the comparison to the NUREG-1465 release to the containment includes consideration of all radionuclides leaving the primary system or ex-vessel fuel to the containment and the environment. The C-SGTR results were included in this sampling.

The Surry UA model includes 17 radionuclide classes (see Table 4-5) and four other non-radioactive structural classes (i.e., not relevant for the source term).[35] The benchmark is currently limited to the noble gases (i.e., the Xe class), all forms of cesium (i.e., Class 2 and the cesium portion of Classes 16 and 17), and all forms of iodine (i.e., Class 4 and the iodine portion of Class 16). The source term results are then put into a dataframe variable for analyzing.

There are three main data outputs from the dataframe to compare to the NUREG-1465 values: (1) table values, (2) horsetail plots, and (3) histograms. The next section presents tables of the values from the Surry UA and their statistical variance with a comparison to the NUREG-1465 values. Examples of a horsetail plot and histogram are also provided to illustrate effective ways that show the data variability. The histograms are formed by subdividing the results into uniform intervals and recording the number of samples in each interval.

Table 4-5. MELCOR radionuclide classes

Class	Class Name	Chemical Group	Representative	Member Elements
1	XE	Noble Gas	Xe	He, Ne, Ar, Kr, Xe, Rn, H, N
2	CS	Alkali Metals	Cs	Li, Na, K, Rb, Cs, Fr, Cu
3	BA	Alkaline Earths	Ba	Be, Mg, Ca, Sr, Ba, Ra, Es, Fm
4	I2	Halogens	I_2	F, Cl, Br, I, At
5	TE	Chalcogens	Te	O, S, Se, Te, Po
6	RU	Platinoids	Ru	Ru, Rh, Pd, Re, Os, Ir, Pt, Au, Ni
7	MO	Early Transition Elements	Mo	V, Cr, Fe, Co, Mn, Nb, Mo, Tc, Ta, W
8	CE	Tetravalent	Ce	Ti, Zr, Hf, Ce, Th, Pa, Np, Pu, C
9	LA	Trivalents	La	Al, Sc, Y, La, Ac, Pr, Nd, Pm, Sm, Eu, Gd, Tb, Dy, Ho, Er, Tm, Yb, Lu, Am, Cm, Bk, Cf
10	UO_2	Uranium	UO_2	U
11	CD	More Volatile Main Group	Cd	Cd, Hg, Zn, As, Sb, Pb, Tl, Bi
12	AG	Less Volatile Main Group	Ag	Ga, Ge, In, Sn, Ag
16	CSI	Cesium iodide	CsI	CsI
17	CSM	Cesium molybdate	Cs_2MoO_4	Cs_2MoO_4
18	Ag	Control rod silver	Ag	Ag (non-radioactive from the control rod)
19	In	Control rod indium	In	In (non-radioactive from the control rod)
20	Cd	Control rod cadmium	Cd	Cd (non-radioactive from the control rod)
21	Sn	Tin from the zircaloy	Structural Sn	Sn (tin released from the oxidation of zircaloy)

[35] The structural, non-radioactive radionuclide classes are important to the overall aerosol behavior. They are important in how they impact aerosol settling and agglomeration of the radioactive releases but not mentioned further here.

4.2.3. Surry UA Source Term Results

The release of the radionuclides occurs in the various phases from various locations (i.e., the fuel rods, the in-vessel debris, revaporized off the in-vessel structures, and from the ex-vessel debris). The data extraction considers all radionuclides that arrive in containment and not their status (e.g., airborne or settled). Because the Surry UA propagates phenomenological uncertainties over one thousand simulations, the accident phase timings, durations, and fission product releases during the various phases are distributions rather than single values. The distributions provide additional insights for comparison to the NUREG-1465 results, which is based on single calculations for each sequence.

The radionuclide values from the Surry UA are reported as fractions of the initial inventory. However, the Surry UA considered 20 unique inventories spanning the time-in-the-cycle. The various radionuclides are at various states of achieving a secular equilibrium and represent different masses as a function of the time-in-the-cycle (e.g., see Section 3.2.1). The additional sophistication of identifying the variations in the inventory masses as a function of the cycle is not presently included (i.e., all results are non-dimensionalized based on the specific inventory sampled in the realization).

4.2.3.1. Comparison to NUREG-1465

Table 4-6 shows the mean, standard deviation, minimum, 5th, 25th, 50th, 75th, and 95th percentile, and maximum values of the Surry UA accident phase start times. While NUREG-1465 does not explicitly provide start times for each phase, the Surry UA results are an interesting quantity to report for other applications (e.g., emergency preparedness or accident management actions). As seen in the table, the start timings between the 5th and 95th percentiles for all phases are relatively close. This means that there is a small variability in the start times for the majority of Surry UA runs, which is somewhat expected since all results are from the same sequence (i.e., a STSBO).

Table 4-6. Accident phase start times (hours)

Metrics	Gap	In-Vessel	Ex-Vessel	Late In-Vessel
NUREG-1465	n/r	n/r	n/r	n/r
Mean	3.9	5.2	10	10
Standard Deviation	2.6	3.1	6.3	6.3
Minimum	2.7	3.2	7.5	7.5
5%	3.3	3.9	8.6	8.6
25%	3.5	4.3	8.9	8.9
50%	3.7	5.0	9.2	9.2
75%	3.7	5.3	9.5	9.5
95%	4.0	5.7	10	10
Maximum	26	31	70	70

n/r = not reported.

The distributions of the Surry UA phase durations are shown in Table 4-7. There are significant deviations in Surry UA phase durations versus the NUREG-1465 results. Each phase from the Surry UA shows an order of magnitude variation. The large variation in the Surry UA durations suggest a large uncertainty when trying to predict duration. While not observed here, some of the variation in the durations stems from very small releases occurring over a protracted time interval and the inclusion of the 0.5 day time-in-the-cycle results.

Table 4-7. Accident durations (hours)

Metrics	Gap	In-Vessel	Ex-Vessel	Late In-Vessel
NUREG-1465	0.5	1.3	2.0	10.0
Mean	1.2	4.9	19	26
Stand. Dev.	0.71	3.4	4.0	5.3
Minimum	0.30	3.2	1.4	1.4
5%	0.52	3.6	13	19
25%	0.57	4.0	17	25
50%	1.6	4.5	19	27
75%	1.6	5.0	21	29
95%	1.9	5.7	26	32
Maximum	5.5	39	31	38

Table 4-8 shows a comparison of the noble gases releases by phase, which are represented in MELCOR as xenon (Xe). Xenon is a non-condensable gas, which is used to identify the start and end of the gap release phase. Some xenon forms in the gap between the fuel and the cladding in the fuel rods. The start of the gap phase is the timing of the first fuel cladding failure (i.e., occurs during the core degradation process). The released xenon circulates through the primary system and enters the containment with the gas discharged to the PRT via the pressurizer SV cycling.[36] A 5% release of xenon to the containment is used to identify a non-trivial release of radionuclides from the fuel (i.e., the end of the gap phase). Since the released xenon remains mobile as a gas, it is the best radionuclide to identify the start of the release phase from the fuel. Xenon is also released from the fuel during the in-vessel core degradation. This is shown by both the NUREG-1465 value and the Surry UA results data indicating ~100% of xenon inventory is released in the gap and in-vessel phases.[37] Unlike the phase durations, the xenon release fractions have a tight distribution meaning there is less uncertainty.

[36] The alternate pathways for release to the containment are not active at this phase of the accident (e.g., RCP seal leakage, the hot leg failure, or the lower head failure). At this time, the leakage through the RCP seals is liquid water. Once the xenon reaches the PRT, it is considered in the containment for the purposes of tracking the source term. Once the PRT pressurizes, the rupture disk will open and the xenon will be released to the containment.

[37] The Surry UA assumed 5% of the xenon is in the gap. The remaining xenon is released during the in-vessel phase due to diffusion processes from the fuel matrix.

Table 4-8. Comparison of the NUREG-1465 and Surry UA fractional xenon releases to the containment for the four phases

Metrics	Gap	In-Vessel	Ex-Vessel	Late In-Vessel
NUREG-1465	0.05	0.95	0.0	0.0
Mean	0.052	0.93	0.012	0.0021
Stand. Dev.	0.0071	0.024	0.020	0.0025
Minimum	0.050	0.74	0.0003	0.0000
5%	0.050	0.90	0.0024	0.0000
25%	0.050	0.93	0.0056	0.0004
50%	0.051	0.93	0.0084	0.0013
75%	0.052	0.94	0.012	0.0028
95%	0.054	0.94	0.021	0.0063
Maximum	0.16	0.95	0.21	0.021

Table 4-9 shows a comparison of the alkali metals releases by phase, which are represented by the various forms of cesium. NUREG-1465 shows a distributed release over the in-vessel and ex-vessel phases, while the Surry UA release of cesium occurs almost entirely during the in-vessel phase. The Surry UA model tracks three chemical forms of cesium (i.e., CsOH, CsI, and Cs_2MoO_4). Although the volatility of the chemical forms vary, MELCOR predicts the in-vessel degradation in the relatively fast-progressing STSBO will release most of the volatile inventory, which includes xenon, cesium, and iodine. Consequently, a key insight is the significantly larger release during the in-vessel phase in the Surry UA than reported in NUREG-1465.

Table 4-9 Comparison of the NUREG-1465 and Surry UA fractional cesium releases to the containment for the four phases

Metrics	Gap	In-Vessel	Ex-Vessel	Late In-Vessel
NUREG-1465	0.05	0.25	0.35	0.1
Mean	0.015	0.74	0.011	0.0095
Stand. Dev.	0.0087	0.12	0.017	0.0095
Minimum	0.0000	0.16	0.0004	0.0000
5%	0.0065	0.53	0.0023	0.0032
25%	0.0088	0.74	0.0054	0.0055
50%	0.014	0.77	0.0081	0.0075
75%	0.019	0.80	0.011	0.010
95%	0.025	0.83	0.019	0.019
Maximum	0.10	0.84	0.17	0.088

Table 4-10 shows a comparison of the halogen releases by phase, which are represented by the various forms of iodine (i.e., I_2 gas and cesium iodide). Like the cesium release results, NUREG-1465 shows the iodine release is distributed over the in-vessel and ex-vessel phases, while the Surry UA release of iodine occurs almost entirely during the in-vessel phase.

Consequently, the majority of the xenon, cesium, and iodine releases occur during the in-vessel phase in the Surry UA. Although there is agreement on the xenon releases with NUREG-1465, NUREG-1465 shows a more balanced release of cesium and iodine between the in-vessel and ex-vessel phases.

Table 4-10. Comparison of the NUREG-1465 and Surry UA fractional iodine releases to the containment for the four phases

Metrics	Gap	In-Vessel	Ex-Vessel	Late In-Vessel
NUREG-1465	0.05	0.35	0.25	0.1
Mean	0.020	0.80	0.016	0.031
Stand. Dev.	0.0084	0.11	0.0090	0.047
Minimum	0.0004	0.24	0.0014	0.0016
5%	0.011	0.58	0.0051	0.0079
25%	0.014	0.80	0.011	0.015
50%	0.018	0.83	0.015	0.020
75%	0.024	0.86	0.019	0.029
95%	0.032	0.88	0.036	0.064
Maximum	0.082	0.89	0.057	0.36

The Surry UA calculations track all radionuclides shown in Table 4-5. This example only shows three radionuclides but could be easily expanded to all the values shown in NUREG-1465 and Table 4-5. Cesium and iodine were selected because they have important health consequences and were included in the key FOMs in the SOARCA UA studies. The xenon results are interesting because they show the start and end of the gap phase and occur without any deposition in the primary system.

4.2.3.2. Horsetail Results

An alternate way to show the Surry UA results is through horsetail plots. The horsetail plot illustrates the variability in all the results in a manner not readily observable in the table values. The time-histories of the iodine releases are shown in Figure 4-2 and illustrate the variability and uncertainty in the Surry UA predictions. The iodine releases start quite early in the accident, which is shown in various statistical values in Table 4-10. While the horsetail figures show the same data as the tables, it allows for more meaningful qualitative insights of the time-histories that is not possible with the end-values presented in the tables. The markedly different 0.5 day time-in-the-cycle results are clearly evident as the slowly developing results.

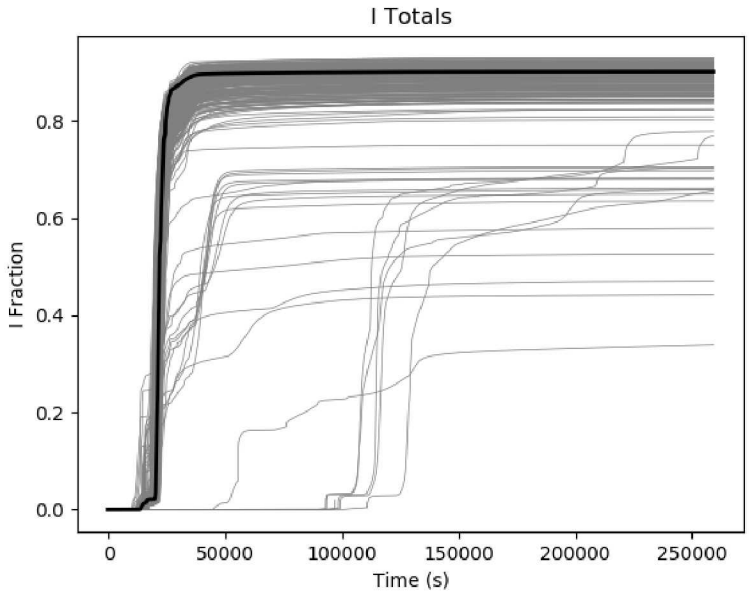

Figure 4-2. Example of a horsetail plot for total iodine fraction in containment as a function of time

4.2.3.3. Histogram Results

Another way to represent the Surry UA data is through histograms. The histograms visually show the distribution for a particular quantity of interest (such as timings, duration, or fission product release fractions) for each phase. A narrow distribution suggests a lower amount of uncertainty in the metric (e.g., phase start time, duration, or magnitude of the release) while wide distributions suggest higher variability and uncertainty. The histogram is an effective way of visualizing the percentiles shown in the tables. As an example, a histogram of late in-vessel duration is shown in Figure 4-3. The x-axis shows the duration of the phase while the y axis shows the number of simulations per bin (bin width ~14 mins). If the majority of simulations are in a few bins, then the distribution is narrow; while if the simulations are spread out in many bins, then the distribution is wide. The distribution shown in Figure 4-3 is quite wide, spanning ~10 hr, which is confirmed in Table 4-7. This corresponds to a large variability or uncertainty in the duration of the late in-vessel phase. The duration reported in NUREG-1465 for late in-vessel phase is much lower than predicted for the Surry UA. Some of the variability in the Surry UA results arise from the time-in-the-cycle sampling.

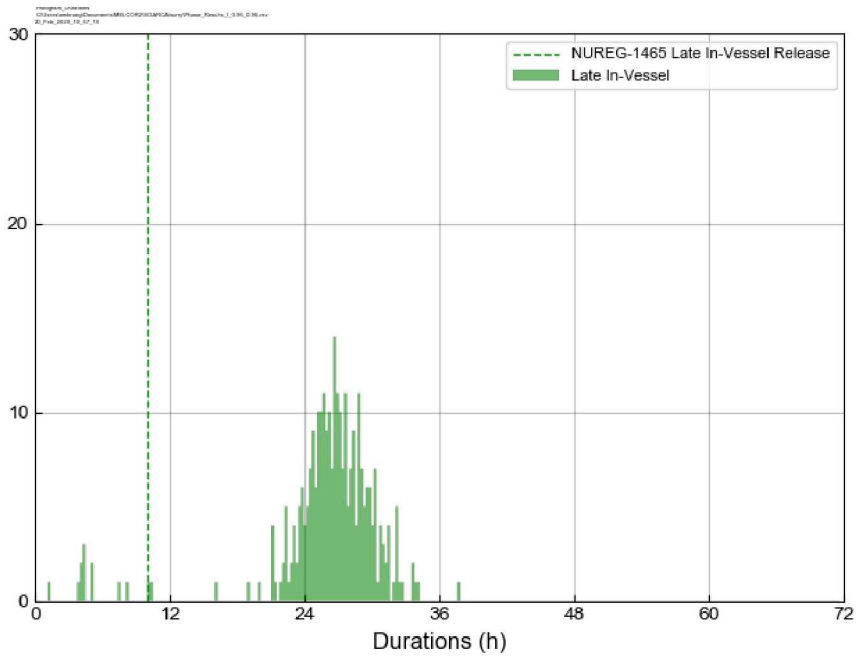

Figure 4-3. Example of a histogram describing the variation in late in-vessel duration

More information can be mined out of the data provided by the Surry UA using a combination of tables, horsetail plots, and histograms. This data can help better understand the conservatisms built into regulatory guidance, such as release fraction data in NUREG-1465. Some unrealized benefits that can be gained from data analysis of Surry UA data is shown in the next section.

4.2.4. Additional Refinement

An additional refinement would be to further characterize how accidents progress than evident in the phases. One way is to rethink the phase characterization to better understand the rate of release to containment. For example, using derivative information, such as the iodine release fraction shown in Figure 4-4, the phases can be split up into: (1) a "bulk release phase" and "rest of release phase" or any number of phases, (2) rate versus duration curves, or (3) a single integral release curve to better characterize how the release occurs. While instantaneous derivatives are quite noisy using Eq. 1, the time evolving derivative in Eq. 2 smooths the derivatives, which is used to calculate the results in Figure 4-4. By smoothing the derivative in this manner or using more sophisticated Python tools, it becomes easier to characterize how fission product release occurs.

$$\frac{\varphi^{n+1} - \varphi^{n}}{t^{n+1} - t^{n}} \qquad \text{Eq. 1}$$

$$\frac{\varphi^{n+1} - \varphi^{n}}{t^{n+1} - t^{0}} \qquad \text{Eq. 2}$$

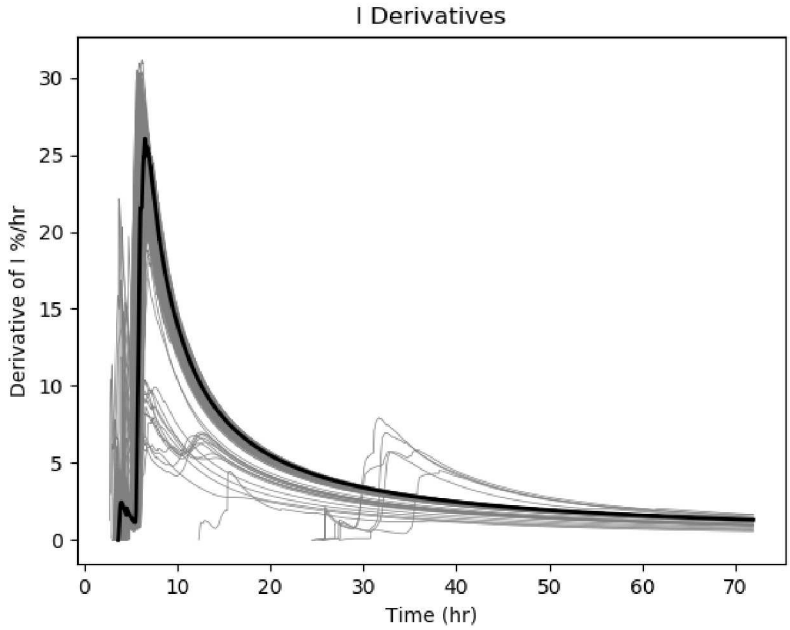

Figure 4-4. Example of a horsetail plot for I fraction derivative in containment as a function of time

As seen in Figure 4-4, the peak iodine release rate occurs at approximately 10 hr. This means the bulk of the iodine is released to the containment during this time. The peak release for most realizations occurs at 10 hr, which is during the in-vessel release phase. Whereas the gap and in-vessel release phases occur over small time intervals, the late ex-vessel and in-vessel phases occur over hours. Either integral accident or phase-specific derivates could be used to better inform an overall release rate or the integral release within the phase. A rate specification could be used to better inform the release to the containment rather than the current approach of a constant release rate for the phase duration.

Finally, one benefit of considering the radionuclide release without regard to phases is evident in Table 4-8 through Table 4-10. The specific metrics for the minimum, the percentiles, and maximum are not representative of the radionuclide inventory in a single realization. For example, the maximum xenon release across all four phases is approximately 1.2 due to different realizations contributing to each maximum phase. Using the releases results over the entire accident ensures mass conservation.

5. SUMMARY

This report highlights the key insights from the three SOARCA UAs but specifically within the scope of the accident progression insights rather than consequence or methodology insights. Although all three studies provide insights into the accident progression and the source term, the scope of each project had different focuses that helped guide the uncertainty parameter selection and corresponding emphasis in the regression evaluations. The common elements from the accident progression insights from the three UA studies were reviewed and organized. The insights focus on the iodine and cesium source term to the environment as the key FOM. The attributes of the iodine and cesium FOM were the parameters that impacted both the magnitude and the timing of the release (e.g., potential for an early containment failure). The key insights are related to (a) the time in the fuel cycle, (b) valve failures, (c) C-SGTRs, (d) hydrogen behavior, (e) containment failure, (f) primary seal leakage, and (f) other source term insights related to modeling uncertainties. Some insights have more information or applicability from one UA versus the other. However, a qualitative discussion is provided about the applicability of the UA findings to other plants.

Time in the cycle

The time in the fuel cycle parameter was an indication of how the fuel burnup influenced the accident progression. The time in the cycle had an integrated impact on the MELCOR accident progression through the magnitude of the decay heat power and the MELCOR and MACCS source term analysis through the mass and make-up of the fission product inventory. It was identified as the most important parameter influencing the accident progression timing, including time of the hot leg rupture, LHF, and containment failure. It was also important to hydrogen production in a non-intuitive manner with more hydrogen production with less burn-up. Through inspection of the Surry and Sequoyah UA results, the containment pressure responses are transitioning from almost no pressurization at 0.5 days to an observable pressurization at 6.25 days. By 25 days into the cycle, the Surry UA is showing a pressurization to containment failure prior to 72 hr. There are many plant specific factors affecting the containment response, but these results provide qualitative insights into the duration of the early burn-up phase. Somewhat surprising, the time in the cycle had a greater importance on the iodine source term, which reaches a secular equilibrium in about 50 days, versus the cesium source term, which grows monotonically in mass throughout the cycle. The higher decay heat as the cycle progressed influenced the magnitude of the late revaporization of gaseous iodine, whereas it had a lower impact on aerosol forms of cesium, which had largely settled prior to containment failure.

Most of the qualitative insights from the time in the cycle from the Surry and Sequoyah UAs will be applicable to all plants. The uncertainty revealed large variations in the radionuclide inventories and decay heats from BOC to EOC. Relative to the timing of the accident progression, the earliest sampled times in the cycle had significantly different behavior until the inventories of shorter-lived isotopes reached a secular equilibrium. An interpretation using the Surry and Sequoyah results suggest this occurs after 25 days. This behavior is expected to be generally consistent for other PWRs and BWRs. The regressions of the key accident event timings show a correlation of the time in the cycle to accelerating the accident progression including hot leg failure, reactor vessel lower head failure, and containment failure. The correlation of these items to a BWR would be the timing to a thermal failure of the SRV, reactor lower head failure, and containment failure. The insights on the accident progression timing as a function of the time in the cycle are qualitatively applicable to all plants.

The time in the cycle was identified as the most important parameter for in-vessel hydrogen production in the Surry UA. The higher quantity of hydrogen at earlier times in the cycle with lower decay heat is expected to be applicable to all plants. The time in the cycle also had an important impact on the source term. The time in the cycle was more important to the iodine release to the environment in both the Surry and Sequoyah UAs than for the cesium release to the environment. The differences were attributed to an increased mobility (i.e., revaporization) and release of the iodine as a function of the decay heat. This is expected to be especially important in BWRs too. The qualitative implications for other plants are expected to be the same but quantitatively impacted by plant-specific containment leakage and failure attributes.

Valve failures

Valve failures were identified as important in all three UAs. A valve failure changes the course of the accident, which may occur from observed failures under design conditions (i.e., a stochastic failure) and thermal failures at degraded severe accident conditions (i.e., calculated, high-temperature conditions where varying differential thermal expansions lead to failures near 900 K). However, there is sparse data and a lack of established expert consensus on how best to model the failure rates under severe accident conditions. Only BWR SRVs experienced thermal failures in the SOARCA UAs, whereas stochastic failures near or below design limits were possible in BWR SRVs, PWR pressurizer SVs, and PWR MSS SVs. A common component of the primary system valve failures was the acceleration of the accident progression and redirection of fission products to the wetwell (BWRs) or the PRT (PWRs).

The type of valve failure (stochastic or thermal) and the failure area were the most important variable effecting the BWR cesium release to the environment. Early stochastic failures had lower source terms whereas later thermal SRV failures retained more fission products in-vessel for subsequent revaporization and created the potential for an MSL failure that bypasses the wetwell (i.e., when the failure area is small). A PWR pressurizer SV failure with a large failure area created conditions for a larger hydrogen burn through a protracted release and circulation of hydrogen in the containment prior to an identifiable ignition source, which was an important over-pressurization challenge for the smaller ice condenser containments.

Combinations of a PWR MSS SV failure with no pressurizer SV failure promoted additional mechanical stress for a C-SGTR. An MSS SV failure was not necessary for a C-SGTR due to other mechanisms to depressurize the secondary (i.e., MSIV leakage). However, no C-SGTRs occurred following a pressurizer SV failure or an SV failure with a small leakage area was necessary. Finally, PWR SV FTCs had other impacts such as delaying hot leg failure and contributing to revaporization sources from the PRT. A failed pressurizer SV with a large failure area delays hot leg failure, which can concentrate large quantities of radionuclides in the PRT. The subsequent revaporization can have an impact when it occurs near or after containment failure. Revaporization from the PRT was not observed in the ice condenser plant due to cooling from the deep containment water pool formed by the melted ice.

The UA analyses identified SV FTC as the key or one of the key uncertain parameters increasing the source term, which is expected to translate to insights in other similar plant designs. All PWRs include pressurizer and MSS SVs. In scenarios with a loss-of-power sequences like the SBOs in the Surry and Sequoyah UAs, the MSS and pressurizer SVs will cycle to release steam and prevent an over-pressurization of the secondary system. With respect to the uncertainty of their failure characteristics, the SV FTC characteristics used in the PWR UAs are judged representative of other

PWRs in the U.S. The quantitative insights are dependent on many plant-specific factors that limit their direct applicability. However, the following qualitative insights are applicable:

- An MSS SV FTC weakly increases C-SGTR occurrences.
- A pressurizer SV FTC with a large failure area can prevent a C-SGTR whereas no FTC or an FTC with a small failure area promotes a C-SGTR.
- A pressurizer SV FTC with a large failure area can delay or prevent hot leg failure.
- A pressurizer SV FTC can concentrate radionuclides in the PRT that may promote their late revaporization.
- A pressurizer FTC with a large failure will increase hydrogen release prior to an ignition source, which contributes to larger hydrogen burns.

The related conclusions for C-SGTR Reactors with a B&W NSSS are judged not applicable because the once-through SGs are less susceptible to hot natural circulation flows from the core.

Overall, the Peach Bottom SRV failure insights are expected to have qualitative applicability to all BWRs. The stochastic and thermal failure characteristics are expected to be similar. The associated thermal challenges to the MSL is also expected to be applicable. The impact of the source term from the various SRV and MSL failures is not expected to be generally applicable due to significant variations in the BWR containment design. However, the responses of the other Mark I containments are expected to be similar to the Peach Bottom with some variations in the timing of the liner melt-through due to the sump size and drywell wall and floor characteristics.

The valve failures are only applicable to transients without power or control of the BWR SRVs or PWR power-operated relief valves. The operator control of these valves provides additional flexibility to regulate the system pressure and eliminate repetitive cycling.

C-SGTRs

A C-SGTR was a very important early and late phase release pathway for PWRs. In every realization with a C-SGTR, a hot leg nozzle rupture also occurred (i.e., the attributes that lead to a C-GTR also promote a hot leg rupture). The realizations with a C-SGTR had a large and early releases of cesium and iodine. The hot leg failure terminated the high leakage flow rate through the C-SGTR. However, the C-SGTR persisted as the dominant pathway for cesium and iodine radionuclide release as the containment pressurized due to ex-vessel CCI. A key insight was that only tubes with flaws progressed to a C-SGTR. If there was a deep flaw, then the failure was predicted in all locations in the SG and not limited to the highest temperature regions. The likelihood of a C-SGTR for the cold and hot upflow regions significantly increased if the non-dimensional flaw depths were greater than 0.8 and 0.68, respectively. The likelihood of a C-SGTR in the peak temperature region significantly increased if either the non-dimensional flaw depth was greater than 0.42 or if the flaw depth was greater than 0.31 with a peak non-dimensional hot plume temperature greater than 0.48 (i.e., near the higher end of the uncertainty range).

Following the C-SGTR, the dense arrangement of the steam generator tubes with grid supporters were very effective at retaining larger aerosols. However, gases and small aerosols slipped past the obstructions with an effective decontamination less than 2. The in-vessel aerosol distribution was skewed towards smaller aerosols as the accident progressed and the larger aerosols settled.
A sensitivity study with multiple C-SGTRs showed a sequential increase in the source term until 3 C-SGTRs. Above 3 C-SGTRs, the incremental adverse impacts were limited by a less significant increase in leakage and controlling leakage on the SG secondary side. The largest source term in the Surry UA was the rare case with 2 C-SGTRs.

The qualitative insights from the Surry UA are applicable to other PWRs with similar hot leg and SG geometries. These include Westinghouse plants with SGs similar to the Model 51 SG, which includes the Model 44 SG. However, the conclusions can be different for other geometries. NUREG-2195 found that the conditional probability of a C-SGTR is about a factor of 10 larger for plants with a shallow inlet SG plenum (e.g., the selected CE plant) than the plants with a deep inlet SG plenum (e.g., a Westinghouse plant with a Model 51 SG). The observations on the flaw depth for a C SGTR from the Surry UA would suggest less severe flaws will fail tubes in a CE plant. Consequently, the Surry UA quantitative insights on flaw depth would not be conservative for a CE plant or other SG designs with large, shallow SG inlet plenums (e.g., the AP1000).

The C-SGTRs are not applicable to B&W plants with once-through SGs. BWRs do not have SGs, so the issue is not applicable for them.

Hydrogen behavior

The behavior and combustion of hydrogen was a focus in the PWR UAs and observed in the BWR reactor building (e.g., as observed in the Fukushima Dai-chi accident). A key part of the UA methodology identified active ignition sources, which included ex-vessel CCI and hot jets above the autoignition temperature from the hot leg, RCP, and PRT. The PWR UAs included several uncertainty parameters to investigate hydrogen ignition and combustion loads. None of the hydrogen burns in the Surry UA threatened a containment over-pressure failure, which is the likely outcome for steel-reinforced concrete containments without steam suppressing attributes (e.g., ice in PWR ice condenser containments or water in BWR Mark III containments). The early burns (i.e., often the first burn) were the largest, especially when the hydrogen can distribute throughout the containment prior to an identifiable ignition source. Only the first burn caused a containment failure in the Sequoyah UA. The late phase burns typically occurred due to a persistent ignition source (i.e., hot jets and CCI) and ignited hydrogen locally and at lower concentrations. Due to a finite and diminishing oxygen content versus growing steam and CCI gas concentrations, the PWR containments dropped below the oxygen threshold that could support combustion. As discussed above, the valve behavior was the most important contributor to the largest hydrogen combustions.

The low likelihood of an early failure of Sequoyah's free-standing steel containment from a hydrogen burn was a key insight. A pressurizer SV had to fail with a large failure area with sufficient time for hydrogen to circulate into the upper containment prior to the first ignition source. Furthermore, the realizations with an early containment failure almost always had a sampled failure pressure of the containment below the median of the failure pressure distribution (i.e., the peak pressure from the hydrogen burn rarely exceeds the median failure pressure). When these criteria aligned, the first burn started in the lower containment due to one of the identified ignition sources (i.e., hot gases from the hot leg, PRT, or RCP) and propagated into the large upper containment. The resulting over-pressure failure challenge yielded a large and early source term if the containment ruptured (i.e., much earlier and larger than most non-early containment failure iodine and cesium releases). If igniters were recovered, then the hydrogen was burned locally at lower concentrations and there was not an over-pressure challenge to the containment. The LTSBO hydrogen sensitivity calculations confirmed that valve failures produced a large hydrogen source to the containment, but multiple ignition sources were predicted that could ignite the mixture before reaching concentration capable of an overpressure failure.

Containment failure

The events contributing to containment failure are themes of the aforementioned insights. Interestingly, the BWR Mark I containment failure showed low importance to ex-vessel debris

movement and drywell head leakage. Every Peach Bottom UA calculation included drywell leakage and drywell liner melt-through (i.e., the uncertainty exploration did not preclude these events). New MELCOR 2.2 calculations with updated ex-vessel debris behavior showed the radionuclide releases with a delayed drywell liner failure were replaced with higher releases from drywell head leakage. Consequently, the impact on the overall radionuclide leakage was minor. Similarly, hydrogen burns in the BWR reactor building occurred in every calculation, which diminished any significant retention benefit. Consequently, the uncertain parameters for reactor building performance were not important for the magnitude of the cesium or iodine source term. The BWR Mark I containment failure dynamics causing a surge of flashing water from the wetwell to spill into the drywell was an interesting insight. The subsequent steam production from the water boiling on the ex-vessel debris and release of any radionuclides were important in accidents with a stochastic SRV failure.

The Surry UA containment failure results show that a steel-reinforced concrete containment failed by over-pressurization from ex-vessel CCI. The CCI heated the containment air, evaporated spilled water on the containment floor, and released non-condensable gases. The containment pressurized to liner failure and towards a rebar failure by 72 hr, which started higher leakage. The leakage rate gradually increased with containment pressure. The source term was generally small due to adequate time for natural gravitational aerosol settling. The free-standing steel containment also experienced the same long-term pressurization from CCI but ruptured at its failure pressure, which quickly depressurized the containment. The design leakage prior to a late containment failure is important for the cesium source term prior to natural gravitational settling, which limits the airborne aerosols mass at time of the late over-pressure failure.

The expected impact of these conclusions to other plants varied. The insights on the late PWR and BWR Mark III containment over-pressure responses from CCI are expected to be qualitatively similar to Surry and Sequoyah for steel-reinforced concrete and free-standing steel containments, respectively. Each BWR Mark II has unique characteristics that impact the ex-vessel debris behavior. The potential for an early drywell liner in a Mark II ranges from low to geometrically impossible. Depending upon the ex-vessel debris behavior and design characteristics allowing debris to enter the wetwell, the corresponding similarity on drywell head leakage could vary (e.g., in some Mark II designs some of the ex-vessel debris may relocate into the wetwell).

Primary system pump leakage

The PWR pump seal leakage was identified as an important generic safety issue in the 1980s and resolved as not warranting generic cost-beneficial safety enhancements. Nevertheless, PWRs have systematically replaced their seals with improved materials that are less susceptible to thermal degradation. More recently, new seals are being installed that are advertised to be capable of sustaining 100% system pressure with fail-safe redundancy and negligible leakage. Consequently, the SOARCA UA insights are evolving. In plants without upgraded, leak resistant seals, RCP seal failures contribute to a faster inventory loss from the primary system, which accelerates the timing to core damage. The leaking seals may have an impact as a potential ignition source from leaking gases above the hydrogen autoignition. This is usually a positive impact because it can burn the released hydrogen locally in the lower containment before it circulates throughout the containment (i.e., a potential for a larger burn).

The BWR seal leakage is important to cooling the ex-vessel debris and delaying the drywell liner melt-through. It is also important for (1) accelerating the inventory loss and associated core melt progression and (2) creating a steam source for containment pressurization prior to vessel failure and through water-debris interactions after vessel failure (i.e., contributes to drywell pressurization

and leakage). The insights on recirculation pump seal leakage from the Peach Bottom and Fukushima Dai-chi calculations are somewhat applicable to other BWRs. The drywell liner melt-through issue is unique to BWRs with Mark I containments. The qualitative insights are expected to be similar with some variations in the effectiveness due to the sump size and drywell wall and floor characteristics. The acceleration of the inventory of loss and early pressurization is applicable for the other BWRs (i.e., Mark II and Mark III containments). However, the impact on ex-vessel debris behavior is expected to be different for the BWR Mark II and Mark III containment designs due to significantly different containment designs.

Other source term insights

Uncertainties in the radionuclide behavior continue to be influential in characterization of the source term. The chemical form of the cesium and iodine was investigated as two parameters in the UAs but there are others. The explored parameters showed importance on the source term. Due to the potential for chemisorption on BWR internal structures (i.e., separators and dryers), the amount of cesium hydroxide was important. The PWR steam generator tubes were an important deposition location but not susceptible to cesium chemisorption due to the Inconel tube construction. The amount of gaseous iodine was important in all calculations due to its long-term mobility for release. The insights from these modeling uncertainties will persist until there is an improved chemistry modeling.

Other applications

The NRC recently published Research Information Letter 20-03 summarizing the numerous uses of the SOARCA project as of 2019. This letter notes that the project's results, insights, computer code models, and modeling best practices have supported NRC rulemaking, licensing, and oversight efforts and facilitated international cooperation and knowledge management. The letter also notes that the SOARCA project has been used or cited in over 325 publications in the open literature, including technical reports, conference papers, journal articles, and dissertations. These publications cover a broad range of research areas, including but not limited to accident-tolerant fuel, reactor safety (including advanced designs), societal risk, and spent fuel storage and transportation, demonstrating the diverse areas in which researchers have referenced or used aspects of the SOARCA project.

New work in this report was performed was performed using the SOARCA calculations as a large database for investigations of the variability and uncertainty in the severe accident progression. The results from the SOARCA UA accident progression calculations contain a wealth of information not previously documented in the NUREG/CRs. The new but related information presented can be used to benchmark or inform regulatory decisions related to severe accidents. The new work includes a benchmark of the NUREG-1465 licensing source term but showing the variability of key accident progression timings and magnitudes of the radionuclide release from the SOARCA UA. The incorporation of the SOARCA UA information into these applications provides additional insights into the variability from severe accident uncertainties that was not previously explored.

6. REFERENCES

[1] NUREG/CR-7155. "State-of-the-Art Reactor Consequence Analyses Project, Uncertainty Analysis of the Unmitigated Long-Term Station Blackout of the Peach Bottom Atomic Power Station." U.S. Nuclear Regulatory Commission, Washington, DC. May 2016.

[2] NUREG/CR-7245. "State-of-the-Art Reactor Consequence Analyses Project: Sequoyah Integrated Deterministic and Uncertainty Analysis." U.S. Nuclear Regulatory Commission, Washington, DC. October 2019.

[3] NUREG/CR-7262 (DRAFT). "State-of-the-Art Reactor Consequence Analyses Project: Uncertainty Analysis of the Unmitigated Short-Term Station Blackout of the Surry Power Station." U.S. Nuclear Regulatory Commission, Washington, DC. August 2019.

[4] Ghosh, S. T., et al. "State-of-the-Art Reactor Consequence Analyses Project Uncertainty Analyses: Uncertainty Analyses for Station Blackout Scenarios." Paper 193-27145, 2019. International Topical Meeting on Probabilistic Safety Assessment and Analysis (PSA 2019), Charleston, SC, April 28-May 3, 2019.

[5] Ghosh, S. T., et al. "State-of-the-Art Reactor Consequence Analyses Project Uncertainty Analyses: Insights on Accident Progression and Source Term." Paper 193-27164, 2019. International Topical Meeting on Probabilistic Safety Assessment and Analysis (PSA 2019), Charleston, SC, April 28-May 3, 2019.

[6] Ghosh, S. T., et al. "State-of-the-Art Reactor Consequence Analyses Project Uncertainty Analyses: Insights on Offsite Consequences." Paper 193-27165, 2019. International Topical Meeting on Probabilistic Safety Assessment and Analysis (PSA 2019), Charleston, SC, April 28-May 3, 2019.

[7] Ghosh, S. T., et al. "State-of-the-Art Reactor Consequence Analyses Project Uncertainty Analyses: Insights on Methodologies." Paper 193-27166, 2019. International Topical Meeting on Probabilistic Safety Assessment and Analysis (PSA 2019), Charleston, SC, April 28-May 3, 2019.

[8] Ghosh, S. T., et al. "State-of-the-Art Reactor Consequence Analyses Project Uncertainty Analyses: Uncertainty Analyses for Station Blackout Scenarios," Paper 193-27166, 9th Conference on Severe Accident Research (ERMSAR), Prague, Czech Republic, March 18-20, 2019.

[9] NUREG-1465. "Accident Source Terms for Light-Water Nuclear Power Plants." Sandia National Laboratories. U.S. Nuclear Regulatory Commission, Washington, DC. February 1995.

[10] Leonard, M. T., et al. "Accident Source Terms for Boiling Water Reactors with High Burnup Cores Calculated Using MELCOR 1.8.5." SAND2007-7697, Sandia National Laboratories. November 2007.

[11] Ashbaugh, S., et al. "Accident Source Terms for Pressurized Water Reactors with High Burnup Cores Calculated Using MELCOR 1.8.5." SAND2008-6664, Sandia National Laboratories. April 2010.

[12] Gauntt, R. O., et al. "Accident Source Terms for Pressurized Water Reactors with High Burnup Cores Calculated Using MELCOR 1.8.5." SAND2016-12954, Sandia National Laboratories. December 2016.

[13] Ghosh, S. T., et al. "Estimating Safety Valve Stochastic Failure to Close Probabilities for the Purpose of Nuclear Reactor Severe Accident Analysis." NRC2017-3538, Proceedings of the Thirteenth NRC/ASME Symposium on Valves, Pumps, and In-Service Testing for Operating and New Reactors. July 2017.

[14] NUREG/CR-7037. "Industry Performance of Relief Valves at U.S. Commercial Nuclear Power Plants through 2007." U.S. Nuclear Regulatory Commission, Washington, DC. March 2011.

[15] M. Zhu and A. Lu. "The Counter intuitive Non informative Prior for the Bernoulli Family." *Journal of Statistics Education*, 12:2. 2004.

[16] NUREG/CR-7110 Volume 1, Rev. 1. "State of the Art Reactor Consequence Analysis Project Volume 1: Peach Bottom Integrated Analysis." U.S. Nuclear Regulatory Commission, Washington, DC. May 2013.

[17] C. F. Boyd, K. W. Armstrong. "Computational Fluid Dynamics Analysis of Natural Circulation Flows in a Pressurized-Water Reactor Loop under Severe Accident Conditions." NUREG-1922, U.S. Nuclear Regulatory Commission, Washington, DC. March 2010.

[18] NUREG-2195 (DRAFT). "Consequential C-SGTR Analysis for Westinghouse and Combustion Engineering Plants with Thermally Treated Alloy 600 and 690 Steam Generator Tubes." U.S. Nuclear Regulatory Commission, Washington, DC. May 2016.

[19] NUREG 1771. "U.S. Operating Experience with Thermally Treated Alloy 600 Steam Generator Tubes." U.S. Nuclear Regulatory Commission, Washington, DC. February 2003.

[20] NUREG-2188. "U.S. Operating Experience with Thermally Treated Alloy 600 Steam Generator Tubes." U.S. Nuclear Regulatory Commission, Washington, DC, February 2016.

[21] NUREG/CR-6791, Revision 1. "Eddy Current Reliability Results from the Steam Generator Mock-up Analysis Round-Robin." U.S. Nuclear Regulatory Commission. October 2009.

[22] Stewart, W. A., A. T. Pieczynski and V. Srinivar. "Natural Circulation Experiments for PWR Degraded Core Accidents." EPRI Report NP-6324-D. 1989.

[23] Stewart, W. A., A. T. Pieczynski and V. Srinivar. "Natural Circulation Experiments for PWR High Pressure Accidents." EPRI Report TR-102815. 1993.

[24] C. F. Boyd, K. Hardesty. "CFD Analysis of 1/7th Scale Steam Generator Inlet Plenum Mixing During a PWR Severe Accident." NUREG-1781, U.S. Nuclear Regulatory Commission, Washington, DC. October 2003.

[25] NUREG-1788. "CFD Analysis of Full-Scale Steam Generator Inlet Plenum Mixing During a PWR Severe Accident." U.S. Nuclear Regulatory Commission, Washington, DC. May 2004.

[26] C. F. Boyd and K. W. Armstrong. "Computational Fluid Dynamics Analysis of Natural Circulation Flows in a Pressurized Water Reactor Loop under Severe Accident Conditions." NUREG-1922, U.S. Nuclear Regulatory Commission, Washington, DC. March 2010.

[27] NUREG/CR-6995. "SCDAP/RELAP5 Thermal-Hydraulic Evaluations of the Potential for Containment Bypass During Extended Station Blackout Severe Accident Sequences in a Westinghouse Four-Loop PWR." U.S. Nuclear Regulatory Commission, Washington, DC. March 2010.

[28] Boyd, C. "CFD Predictions of Severe Accident Natural Circulation Flows in a Combustion Engineering PWR." ADAMS Accession No ML16068A170, U.S. Nuclear Regulatory Commission, Washington, DC.

[29] U.S. NRC. "State-of-the-Art Reactor Consequence Analyses (SOARCA) Project: Sequoyah Integrated Deterministic and Uncertainty Analyses." (Draft Report) ADAMS Accession No ML16096A374, U.S. Nuclear Regulatory Commission. 2016.

[30] Wagner, K., et al. "MELCOR 2.2 Benchmarks of Peach Bottom NUREG/CR-7155 Uncertainty Analysis." (Draft Report) SAND2020-XXXX, Sandia National Laboratories. January 2010.

[31] NUREG/CR 6920. "Risk Informed Assessment of Degraded Containment Vessels." U.S. Nuclear Regulatory Commission, Washington, DC. June 2006.

[32] NUREG/CR 6906. "Containment Integrity Research at Sandia National Laboratories, An Overview." U.S. Nuclear Regulatory Commission, Washington, DC. March 2006.

[33] NUREG/CR 6433. "Containment Performance of Prototypical Reactor Containments Subjected to Severe Accident Conditions." U.S. Nuclear Regulatory Commission, Washington, DC. August 1996.

[34] NUREG/CR 7149. "Effects of Degradation on the Severe Accident Consequences for a PWR Plant with a Reinforced Concrete Containment Vessel." U.S. Nuclear Regulatory Commission, Washington, DC. June 2013.

[35] NUREG/CR-5528. "An Assessment of BWR Mark-II Containment Challenges, Failure Modes, and Potential Improvements in Performance." U.S. Nuclear Regulatory Commission, Washington, DC. July 1990.

[36] NUREG/CR-5529. "An Assessment of BWR Mark-III Containment Challenges, Failure Modes, and Potential Improvements in Performance," U.S. Nuclear Regulatory Commission, Washington, DC. July 1991.

[37] "Type C Containment Isolation Valve Performance." EPRI Report Number 1022599, ADAMS Accession No ML110970450. ERPI, Palo Alto, CA. March 2011.

[38] U.S. NRC. "State-of-the-Art Reactor Consequence Analyses (SOARCA) Project: Surry Integrated Deterministic and Uncertainty Analyses." (Draft Report) ADAMS Accession No ML16096A374, U.S. Nuclear Regulatory Commission, Washington, DC. 2016.

[39] U.S. NRC. "Closeout of Generic Safety Issue 23, Reactor Coolant Pump Seal Failure." ADAMS Accession No ML993370509, U.S. Nuclear Regulatory Commission, Washington, DC. November 8, 1999.

[40] Dominion. "Virginia Electric and Power Company (Dominion) Surry Power Station Unit I Compliance Letter in Response to the 12, 2012 Commission Order Modifying Licenses with Regard to Requirements for Mitigating Strategies for Beyond-Design-Basis External Events, Order Number Ea-12-049." ADAMS Accession No ML15209A503, U.S. Nuclear Regulatory Commission, Washington, DC. July 22, 2015.

[41] SAND2016-0232. "Fukushima Daiichi Unit 1 Accident Progression Uncertainty Analysis and Implications for Decommissioning of Fukushima Reactors – Volume I." Sandia National Laboratories. January 2016.

[42] NUREG/CR-5732. "Iodine Chemical Forms in LWR Severe Accidents." U.S. Nuclear Regulatory Commission, Washington, DC. April 1992.

[43] "Phebus Fission Product (Phebus-FP) Program." ADAMS Accession No ML081330474. May 30, 2008.

[44] NUREG/CR-7110, Volume 2, Rev. 1. "State-of-the-Art Reactor Consequence Analysis Project Volume 2: Surry Integrated Analysis." U.S. Nuclear Regulatory Commission, Washington, DC. January 2012.

[45] "Calculation of Distance Factors for Power and Test Reactor Sites," TID-14844, ADAMS Accession No ML021720780, U.S. Nuclear Regulatory Commission, Washington, DC. March 1962.

[46] Leggett, C. "Benefits and Uses of the State-of-the-Art Reactor Consequence Analyses (SOARCA) Project." ADAMS Accession No ML20100J883, U.S. Nuclear Regulatory Commission, Washington, DC.

DISTRIBUTION

Email—Internal

Name	Org.	Sandia Email Address
Technical Library	01977	sanddocs@sandia.gov

Email—External (encrypt for OUO)

Name	Company Email Address	Company Name

This page left blank

This page left blank

Sandia National Laboratories

Sandia National Laboratories is a multimission laboratory managed and operated by National Technology & Engineering Solutions of Sandia LLC, a wholly owned subsidiary of Honeywell International Inc. for the U.S. Department of Energy's National Nuclear Security Administration under contract DE-NA0003525.